UNIVERSITY OF CANTERBURY

MASTERS THESIS

Effect of Matrix Additives on the Mechanical Properties of Pultruded Composites

---

Anton Jakob GOOD

A thesis submitted in fulfilment of the requirements

for the degree of Master of Engineering

in the

Department of Mechanical Engineering

Declaration of Authorship

- This work was done wholly or mainly while in candidature for a research degree at this University.
- Where any part of this thesis has previously been submitted for a degree or any other qualification at this University or any other institution, this has been clearly stated.
- Where I have consulted the published work of others, this is always clearly attributed.
- Where I have quoted from the work of others, the source is always given. With the exception of such quotations, this thesis is entirely my own work.
- I have acknowledged all main sources of help.
- Where the thesis is based on work done by myself jointly with others, I have made clear exactly what was done by others and what I have contributed myself.

Signed:

_____

Date:

_____

Abstract

Pultrusion is an industrial process for the manufacture of fibre-reinforced composites having highly aligned continuous fibre reinforcement. In this work, the effect of processing conditions (temperature) and material composition (filler type, filler content, release agents) on the mechanical properties of pultruded glass fibre-reinforced polymer matrix composites was investigated. The processing-property relationships of the pultruded composites were assessed by measuring the tensile and flexural behaviour, short beam strength and curing behaviour. An empirical model is developed to predict the density of the composites, based on the volume fraction of glass fibre, filler additions and shrinkage behaviour. The study shows that significant improvements in the tensile (>75%), flexural (>15%) and interlaminar shear strength (>50%) in pultruded composites, including waste reduction and decreased manufacturing costs, are possible by manipulating the processing conditions and composition of the resin component.

Acknowledgements

I would like to extend my gratitude to a number of people, without whom this project would not have been possible. Firstly, I would like to thank Mr. Stuart Hay from Gracol Composites for reaching out to the University of Canterbury and Callaghan Innovation in an effort to seek help in improving his products. Mr. Hay has been enthusiastic and helpful for the entirety of the project. I would also like to thank the other employees at Gracol Composites including Mark, Hotse and Roger who have proved to be an invaluable source of knowledge; they have assisted with achieving the project goals, providing hints when I was stuck, but also allowing me to learn for myself.

I would like to thank A/Prof. Mark Staiger for supervising this project, providing assistance and guiding me throughout the last 18 months.

Mr. Garry Cotton and Mr. Ken Brown from the University of Canterbury mechanical workshop are greatly acknowledged for their advice on manufacturing of components and providing access to the workshop facilities in the Department of Mechanical Engineering, University of Canterbury.

Mr. Kevin Stobbs and Mr. Mike Flaws also provided training in materials testing and microscopy.

Mr. Gerry Kirk assisted with the design and manufacture of electronic control systems, as well as providing valuable career and life advice.

I cannot forget to acknowledge my family, without my parents hard work and support throughout my life I would not have been in a position to begin this project in the first place. My brother has always been a person to bounce ideas off and has also been involved in field trialling products from Gracol Composites. My girlfriend Jane has been by my side throughout the entire project and has helped me stay sane.

Finally, I would like to thank the University of Canterbury for providing me with my education as an Engineer and helping me to reach my full potential and Callaghan Innovation for providing financial assistance.

Contents

List of Figures

List of Tables

List of Abbreviations

ASTM	**A**merican **S**ociety for **T**esting and **M**aterials
CAD	**C**omputer **A**ided **D**esign
CSM	**C**hopped **S**trand **M**at
CSV	**C**omma **S**eparated **V**ariable
DMA	**D**ynamic **M**echanical **A**nalysis
EDS	**E**nergy **D**ispersive *X*-ray **S**pectroscopy
FE	**F**inite **E**lement
GFRP	**G**lass **F**ibre **R**einforced **P**olymer
HDPE	**H**igh **D**ensity **P**oly**E**thylene
HRC	**H**ardness **R**ockwell **C** scale
ISO	**I**nernational **O**rganization for **S**tandardization
LPA	**L**ow **P**rofile **A**dditive
MEKP	**M**ethyl **E**thyl **K**etone **P**eroxide
PHR	**P**er **H**undred **R**esin
PID	**P**roportional **I**ntegral **D**erivative
PWM	**P**ulse **W**idth **M**odulation
RMG	**R**andom **M**icrostructure **G**eneration
RTCS	**R**esin **T**emperature **C**ontrol **S**ystem
RVE	**R**epresentative **V**olume **E**lement
SEM	**S**canning **E**lectron **M**icroscopy
UV	**U**ltra**V**iolet light

Chapter 1

Introduction

1.1 Background and purpose

Pultrusion is an efficient manufacturing process for the production of continuous lengths of fibre-reinforced polymer matrix composite materials having a constant cross-section [4]. Pultrusion has been a commercial fabrication process since the early 1950s. Pultruded profiles exhibit exceptional chemical, electrical and mechanical properties and are thus suitable for use in many high performance industries (Table 1.1). Material and product formulations for the pultrusion process are often developed through trial and error without rigorous experimental regimes in an industrial setting. Such development methods may result in suboptimal properties in one or more aspects.

The purpose of this research is to explore the effects of matrix additives on the mechanical properties of pultruded composites, with the aim of developing a new resin formulation suitable for use in the pultrusion of high performance composites and to develop a model for prediction of microstructural properties.

Fillers and other additives play a major role in determining the properties of pultruded composites [5]. The pultrusion literature reports on the general effects of fillers and additives on the mechanical properties of pultruded composites, particularly with regard to pultruded glass fibre reinforced polyester matrix composites. However, the literature concerning pultruded glass fibre reinforced polyurethane matrix composites is sparse. Therefore, the present work aims to explore the effects of the additive type, particle size and content on the mechanical (tensile, flexural and short beam) properties of pultruded glass fibre reinforced composites based on a polyurethane matrix. The tensile, flexural and shear strength of the pultruded composites was measured as a function of the additive type and content. A

TABLE 1.1: Applications of pultruded composite materials

Field	Desired Properties	Example Uses
Automotive	Mechanical strength, low density, tight dimensional tolerances, repeatable properties	Wheel components, suspension components, steering components
Construction	Mechanical strength, low density, fire stability, thermal insulation, easy alteration	Frames, walkways, stairs, structural beams, walling, fencing, concrete reinforcement
Electrical	Low conductivity, moisture resistance	Ladders, electrical junction boxes, cable support conduits
Harsh environments	Chemical stability, fatigue resistance, UV stability	Boat trailers, waste water, dynamic sculptures
Decoration	Simplicity of profiles, price	Curtains, frames, covers
Sport	Durability, low density, mechanical strength, price	Arrows, bow limbs, fishing poles, kite frames, ski poles

secondary objective was to develop a model to predict the density and packing properties of pultruded composites in order to capture the effects of fibre and additive size distributions.

1.2 Thesis outline

The thesis is divided into the following chapters. Chapter 1 introduces the topic of the thesis, giving motivation and objectives of the project. Chapter 2 provides a literature review and description of the pultrusion process, highlighting some of the gaps in knowledge in the existing literature and the research questions that emerge. Chapter 3 describes the general experimental procedures used in this research. Chapter 4 details the lab scale pultrusion machine specifically developed for this research. Chapter 5 is concerned with the particle size distributions of the fillers considered in this research. Chapter 6, 7 and 8 examine the effects of filler properties on the tensile, flexural and short beam properties, respectively. Chapter 9 attempts to describe the microstructure of the pultruded composites using statistical modelling. Chapter 10 provides the main conclusions and recommendations for future work arising from this study.

Chapter 2

Literature Review

2.1 Introduction to the pultrusion process

During the pultrusion process, fibres are mechanically drawn through an impregnation bath of uncured matrix resin (Figure 2.1). The resin impregnated fibres then pass through a heated die that acts to form the cross-section and cure the thermosetting resin. The pultruded material is then parted to the desired length by using a flying cut-off saw.

The continuous fibre reinforcement used in the pultrusion process is available in various forms including unidirectional rovings (untwisted bundles of fibre), continuous strand (random) mat, or continuous woven mat. A surfacing veil may also be incorporated into the surface of the pultruded material to improve the surface finish and/or environmental stability of the product. The matrix resin is continuously pumped from a reservoir into the impregnation bath to ensure constant supply and uniform temperature. Typically, the resin will contain additives including catalysts, fillers, stabilisers, pigments and flame retardants depending on the required product properties.

The heated die is a multi-part mould typically machined from tool steel with a length between 500 and 1000 mm. The mould face is highly polished and mostly runs parallel to the pulling axis for the entire length of the die. Rounded inlet shoulders are also used to reduce fibre damage and provide a steady pressure rise within the fibre/resin system that assists with reducing the void content [6]. Typically, the die is heated via electrical resistance heaters in the form of platens or cartridges. Alternatively, heat to the die may be provided by circulating a fluid (such as oil or steam) within passages that have been machined into the die.

The pulling mechanism may involve using a hand-over-hand unit or continuous roller

puller. Generally a continuous roller puller is used for simple rectangular or circular profiles, while a hand-over-hand unit is used for more complex profiles such as I-beams and rectangular hollow sections. The pulling mechanism is also used to control the pultrusion speed, controlling the curing extent of the composites.

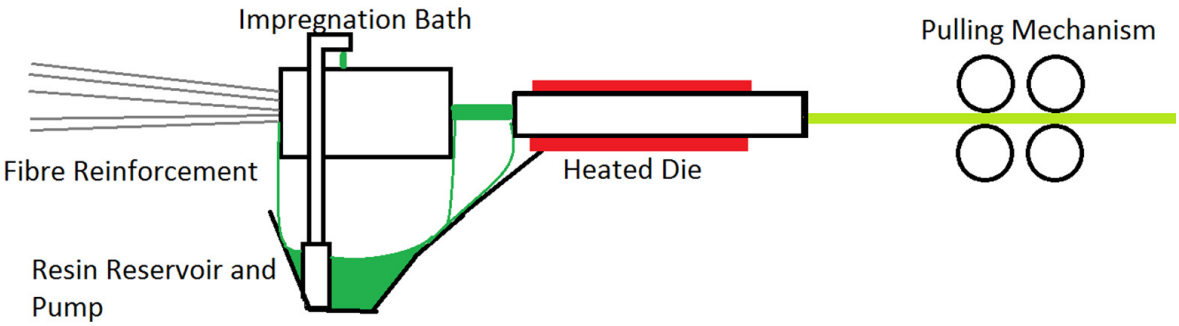

FIGURE 2.1: Schematic layout of the pultrusion process.

2.2 Resin formulation materials and additives

2.3 Effects of resin temperature on the pultrusion process

The viscosity and curing time of thermosetting resins are highly sensitive to temperature. The temperature of operating environments in many industrial settings tends to be highly variable due to a low degree of control. However, the resin impregnation and curing behaviour may be decoupled from environmental variation by directly controlling the temperature of the resin bath during the process.

Borges *et al.* [7] studied the influence of bath temperature (30 - 70 °C) on the processing robustness and properties of pultruded glass fibre reinforced rods containing an unsaturated polyester resin (UCEFLEX ISO 1005 from Elekeiroz). Resin viscosity and catalyst (benzoyl peroxide) stability were too low for successful pultrusion at temperatures greater than 50 °C. In-die curing time was found to decrease from 120 to 95 seconds with an increase of resin temperature from 30 to 50 °C. Increasing resin bath temperature resulted in higher tensile strength, elongation at break and hardness. However, the elastic modulus decreased linearly from 34.6 GPa at 30 °C to 31.2 GPa at 50 °C with void content increasing from 4.85 to 6.95 vol%. Resin fibre wet-out was increased as the resin bath temperature was increased due to a decrease in resin viscosity. However, most of the excessive loss of resin from the glass fibres prior to entering the die was observed at higher temperatures. The allowable

resin viscosity was found to be between 400 and 5000 mPa s. While the curing time was significantly reduced at temperatures above 60 °C. It was recommended that the pultrusion process be operated using a resin bath temperature between 30 and 50 °C. Flexural properties were not examined as a part of the study, nor were the effects of fillers.

Chen *et al.* [8] examined the effect of bath temperatures (25 -55 °C) on the polymerisation of furfuryl alcohol during the pultrusion process. A resin bath temperature of 25 °C resulted in an extended pot life and ideal viscosity range over an 8 h period (700 mPa s to 1000 mPa s). No mechanical properties were considered in the study and no consideration was given to fillers.

Resin bath temperature control has been shown as an effective method for controlling the viscosity of uncured resin during pultrusion and may result in improved mechanical properties in pultruded composites.

2.4 Effect of additives on the mechanical properties of pultruded composites

Additives are added to the resin primarily for two reasons. Additives can be used to reduce the cost of the final products by reducing the resin content. Additives may also improve the surface finish of the final products by altering interactions at the profile-die interface. Additionally, additives may be used to improve flammability or environmental resistance of pultruded composites. Additives have the potential to significantly alter the mechanical properties of pultruded materials with both positive and negative effects being possible.

Landon *et al.* [9] studied the effects of particle diameter of a spherical glass bead filler on the tensile strength of a cast thermosetting polyurethane resin. The tensile strength was found to decrease linearly with increasing particle diameter, with a maximum dependence of tensile strength on particle diameter at a filler volume fraction of 0.2. Fibre reinforcement was not used in composites considered in the study.

The flexural strength of pultruded glass fibre reinforced polyurethane matrix composites was increased with both mica and calcium carbonate filler contents between 0 and 40 parts per hundred resin (phr), Chen *et al.* [10]. Calcium carbonate provided greater improvements in flexural strength compared to mica. The calcium carbonate and mica had a particle

sizes of 350 and 325 mesh, respectively. No other particle sizes or loading conditions were examined in the study.

The influence aluminium based fillers (20 - 30 vol%) on the microstructure and flexural properties of pultruded glass fibre composites with isophtalic and vinyl ester resins was reported by Paciornik *et al.* [11]. A method of digitally analysing scanning electron micrographs was developed to automate the measurement of the glass fibre content, distribution of glass fibre diameters and filler and resin content. Glass fibres within most polymer composites tend to be clustered, rather than uniformly distributed. Increasing filler content from 20 to 30 vol% resulted in an increase in flexural modulus from 10 to 12 GPa. The type of aluminium based filler used in the study was not reported.

Boukhili *et al.* [12] examined the physical and mechanical properties of pultruded glass-fibre composites ($v_f = 51.6\%$) containing clay fillers and low profile additives (LPAs). LPAs are thermoplastic polymers that provide improved shrinkage control in thermosetting resins. Clay powder with a mean particle size of 4.8 µm was used as a filler. Polyvinyl acetate (PVAc) was used as an LPA in a general purpose unsaturated polyester resin. The filler and LPA loading between 0 - 40 phr and 0 - 20 phr, respectively. The interlaminar shear strength of the pultruded composites was slightly sensitive to the filler loading. Span to thickness ratio (L/d) was varied from 11 to 24 to study the interaction of shear and tensile stresses in flexural tests. Specimens failed through interlaminar shear at L/d = 11 (τ_f = 40 MPa, σ_f = 840 MPa). The flexural strength was not influenced by the filler loading at L/d = 16 and 24 (σ_f = 1100 MPa), with tensile and compressive stresses being dominant in comparison to shear stresses. The standard L/d ratio of 4 for short beam testing was found to be too low as the specimens failed by compressive yield under the loading nose rather than by interlaminar shear failure. The addition of the LPA reduced the cure shrinkage due to microvoid formation. The LPAs that similar effects on the mechanical properties as the fillers. The study did not consider the effects of different filler particle diameters.

The catalyst type, LPA content and $CaCO_3$ filler content may each contribute to the formation of microvoids as reported by Zhang *et al.* [13]. The volume fraction of voids has been observed to increase from 0.86 to 1.89% using 14.3 - 29 wt% calcium carbonate filler with an average particle size of 7 µm. The appearance of the cured resin became opaque with increasing filler loading. The void content was also found to be a function of the catalyst. The void fraction was 13% when using a tert-Butyl peroxybenzoate (TBPB) catalyst.

The use of a methyl ethyl ketone peroxide (MEKP) catalyst resulted in a void content of 7%. The void formation was reduced by using an applied pressure. Zhang suggests calcium carbonate filler assists in the formation of microvoids through the nucleation of gas bubbles. The TBPB catalyst is proposed to react with the $CaCO_3$, releasing CO_2 that then acts as an unintentional blowing agent.

Gupta *et al.* determined the effects of carbon black, short bagasse fibre and calcium carbonate fillers on the tensile strength of pultruded glass fibre composites using a Taguchi analysis [5]. The tensile strength was observed to increase with increasing bagasse fibre content and decrease with increasing calcium carbonate and carbon black content.

There has been little work on the effects of mould release agents on the short beam strength of pultruded composites. Irfan *et al.* [3] observed significant reductions in mechanical properties of pultruded composites using epoxy and polyurethane resins manufactured with an internal mould release agent. The flexural strength was observed to increase by 50% when the mould release agent was applied externally to the profile rather than mixed with the resin. Furthermore, the interlaminar shear strength of the composites was increased by up to 40% where the mould release agent was applied externally rather than dispersed throughout the resin mixture. The use of an internal mould release (INT-PUL-24) agent appears to reduce the interfacial bonding strength between the matrix and glass fibres due to incomplete migration of the release agent to the surface of the composite, resulting in a decrease in the interlaminar shear strength.

Previous studies have shown the mechanical properties of pultruded composites are a function of the morphology and chemistry of additives, with voids and poor fibre-matrix bonding being responsible for reduced properties. No studies have considered the effects of filler particle size and content in pultruded polyurethane matrix composites.

2.5 Modelling the effects of additives on pultruded composite properties

The increasing demand of composite materials in industry calls for cost-effective methods to accurately predict properties of the composites based on their constituent components. Traditional methods for characterising composites involve full factorial and Taguchi experimental campaigns. Physical experiments require significant human, infrastructure and time

resources that are costly. An increasing trend in the composites industry is to complement and/or replace experimental work with numerical processes capable of rapidly providing the same information at a lower cost. Significant research has been conducted into the generation and analysis on representative microstructures of long fibre reinforced composite materials.

Park *et al.* [14] studied the effects of filler and void content on the mechanical properties of pultruded composites under shear loading. Various analytical models were used to predict the bulk properties of the pultruded composites based on the filler type, filler loading and void content. Park *et al.* used a clay powder filler consisting of hexagonal platelets (0.4 - 6.0 µm diameter). It was observed that the shear modulus of the pultruded composites could be accurately predicted using the Halpin-Tsai and Mori-Tanaka models when the filler and void content are taken into account. However, the effect of filler particles on the packing efficiency of the glass fibres and therefore the influence on ultimate strength properties was not considered.

The effects of fibre packing on the elastic properties of a transversely random distributed, longitudinally unidirectional glass-epoxy composite was described by Gusev *et al.* [15]. The glass fibre diameter distribution and volume fraction of a unidirectional glass fibre composite was determined. Monte Carlo simulations were used to generate random microstructures containing glass fibres with a pre-determined diameter distribution. The elastic constants of the composite were predicted by an FEA model based on the generated microstructures to within a few percent. Modelling of the composite microstructure using either hexagonal or square packing arrangements produced significant errors in the predicted properties, as did the Halpin-Tsai, Tendon-Weng and Wilczynski models. Microstrucutre analysis as a part of the study showed glass fibres in real composites are not regularly packed and should be considered as having a random packing array. The glass fibre diameter was observed to have little influence on the elastic properties of the composite. However, the randomness of the packing arrangement affected the accuracy of the model. The use of numerical methods to complement or possibly replace phenomenological models for predicting elastic properties of composite materials was recommended. However, a limitation of the study was that fillers were not considered.

Random microstructure generation (RMG) has also been used as a method for predicting elastic properties of real and simulated fibre arrangements in unidirectional long fibre

composites with high volume fractions by Melro *et al.* [16] and Romanov *et al.* [17]. Representative volume elements (RVE) of sample microstructures were generated with RMG. Randomised minimum fibre spacings of between 0 and 7% of the radius of the fibre were implemented [15]. Finite element (FE) analysis based on the RVEs was in close agreement with experimental values. However, the effects of filler or variations in the fibre diameter on the packing efficiency were not considered.

A modified nearest neighbour algorithm method similar to the RMG method was developed for RVEs as reported by Wang et al. [18]. The microstructure was generated by placing fibres around a central fibre using probability density functions to describe the angular position and radial distance. The method is slower than earlier RMG work although produces more representative RVEs. The RVEs were used to perform 2D and 3D FE analysis to predict the elastic moduli and Poisson's ratios of a carbon fibre composite, achieving good agreement with experimental properties in the longitudinal direction, although underestimating the properties in other loading conditions. Filler particles were once again not considered in these models.

While significant work has been performed regarding the generation of representative microstructures for composites with unidirectional reinforcement, there is no published work regarding stochastic modelling of the effects of particulate additives.

2.6 Summary

Resin viscosity is an important factor in the production of pultruded composites and temperature control has been shown to be an effective means of improving the properties of pultruded composites containing polyester resin.

Tests regarding the effects of additives on pultruded composites are generally only limited to one loading condition in the literature, with most work being presented on the flexural properties.

Modelling of unfilled pultruded composites through statistical generation of microstructures is a well understood field, however no work has been published on the generation of microstructures for pultruded composites containing particulate fillers.

This research sets out to develop a lab-scale pultrusion machine with a resin temperature control system that will be used to to produce composites containing various additives. The

composites will then be tested under tensile, flexural and short beam loading to characterise the effects of the additives. A statistical microstructure generation model will be developed to aid in the prediction of the density and glass packing fraction of pultruded composites.

Chapter 3

Experimental Procedures

3.1 Materials

3.1.1 Resin

Two resins were used in this research, Plexinate P100 and Plexinate P200. Both resins were manufactured by Plexinate Ltd. Tables 3.2 and 3.1 give the properties of liquid and cured P100 resin, respectively. No datasheet is available for the Plexinate P200 resin.

TABLE 3.1: Properties of liquid P100 resin

Property	**Value**
Polyurethane polymer content	55%
Styrene content	42-43%
Methyl methacrylate content	2-3%
Isocyanate content	0%
Viscosity at 25 °C	200 −350mPas
Specific gravity	1.043

TABLE 3.2: Physical properties of unfilled Plexinate P100 castings

Property	**Value**
Tensile strength	87 MPa
Flexural strength	131 MPa
Tensile modulus	3.9 GPa
Flexural modulus	3.8 GPa
Heat deflection temperature	135 °C
Elongation at break	3.5%
Barcol hardness	42-44
Specific gravity	1.1

The resins are based on a mixture of polyurethane polymer and styrene as a reactive solvent. Both resins are cured at elevated temperatures with heat activated peroxides (Section 3.1.4). P100 is intended to be used as a base resin, while P200 is added in small quantities ($\approx$ 10 parts per hundred resin (phr)) to improve the flexural properties of pultruded composites and reduce the peak exotherm temperature within the pultrusion die during curing of thick profiles.

3.1.2 Glass fibres

The glass fibres used in this research were Jushi Direct Roving (DR) 312 (Table 3.3). The glass rovings are coated with a silane based binder and are designed for the pultrusion process.

The linear density of the rovings is given in grams per metre (or tex). Two types of Jushi DR 312 roving with linear densities of 4400 and 9600 tex were used for this research.

TABLE 3.3: Jushi Direct Roving 312 glass roving properties

Property	**4400 tex**	**9600 tex**
Glass type	E-glass	E-glass
Filament diameter	23 µm	34 µm
Roving area	1.73 mm^2	3.77 mm^2
Tensile strength	2513 MPa	2513 MPa
Tensile modulus	79.16 GPa	79.16 GPa
Shear strength	67 MPa	67 MPa

3.1.3 Fillers

Talc and limestone fillers were investigated in this research. Talc is a clay mineral composed of hydrated magnesium silicate with the chemical formula $H_2Mg_3(SiO_3)_4$ (specific gravity (s.g.) = 2.58-2.83).

Limestone primarily consists of calcium carbonate ($CaCO_3$), in the form of calcite (s.g. = 2.711) and aragonite (s.g. = 2.83). Both talc and calcium carbonate exhibit thermal stability up to 800 °C. Talc is slightly soluble in dilute mineral acids while calcium carbonate reacts with acids to release carbon dioxide.

3.1.4 Other additives

Two catalysts were added to the resin formulation in this research, Norox Pulcat AWM and Norox TBPB. Norox Pulcat AWM is a proprietary peroxide solution designed for cure initiation of unsaturated polyester and vinyl ester resins in the pultrusion process (Table 3.4). Norox TBPB is a liquid consisting of pure tert.Butylperoxybenzoate and is used as a radical source in the polymerization of styrene and methacrylates (Table 3.5). Norox recommends the addition of Pulcat and TBPB to resin formulations at 1.5 and 1.0 phr, respectively.

TABLE 3.4: Norox Pulcat AWM properties

Property	**Value**
Active oxygen	8.7-9.0%
Specific gravity	1.0
Viscosity at 25 °C	14.5 mPa s
Flash point	60 °C
Appearance	Colourless liguid

TABLE 3.5: Norox TBPB properties

Property	**Value**
Active oxygen	8.16 w%
Specific gravity	1.04
Viscosity at 20 °C	8.0 mPa s
Flash point	60 °C
Appearance	Yellow liguid

Two mould release agents were added to the resin formulation in this research, Mold Wiz INT-PUL-24 and zinc stearate. Mold Wiz INT-PUL-24 is a process aid additive designed specifically for the pultrusion process and is a proprietary blend of organic fatty acids, esters and amine neutralising agents (Table 3.6). The manufacturer recommends the addition of Mold Wiz INT-PUL-24 at 1 phr.

Zinc stearate was provided by Amtrade New Zealand Ltd. and is a soft, white powder consisting of a metal soap that is used as a release agent and lubricant in industrial processes. Zinc stearate has a density of 1.095 g cm^{-3} and melts at 120-130 °C.

TABLE 3.6: Mold Wiz INT-PUL-24 properties

Property	Value
Specific gravity	0.962
Viscosity at 25 °C	100 −180mPas
Flash point	152 °C
Appearance	Colourless liguid

3.2 Preparation of uncured matrix resin

Uncured matrix resin was prepared using a standardised base component formulation (Table 3.7) with a base resin reference mass of 200 g.

Components were weighed using an AVERY TB-061 600 gram precision scale to within 0.1 g. Fillers were added to the resin formulation when required for experiments. All components were added to a mixing vessel and stirred for 5 minutes using an electrically powered stirrer and left to rest for 15 minutes prior to being added to the resin bath of the pultrusion machine. The zinc stearate powder and fillers were conditioned at 23 °C and 50 % relative humidity for a minimum of one week prior to use. Remaining components were used in the as-received condition.

TABLE 3.7: Components used in the neat resin.

Component	Weight (phr*)	Weight (%)
Plexinate P100 polyurethane resin	100 (base reference)	85.0
Plexinate P200 polyurethane resin	10	8.5
Norox Pulcat AWM catalyst	1.5	1.3
Norox TBPB catalyst	1.0	0.85
Zinc stearate powder (Amtrade New Zealand Ltd.)	5.0	4.2
Mold Wiz INT-PUL-24	0.5	0.42

* phr = parts per hundred resin

3.3 Production of pultruded composites

Two different pultrusion machines were used in the production of the glass fibre-polyurethane composites (GFRP). A full scale production machine was used for producing 12.7 mm diameter rods. A small-scale experimental pultrusion machine (GEC-EXP1) was used to produce 3.2 and 5.0 mm diameter rods and 15(w) x 3.5 (t)mm flat bars.

The die temperature was maintained at 150 °C, pull speed at 250 mm min^{-1} and resin bath temperature at 25 °C for all production runs. Table 3.8 gives the theoretical glass content of each composite manufactured for the study. The first and final two metres of each production batch were discarded, with the remaining product being cut to length for testing. The pultrusion machine was cleaned between production runs to avoid contamination. No post-curing was performed on the composites.

TABLE 3.8: Glass content of experimental composites.

Profile	**Number of rovings**	**Expected fibre volume (%)**
12.7 mm diameter rod, 4400 tex	35	47.8
12.7 mm diameter rod, 9600 tex	16	47.6
3.2 mm diameter rod, 4400 tex	3	64.5
5.0 mm diameter rod, 4400 tex	7	61.7
15(w) x 3.5 (t)mm flat bar, 4400 tex	20	65.9

3.4 Materials characterisation

All specimens were conditioned at the laboratory conditions for a minimum of 48 hours prior to testing. Tests were performed at a temperature of 23 °C and relative humidity of 50%. Displacement, time and load were recorded to a DAT file for later analysis using MICROSOFT EXCEL and MATLAB.

3.4.1 Dynamic mechanical analysis

Dynamic mechanical analysis (DMA) was carried out according to ASTM D7028 [19] using a TA Instruments Q800 Dynamic Mechanical Analyser. Two specimens from each batch were cut to a length of 40 mm. Each specimen was tested twice in order to detect changes in cure behaviour induced by using a different filler. Each test was run from 30 to 200 °C at a ramp rate of 5 °C min^{-1}. Testing was conducted in single cantilever mode using a span of 17.5 mm. The oscillation frequency was 1 Hz and the amplitude of oscillation was 20 µm with no pre-load on the sample.

Polymer composites are viscoelastic materials. In response to an applied force a viscoelastic material exhibits behaviour that is a mixture of a viscous liquid and an elastic solid

- having both a viscous (E'', loss modulus) and elastic (E', storage modulus) component. The ratio of the loss modulus to the storage modulus is defined as the loss tangent (Equation 3.1), giving a measure of damping capacity of a polymer.

$$\tan\delta = \frac{E''}{E'} \tag{3.1}$$

The glass transition (T_t) was determined using the maximum in the damping (i.e. peak in tan(δ)). The onset of the glass transition temperature (DMA T_g) was determined by finding the intersection of a line tangent to the storage modulus in the initial plateau region and a line tangent to the storage modulus midway between the upper and lower plateau regions.

3.4.2 Density measurements

Density measurements were performed in accordance with ASTM D792 [20] using a Metler Toledo XP105 equipped with a density testing kit (Figure A.1). Two replicates from each batch of composite material were tested. Distilled water at a temperature of 23 °C was used as the immersion fluid. The apparent mass of each sample was measured in air and recorded to the nearest 1 mg. The sample was then immersed in the vessel and all air bubbles were removed from the surface of the sample using a wire. The apparent mass of the immersed sample was then measured and recorded to the nearest 1 mg.

The density of the sample was calculated using Equation 3.2,

$$\rho = D \times \frac{a}{a-b} \tag{3.2}$$

where ρ is the density of the sample in kg m^{-3}, D is the density of water from Table 3.9, a is the apparent mass of the sample in air in g and b is the apparent mass of the sample when immersed in the vessel in g.

TABLE 3.9: Standard water density, from ASTM D792 - 13

°C	ρ=/kg m^{-3}									
	0.0	0.1	0.2	0.3	0.4	0.5	0.6	0.7	0.8	0.9
21	997.9948	9731	9513	9294	9073	8852	8630	8406	8182	7957
22	997.7730	7503	7275	7045	6815	6584	6351	6118	5883	5648
23	997.5412	5174	4936	4697	4456	4215	3973	3730	3485	3240
24	997.2994	2747	2499	2250	2000	1749	1497	1244	0990	0735
25	997.0480	0223	9965[B]	9707[B]	9447[B]	9186[B]	8925[B]	8663[B]	8399[B]	8135[B]

[A]Obtained from *CRC Handbook of Chemistry and Physics*, 78th edition, 1997-1998.
[B]The leading figure decreases by 1.

3.4.3 Tensile testing

The pultruded rods were tensile tested in accordance with ASTM D3916. Tensile testing clamp fixtures were designed in CAD to exceed the requirements set out in ASTM D3916 for the 3.2 and 12.7 mm diameter rods (Figure A.2). The clamps were fabricated from mild steel and aluminium alloy (6061) for the 3.2 and 12.7 mm diameter rods, respectively (Figure A.3). Aluminium alloy was found to be not durable enough for the quantity of tests which were to be performed as part of this experiment.

The clamps were designed so as to exceed the minimum required clamping length by fully utilising the clamping area the MTS 810's hydraulic clamps. The compressive stress imparted on the rod during clamping was minimised using the above approach, allowing for accurate and consistent measurements of tensile strength for each rod type.

An MTS 810 load frame equipped with a 100 kN load cell was used for tensile tests on the 3.2 mm diameter rods and a Satec heavy duty tensile-compression testing rig with a 1 MN load cell was used for tensile tests on the 12.7 mm diameter rods.

Specimen lengths for the 3.2 and 12.7 mm diameter rods were 500 and 950 mm, respectively. Large specimen lengths were required, to ensure a relatively constant stress throughout the gauge length and minimise the effects of potential concentric and angular misalignment of the specimen. Concentric and angular misalignment was minimised by using alignment jigs when installing the clamp fixtures on the MTS 810 and Satec machines.

Five specimens were selected at random from each batch of composite and their average diameter was determined using a set of digital callipers based on 5 measurements. Rods were set up for testing using a clamping pressure of 10 MPa.

The cross-head displacement rate was set to a constant 5.0 mm min^{-1} until failure occurred. The failure mode, location and duration was recorded. The test result was discarded if a specimen failed within the clamps or at a flaw.

The tensile strength of each sample was calculated using Equation 3.3,

$$\sigma_t = \frac{4P}{\pi D^2} \tag{3.3}$$

where σ_t is the tensile strength in MPa, P is the load in kN and D is the diameter of the rod in mm.

3.4.4 3-Point flexural testing

Rectangular specimens with nominal dimensions of 15(w) x 3.5 (t)mm and an edge fillet radius of 0.2 mm were produced for each type of filler and content using a die with rectangular profile. 3-point flexural testing was carried out in accordance with ASTM D790 using an MTS 810 load frame equipped with a 100 kN load cell (Figure 3.1). The span to thickness ratio was 16:1 and the support and loading nose diameter was 10 mm.

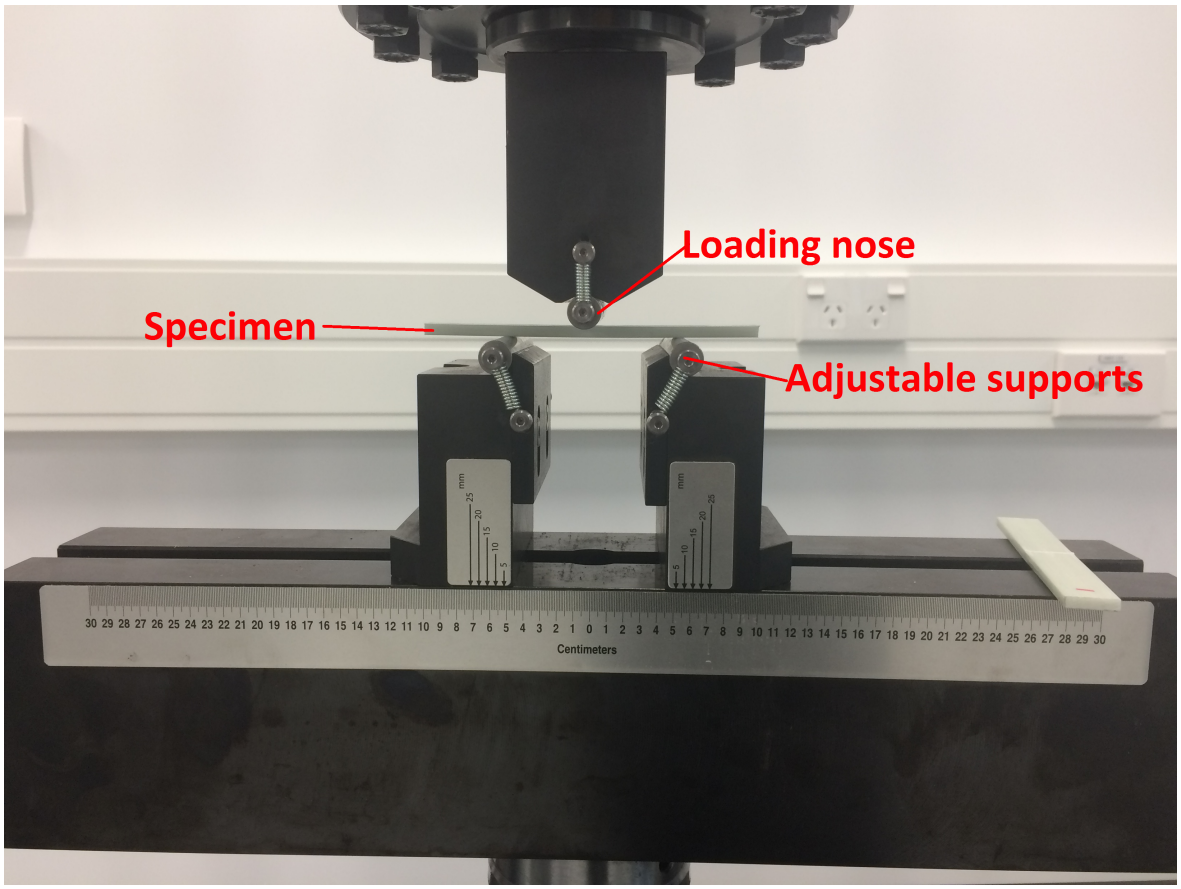

FIGURE 3.1: 3-point flexural test performed to ASTM D790 on a 15 x 3.5 mm rectangular pultruded bar.

Five samples were selected at random from each batch and their dimensions were measured at five points along their length. The cross-head displacement rate (1.49 mm min^{-1}) was calculated using Equation 3.4,

$$R = \frac{ZL^2}{6d} \tag{3.4}$$

where R is the displacement rate in mm min^{-1}, Z is the strain rate of the outer fibre in mm mm^{-1} min^{-1} (0.01) and d is the depth of the section in mm. The failure load was defined as the peak load obtained during the test.

The flexural strength of each sample was calculated using Equation 3.5,

$$\sigma_f = \frac{3PL}{2bd^2} \tag{3.5}$$

where σ_f is the flexural strength in MPa, P is the load in N, L is the span in mm, b is the width of the section in mm and d is the depth of the section in mm.

The failure strain of each sample was calculated using Equation 3.6,

$$\epsilon_f = \frac{6Dd}{L^2} \tag{3.6}$$

where ϵ_f is the flexural strain in $\mathrm{mm\,mm^{-1}}$, D is the maximum deflection in mm, L is the span in mm and d is the depth of the section in mm.

The flexural chord modulus was calculated using Equation 3.7,

$$E_f = \frac{\sigma_{f2} - \sigma_{f1}}{\epsilon_{f2} - \epsilon_{f1}} \tag{3.7}$$

where E_f is the flexural chord modulus in MPa, σ_{f2} and σ_{f1} are the stresses at predefined points and ϵ_{f2} and ϵ_{f1} are the strains at the predefined points. Due to the linear response of the materials, σ_{f1} and ϵ_{f1} were taken to be zero while σ_{f2} and ϵ_{f2} were taken to be the failure stress and failure strain, respectively.

3.4.5 Short beam testing

Rectangular specimens with nominal dimensions of 15(w) x 3.5 (t)mm and an edge fillet radius of 0.2 mm were produced for each type of filler and content. Short beam testing was carried out in accordance with ASTM D2344 [21] to determine the short beam strength. Special short beam loading fixtures were designed with CAD and fabricated from 4340 steel (60 HRC) to meet the requirements of ASTM D2344(Figure A.4).

Ten samples were selected at random from each batch and dimensions were measured at five points to obtain average dimensions.

Figure 3.2 shows a short beam loading test with a larger (13 mm) diameter loading nose compared to the ASTM standard. The larger loading nose was used to minimise localised compressive failure as was reported by Boukhili *et al.* [12]. The cross-head displacement rate was $1.0\,\mathrm{mm\,min^{-1}}$. Constant displacement rate loading was performed on the samples, with

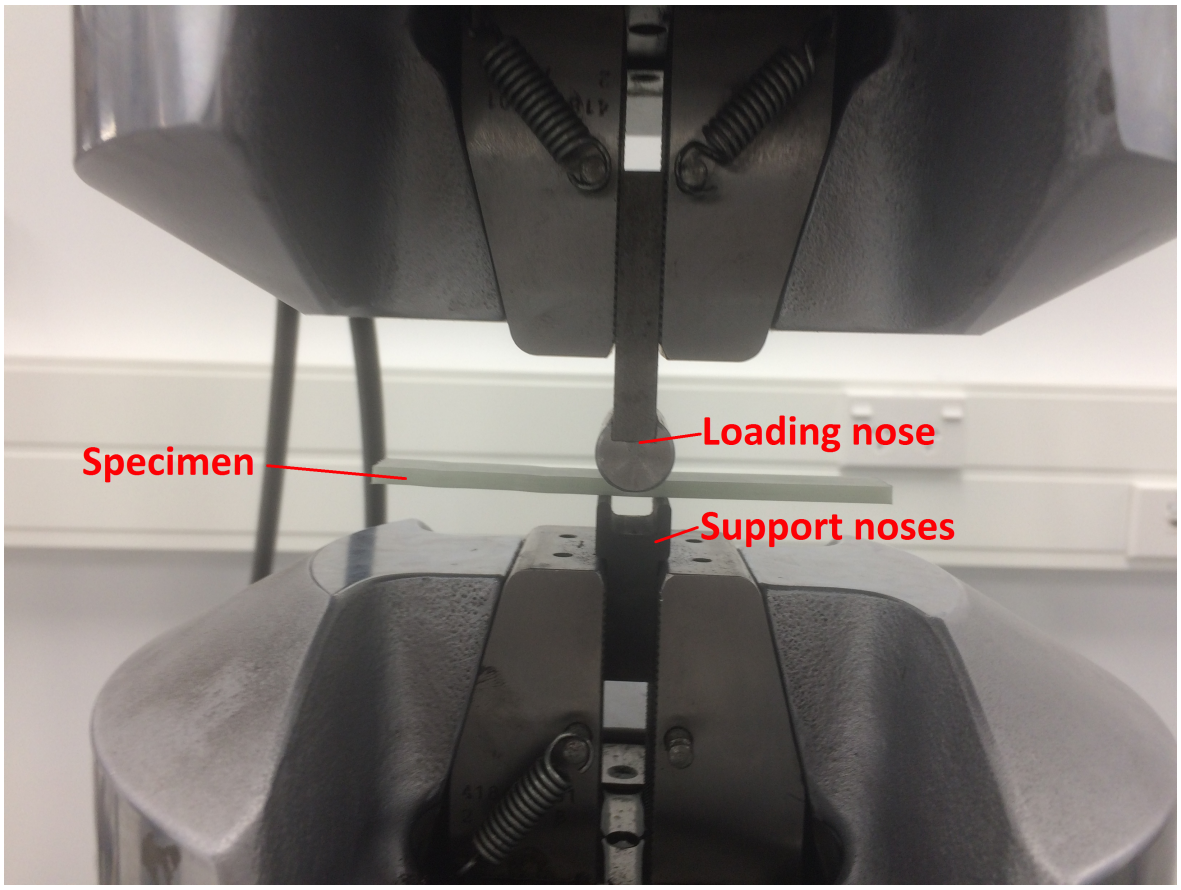

FIGURE 3.2: Short beam loading test with larger diameter loading nose to reduce likelihood of localised compressive failure.

an initial displacement of 0.25 mm above the sample and a final displacement of 1.00 mm as all specimens failed between 0.5 and 1.0 mm displacement. The failure load for each sample was defined as the peak load obtained during the test.

The short beam strength of each sample was calculated using Equation 3.8,

$$S = \frac{0.75P}{b \times h} \tag{3.8}$$

where S is the short beam strength in MPa, P is the load in kN, b is the width of the section in mm and h is the thickness of the section in mm.

Chapter 4

Development of a lab-scale pultrusion machine

4.1 Introduction

Fluctuations in the ambient temperature affects the performance of the pultrusion process [7]. Industrial settings often do not incorporate precise climate control systems for pultrusion. The daily range in temperature in Christchurch is approximately 10 °C, with a seasonal variation of approximately 12 °C (Table 4.1) [22]. A temperature increase of 10 °C results in a decrease of resin viscosity of up to 400 mPa s, significantly affecting fibre wet-out in pultruded composites [7]. Resin bath temperature control was developed as a part of this research in order to maintain a suitable constant resin viscosity to account for daily and seasonal variations in temperature. An experimental scale pultrusion machine (GEC-EXP1), was developed in conjunction with the resin bath temperature control system.

TABLE 4.1: Climate data for Christchurch, New Zealand

Month	Jan	Feb	Mar	Apr	May	Jun	Jul	Aug	Sep	Oct	Nov	Dec
Average high °C	22.4	21.9	20.0	17.3	14.2	11.4	10.7	12.2	14.6	16.9	19.0	20.9
Daily mean °C	17.1	16.8	15.0	12.1	9.0	6.2	5.7	7.1	9.3	11.5	13.6	15.7
Average low °C	11.8	11.6	9.9	6.8	3.8	1.1	0.7	2.0	4.0	6.1	8.1	10.6

The GEC-EXP1 pultrusion machine is a small scale, instrumented experimental pultrusion machine specifically designed for rapid experimentation with varying resin systems with small cross-section profiles. Pultrusion rates of up to 600 mm min^{-1} were possible, while die lengths of up to 600 mm are accommodated with a maximum heater power of

2000 W being provided to a single zone heater array. Profiles with cross-sectional areas of up to 50 mm^2 were pultruded with the machine. The resin temperature is controlled through a double walled resin bath with a heat transfer fluid composed of automotive coolant and a 2000 W heating element with forced circulation. Figure 4.1 shows a CAD rendering of the double walled resin bath.

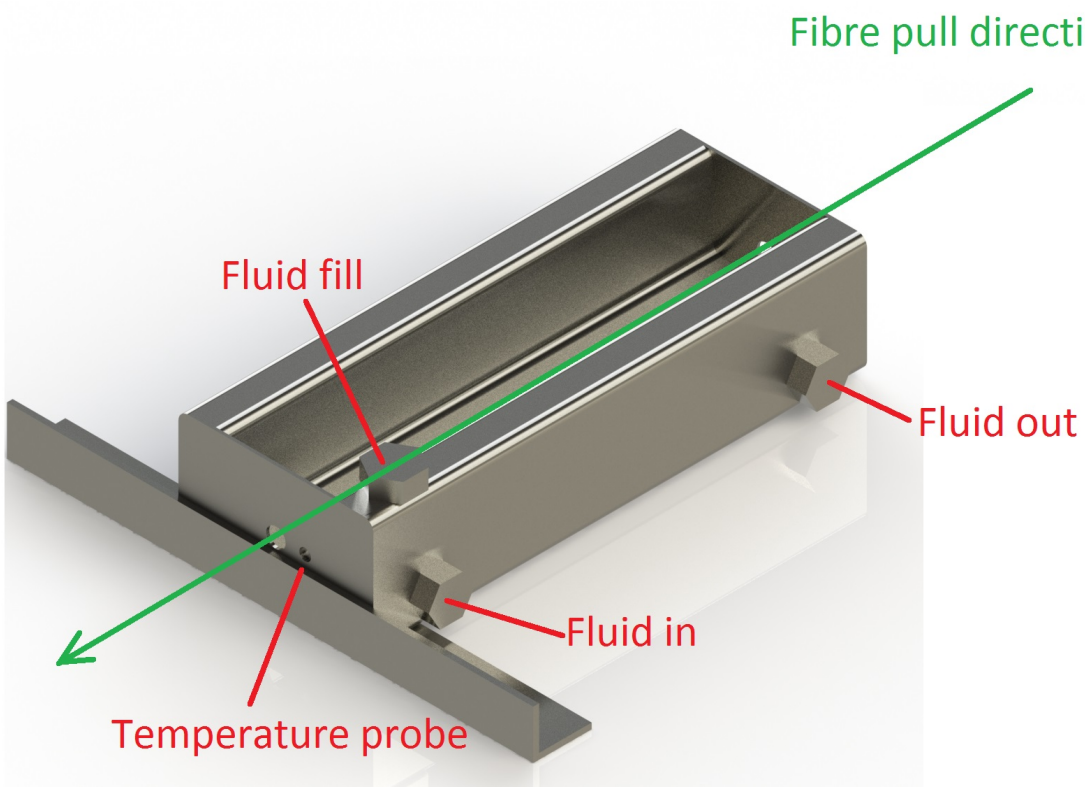

FIGURE 4.1: CAD rendering of the double walled resin bath.

The GEC-EXP1 pultrusion machine is fully programmable, using an ATmega328 micro controller. The ATmega328 controller board has four noise reduced 5 V analogue inputs and one noise reduced amplified analogue input. In terms of outputs, the controller board operates three solid state relay AC switches and two (diode protected) MOSFET DC switches, giving a total of 5 outputs (Figure 4.2). The GEC-EXP1 pultrusion machine is pictured during early trials, producing 3.2 mm diameter rods in Figure 4.3.

The controller board for the GEC-EXP1 is designed in such a way that it can be used in conjunction with a large scale production pultrusion machine. The controller board is only used for resin bath temperature control and die temperature monitoring duties when used with a large scale machine.

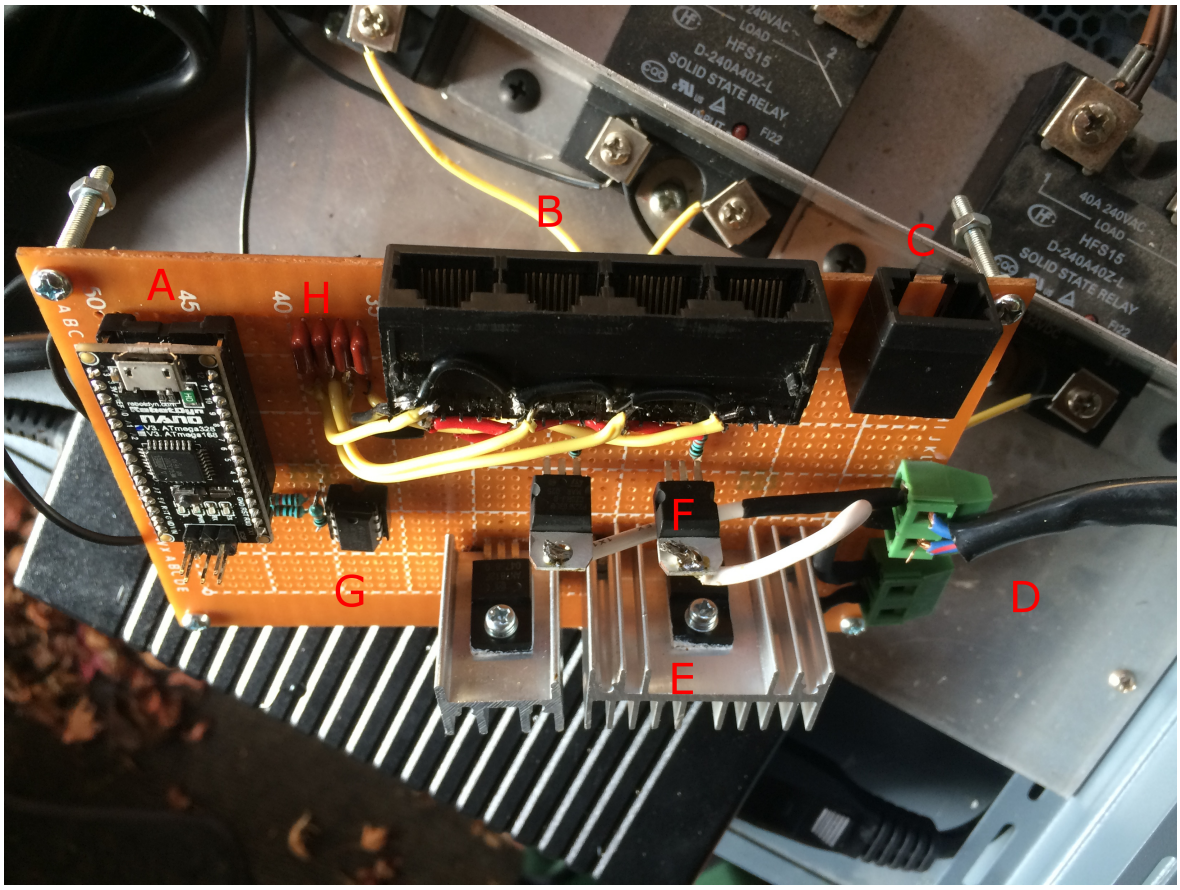

FIGURE 4.2: Control board for the GEC-EXP1 pultrusion machine. A: Microcontroller, B: Analogue inputs, C: Amplified analogue input, D: High current digital outputs, E: Voltage regulators, F: MOSFETs for switching high current outputs, G: Operational amplifier, H: Noise reduction capacitors

4.2 Systems

4.2.1 Instrumentation

Instrumentation on the GEC-EXP1 machine is provided by temperature sensors located within the die, resin bath and heat transfer fluid. The temperature sensors are connected to an ATmega328 micro controller using capacitive noise-reduced input channels. The ATmega328 micro controller has 10-bit analogue-to-digital (ADC) conversion, giving a temperature resolution of 0.5 °C for the temperature probes located within the resin bath and heater fluid (LM35 precision centigrade temperature sensor). The temperature of the die is measured using a K-type thermocouple.

The signal from the thermocouple is amplified using a noise-reduced op-amp circuit and cold junction compensation is provided by a reference LM35 temperature sensor. The temperature resolution of the die is 1.0 °C.

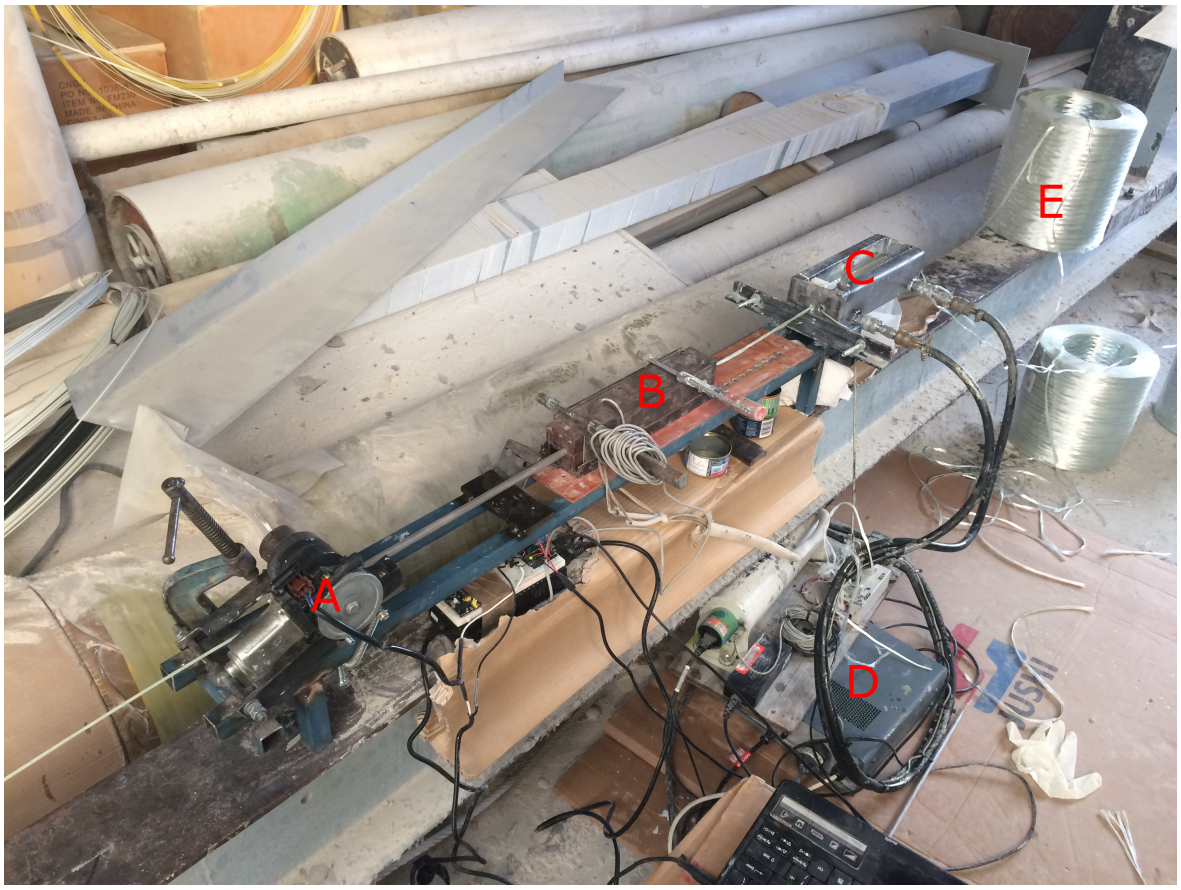

FIGURE 4.3: GEC-EXP1 pultrusion machine. A: Pulling mechanism, B: Heated Die, C: Heated resin bath, D: Controller, E: Roving supply

Software was written using GNU OCTAVE to monitor and log temperature and state data through serial communication with the GEC-EXP1 controller. Data is stored in a CSV text file and can be analysed in MICROSOFT EXCEL and MATLAB to allow for determination of optimal control parameters for various resin bath configurations.

Figure 4.4 shows the data logging software operating on a laptop at the factory. The data logging software produces a real time display of heater temperature, resin bath temperature, heater power and die temperature.

4.2.2 Temperature control

A low pressure inductive pump from automotive applications is used to pump the heat transfer fluid (distilled water mixed with 50 vol% ethylene glycol automotive coolant). The coolant is primarily used for its corrosion inhibiting properties. The heater consists of a cylindrical tank with a 2.0 kW resistive electrical heating element. There are guide plates

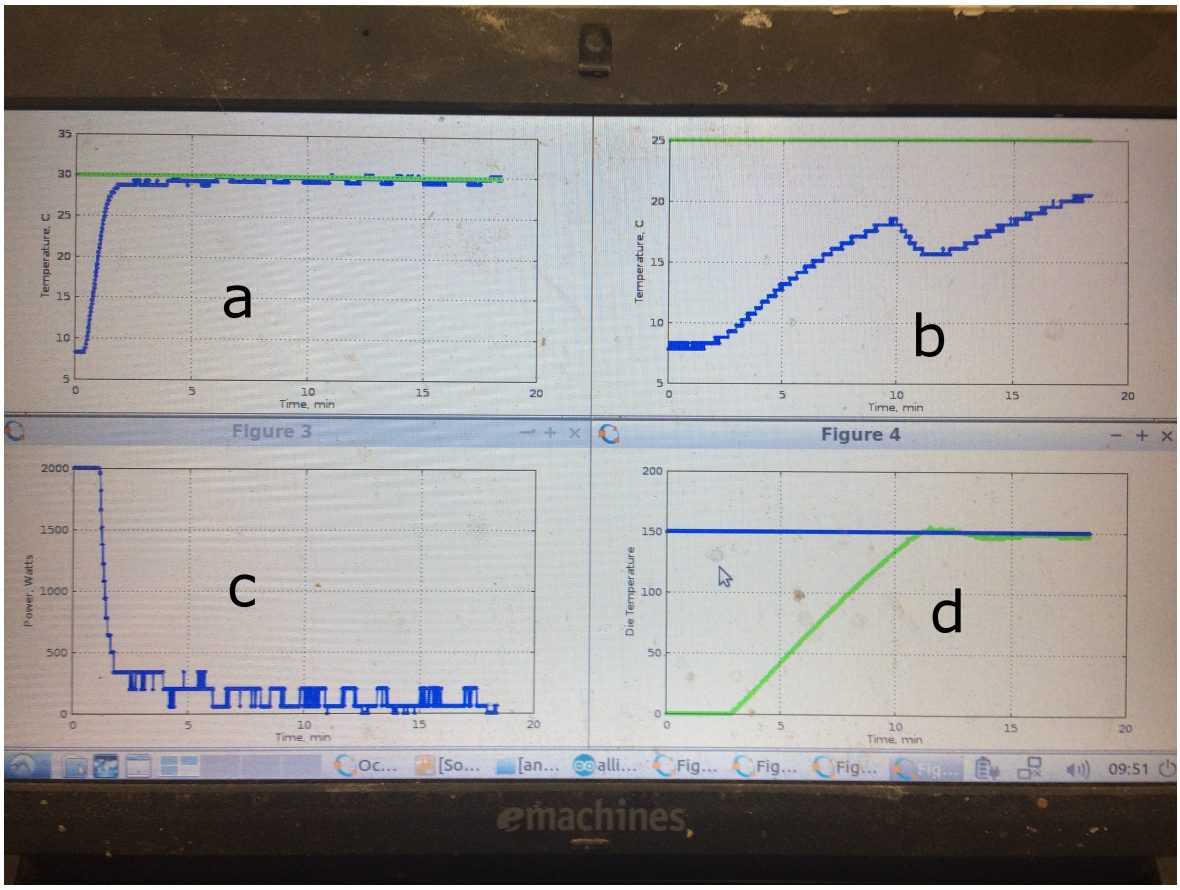

FIGURE 4.4: Data logging software for the GEC-EXP1 pultrusion machine, operating in GNU OCTAVE. Datalogging software plots heater temperature (a), resin bath temperature (b), heater power (c) and die temperature (d) in real time.

within the tank to encourage circulation of the fluid and minimise stagnation around the heating element.

4.2.3 Traction system

Tractive effort is provided by a 12 V DC worm drive motor. The motor is coupled to a shaft with a rubber roller. There is a second rubber roller on an idler shaft below the driven roller. Motor speed is controlled using (pulse width modulation) PWM - high (31 250 Hz) and low frequency (1 Hz). The motor operates in open loop speed control and as such the speed must be manually adjusted for each profile and resin formulation.

4.3 Simulation

A numerical model was developed using GNU OCTAVE to simulate the thermal performance of the resin temperature control system. The purpose of this model is two-fold: (i) aid the development of a robust control algorithm and (ii) development of the live data plotting application. Figure 4.5 shows a series of plots generated by the simulation of the RTCS control system, while Figure 4.6 shows the experimental validation of the simulated RTCS control system. The system deviated from theoretical predictions beyond the first transient period. The issue is not significant, since pultrusion machines are constantly consuming resin and thus the quantity of resin within the bath is in a state of flux, which is not accounted for within the model. For machine utilisation optimisation, anything beyond the first transient is not of concern as the main benefit of the RTCS is to allow for fast initial starting of the machine followed by generally constant operating conditions. Whether the RTCS begins its second heating cycle at 25 minutes or 28 minutes is of little concern to the behaviour of the pultrusion machine, as long as the temperature of the resin bath remains within tolerance.

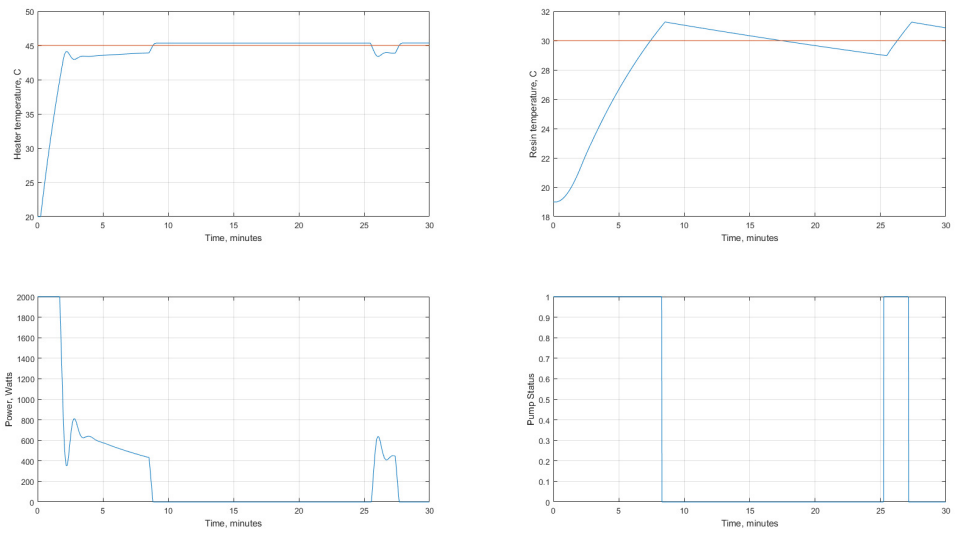

FIGURE 4.5: Simulation of the resin temperature control system performance. The simulation was used to tune control parameters of the system.

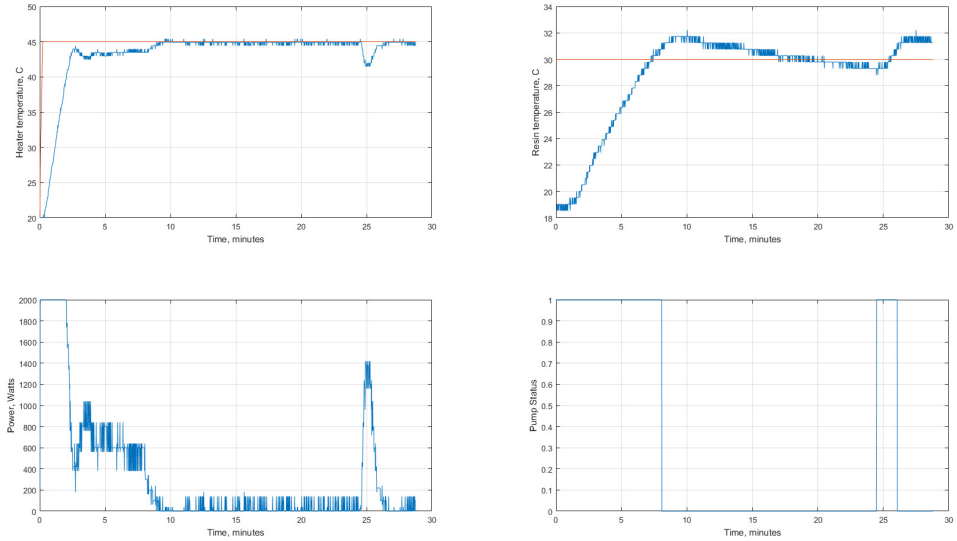

FIGURE 4.6: Experimental validation of simulated resin temperature control system performance.

4.4 Summary

A fully instrumented lab-scale pultrusion machine with closed loop resin temperature control was developed. The resin temperature control system allows for consistent performance of the pultrusion process and can be used to produce composites with minimal batch-to-batch variation caused by environmental effects, allowing for accurate determination of the effects that processing conditions and resin formulation have on pultruded composites. The remainder of the thesis covers the material characterisation of the composites produced with the lab-scale pultrusion machine and resin temperature control system.

Chapter 5

Characterisation of the particle size distribution of fillers

5.1 Introduction

The particle size distribution of various filler products was measured prior to experimentation on the mechanical properties of pultruded composites. The correlation between the filler particle sizes, processing robustness and mechanical properties of the final composites was then able to be analysed in later chapters.

5.2 Experimental methods

5.2.1 Materials

Three different talc filler products were analysed: Rebain DC325T-FIR, Liaoning DC325 and Liaoning DC325-995. Four different filler products of the Omyacal trade name which were used in the subsequent experiments were also analysed: Omyacal 1T, Omyacal 2, Omyacal 5, and Omyacal 10.

Rebain DC325T-FIR is described as a medium purity magnesium silicate with up to 50% impurities with a minimum of 98% of particles passing through a 325 mesh screen. Liaoning DC325 and DC325-995 are described as a fine white high quality natural magnesium silicate (Table 5.1) with a minimum of 98 and 99.5% of particles passing through a 325 mesh screen, respectively..

Omyacal 1T is described by the manufacturer as a high grade natural limestone, milled for fineness and surface treated to make it oleophilic and hydrophobic for ease of dispersion.

TABLE 5.1: Typical chemical analysis of Liaoning products [1]

Component	Weight (%)
SiO_2	min 55
MgO	min 30
CaO	max 3
Fe_2O_3	max 0.5
Al_2O_3	max 0.5

The remaining Omyacal products are described as high grade natural limestone, milled for fineness. Omyacal products primarily consist of calcium carbonate with small quantities of other minerals (Table 5.2).

TABLE 5.2: Typical chemical analysis of Omyacal products [2]

Component	Weight (%)
$CaCO_3$	98.0
$MgCO_3$	0.8
Fe_2O_3	0.1
HCl insoluble content	1.1

5.2.2 Particle size measurement

A micrometrics Saturn DigiSizer II High-Definition Particle Size Analyser was used to determine the particle size distributions of the fillers. The Saturn Digisizer II uses light scattering analysis to measure the particle size distributions of powdered samples with particle sizes ranging from 40 nm to 2.5 mm as an equivalent spherical diameter. All samples used for the measurement of the particle size distribution were taken in a representative manner from freshly opened 25 kg sacks. The contents of the bags were mixed thoroughly and a sample of approximately 100 mL of each filler type was taken to be analysed.

All samples used for particle size distribution analysis were taken in a representative manner from freshly opened 25 kg sacks. The contents of the bags were mixed thoroughly and a sample of approximately 100 mL of each filler type was taken to be analysed. Thus, the results of these tests are expected to be substantially fair and representative of the product.

5.3 Results and discussion

Table 5.3 gives the mean, median and advertised median particle diameters for each filler type.

TABLE 5.3: Average particle diameters of filler products.

Product	**Mean** (µm)	**Median** (µm)	**Advertised median** (µm)
Omyacal 1T	117	105	1.7
Omyacal 2	10.8	3.28	2.5
Omyacal 5	10.1	4.88	5.0
Omyacal 10	12.1	7.62	9.0
Rebain DC325T-FIR	18.7	15.2	N/A*
Liaoning DC325	18.4	12.8	N/A
Liaoning DC325-99.5	17.3	12	N/A

*N/A = not available

The particle size distribution of Omyacal 1T (median = 105 µm) was unexpected as the nominal median particle size was specified as 1.7 µm (Figure 5.1). The source of the above discrepancy is likely due to the partial agglomeration of individual micron-scale particles, leading to measured particle diameters on the order of hundreds of microns, evidenced by the presence of significant quantities of sub-0.1 µm particles not observed in the remaining products. The large median particle diameter for the Omyacal 1T filler was also observed in practice as a variance in texture when sifting through a quantity of the filler by hand. The mixing of Omyacal 1T with the resin was more difficult compared to that of other fillers as the particles tended to agglomerate.

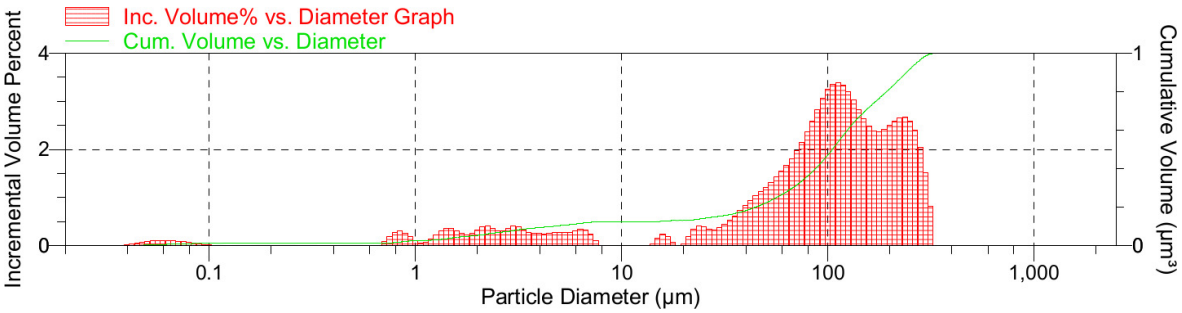

FIGURE 5.1: Particle size distribution of Omyacal 1T.

The implication of the results for particle size distribution analysis for Omyacal 1T indicate that significant stress concentrations are likely to be introduced to the microstructure of a pultruded composite manufactured using Omyacal 1T as a filler. Stress concentrations occur as a result of fibre crimping where large agglomerates of particles are forced to be packed into the spaces between fibres. The mean diameter of each glass fibre is approximately 23 µm for the Jushi direct rovings which were used for these experiments. Thus, if assuming an ideal fibre packing arrangement the maximum particle size is 3.6 µm. Thus,

the volume percentage of unidirectional glass reinforcement within a pultruded composite is expected to decrease in order to accommodate the observed median particle size of 105 µm, that also results in increased pulling force. The above effects on glass packing and pulling force were observed during the production of pultruded composites. However the agglomerations of Omyacal 1T particles appeared to break down at high filler contents, resulting in only moderate increases in the pulling forces and cross-sectional dimensions.

Particle size distributions for the other Omyacal filler types were as expected (Figure 5.2, Figure 5.3, Figure 5.4), with median particle diameters being within 2-3 µm of the specified particle diameters. Omyacal 10 was predicted to suffer from fibre crimping and lower fibre volume fraction due to having a median particle size of 7.62 µm. Consequently, a significant increase in pulling force (increased by a factor of 10) was measured during pultrusion with a high filler (Omyacal 10) content, accompanied by a significant increase in sample cross-sectional area (increased by 1.8%).

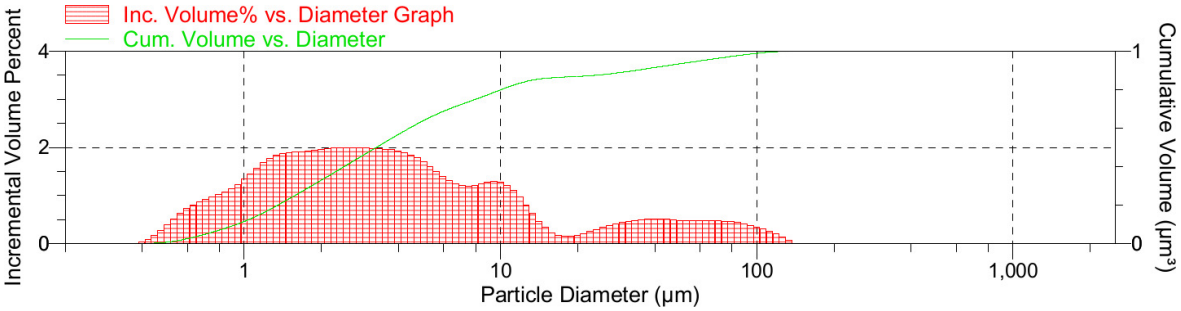

FIGURE 5.2: Particle size distribution of Omyacal 2.

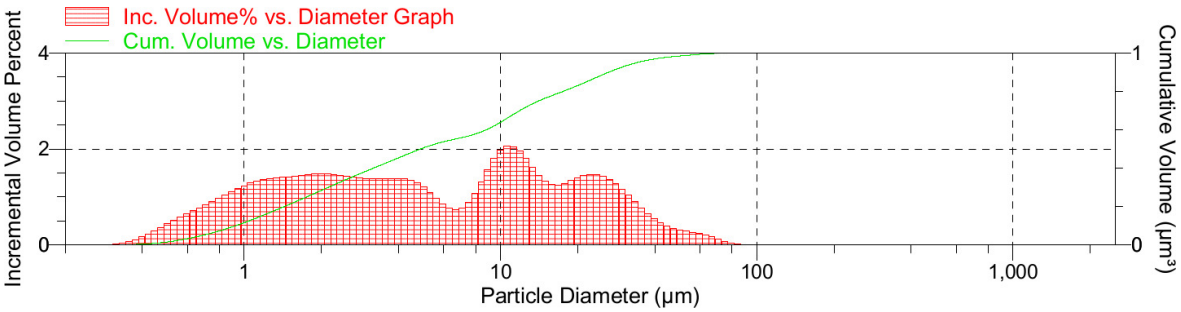

FIGURE 5.3: Particle size distribution of Omyacal 5.

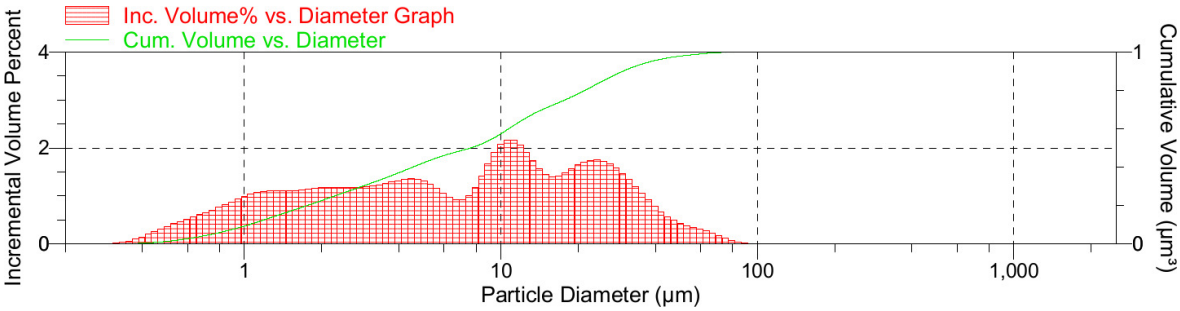

FIGURE 5.4: Particle size distribution of Omyacal 10.

The similarities in peak shapes and locations for incremental volume percentage vs. particle diameter between Omyacal 10 and Omyacal 5 indicate that Omyacal 5 may actually be a blend of Omyacal 10 and another product, such as Omyacal 2. Thus, similar crimping issues as experienced with Omyacal 10 at high filler content could be expected using Omyacal 5 as a filler.

All three of talc fillers were observed to have similar median particle diameters, with Rebain DC325T-FIR exhibiting the largest median diameter of 15.2 µm (Figure 5.5, Figure 5.6, Figure 5.7). The large particle diameters suggests significant issues with fibre crimping at high filler content.

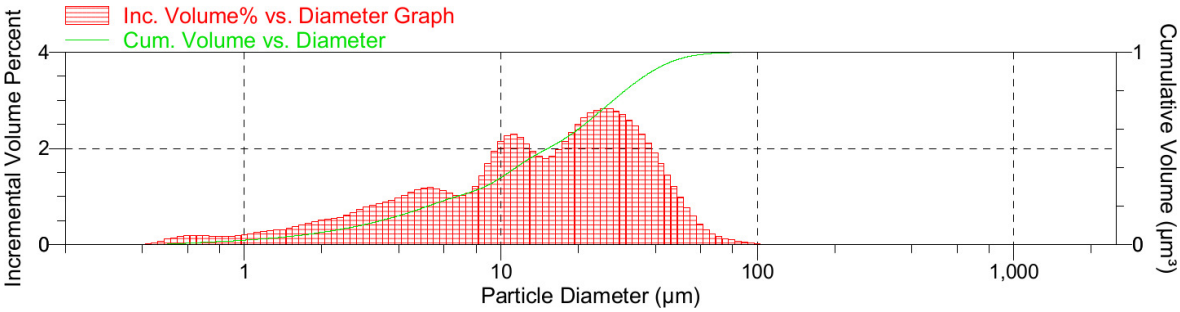

FIGURE 5.5: Particle size distribution of Rebain DC325T-FIR talc.

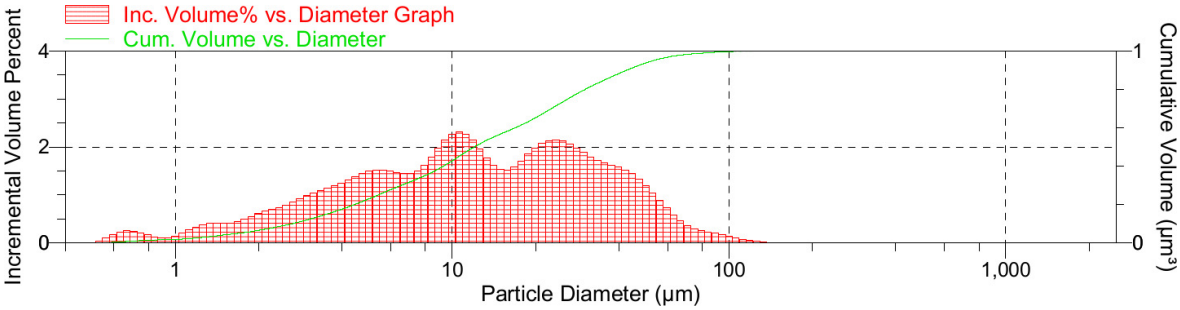

FIGURE 5.6: Particle size distribution of Liaoning DC325 talc.

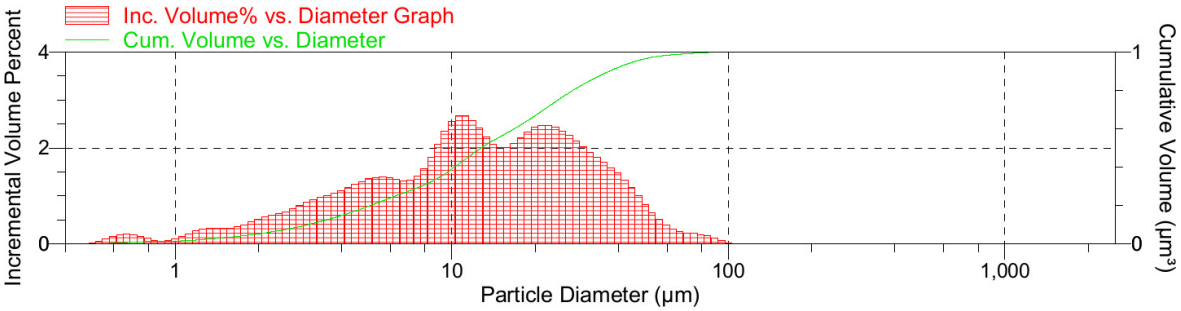

FIGURE 5.7: Particle size distribution of Liaoning DC325-99.5 talc.

The mode particle diameter for Rebain DC325T-FIR was 25.1 µm, which is on the same order of magnitude as the diameter of the glass fibres and significantly larger than the mode particle diameters of both Liaoning DC325 (10.6 µm) and Liaoning DC325-99.5 (11.2 µm) fillers. The large mode particle diameter also suggests that Rebain DC325T-FIR may suffer from increased fibre crimping compared to that of the Liaoning products.

The incremental volume percentage vs. particle diameter graphs for both of the Liaoning products indicates that both products were from a similar batch of raw materials, with the Liaoning DC325-99.5 product exhibiting slightly less variation in particle diameter compared to the Liaoning DC325 product. The results were expected as the Liaoning DC325-99.5 product is a slightly more refined version of Liaoning DC325 - with a rating of 99.5% of the particles being able to pass through 325-mesh screening. The implication of the results is that the final properties of a pultruded composite manufactured using Liaoning DC325-99.5 filler should exhibit less variation than if manufactured using Liaoning DC325 filler.

5.4 Summary

The particle size distributions of filler products were measured, the talc fillers were found to have higher median particle diameters than the calcium carbonate fillers. However, Omyacal 1T exhibited agglomeration and had a median particle diameter of 105 µm. The median particle diameter is predicted to have an effect on the mechanical properties of pultruded composites, with larger particles being expected to reduce the tensile strength through the effects of fibre crimping.

Chapter 6

Effect of fillers on the tensile properties of pultruded composites

6.1 Introduction

The tensile properties of composite materials provide important information regarding their performance as a function of formulation and processing parameters. Unidirectional glass fibre reinforced pultruded composites exhibit linear elastic behaviour followed by brittle failure with no yield point [5]. Tensile tests do not impart significant secondary loading conditions such as shear, flexural or compressive loading on the specimens, giving relatively accurate representations of product properties that may be used for design purposes. Jilken *et al.* observed decreasing tensile strength with increasing mineral filler content in polypropylene composites [23]. Zaini *et al.* reported declining tensile properties with increasing filler content and improved tensile strengths with large filler particles in polypropylene/oil palm wood flour composites[24]. No studies have been reported regarding the effects of fillers on the tensile properties of pultruded composites.

6.2 Experimental methods

Both ASTM D3916 and D7205 are suitable methods for obtaining the tensile properties of pultruded composites. ASTM D3916 utilises clamps to grip the test specimens while ASTM D7205 specifies cast in place anchors. Cast in place anchors provide the benefit of not imparting compressive loading on the surface of the specimens, but they are expensive and time consuming to produce, making them unattractive for a full factorial experiment. Clamps as

specified by ASTM D3916 have the benefit of being reusable an indefinite number of times, reducing the cost of experimentation. However, the clamps produce a compressive load on the specimens that may induce local damage in the form of splitting resulting in inaccurate tensile strength values [25]. All tensile tests were performed in accordance with ASTM D3916, due to the large number of tests to be performed for this study.

An experiment was performed to determine the baseline tensile strength of products based on the resin formulation in Table 6.1 and to compare these results with competitive filler products (talc powders) and alternative filler products (calcium carbonate powders). Three talc powder fillers were used, Rebain DC325T-FIR, Liaoning DC325 and Liaoning DC325-99.5. Omyacal 10 was used as the alternative product in this experiment as the particle sizes of Omyacal 10 are comparable to those in the three talc powder fillers (Table 5.3).

TABLE 6.1: Baseline resin formulation.

Material	**Weight (phr)**	**Weight (percent)**
Plexinate P100 polyurethane resin	100 (base reference)	69.9 %
Plexinate P200 polyurethane resin	10	7.0 %
Norox Pulcat AWM catalyst	1.5	1.1 %
Norox TBPB catalyst	1.0	0.70 %
Zinc stearate powder (Amtrade New Zealand Ltd)	5.0	3.5 %
Mold Wiz INT-PUL-24	0.5	0.35 %
Rebain DC325T-FIR	25.0	17.5 %

Unpigmented 12.7 mm diameter pultruded rods were produced using Rebain DC325T-FIR filler at a content of 25 phr, in batches using 4400 tex rovings and 9600 tex rovings. These rods were then tested according to ASTM D3916 [26] to determine their tensile strength. Due to the higher resource and time requirements associated with testing larger diameter rods, further testing was carried out on smaller diameter rods (3.2 mm.

Unpigmented 3.2 mm diameter pultruded rods were produced for each type of filler and content. The rods were tested according to ASTM D3916 [26] to determine their tensile strength. Dynamic mechanical analysis (DMA) was also performed on one sample from each batch to observe the curing behaviour of each product.

Figure 6.1 shows a 12.7 mm diameter rod after being tensile tested according to ASTM D3916. The sample exhibited a complete non-localised failure across the entire testing span.

Such a failure indicates that the sample failure did not initiate within the clamps or at some fortuitous flaw within the testing span and as such the failure is considered to be purely tensile.

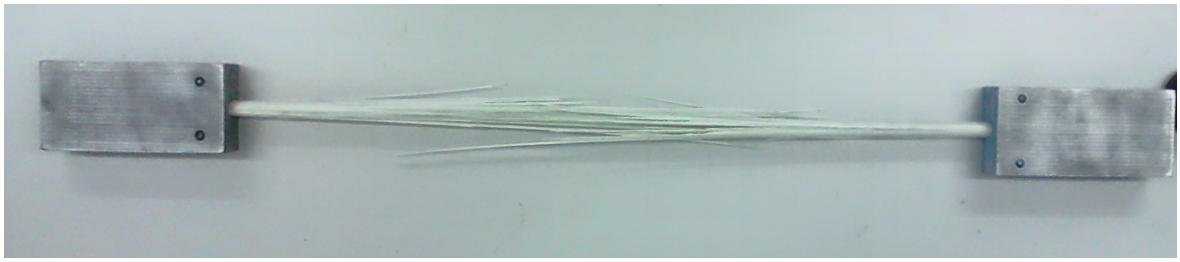

FIGURE 6.1: Photograph of typical tensile fracture of a 12.7 mm diameter rod.

6.3 Results and discussion

6.3.1 Effect of filler type on tensile properties of pultruded composites

The tensile strength of the 12.7 mm diameter rods was found to be approximately 500 $\pm$30MPa for products produced using 4400 tex rovings and 460 $\pm$25MPa for products produced using 9600 tex rovings (Figure 6.2). This represents a reduction in strength of between 8% and 10%. Other research indicates that for glass fibres of differing diameters there is no measured difference in tensile strength if the glass fibre production parameters are kept constant [27]. However, it is generally not possible to maintain the processing parameters in industrial settings between different types of glass rovings. Thus, differences in strength between glass rovings of differing fibre diameters is expected. Ramsteiner *et al.* reported similar decreases in strength with an increase in glass fibre diameter [28]. In contrast to work by Irfan *et al.*, increased pulling speed was found to decrease the tensile strength of the 12.7 mm diameter rods [3]. The resin component of the composite may not have achieved a full cure at higher pulling speeds, thus all further experiments were performed at a pulling speed of 250 mm to ensure full curing.

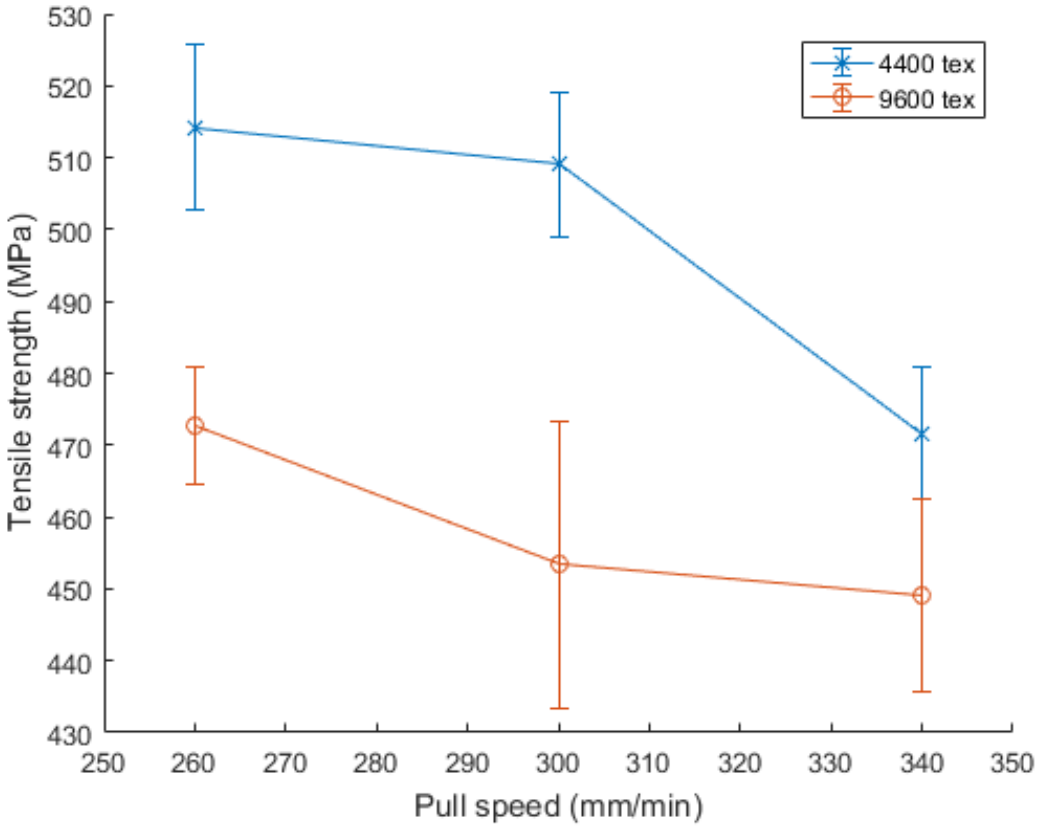

FIGURE 6.2: Tensile strength as a function of pultruion speed and roving tex 12.7 mm diameter rods with 25 phr of Rebain DC325T-FIR. Error bars represent 95% confidence interval.

The tensile strength of the 3.2 mm diameter rods filled with talc powder was low ($\approx$ 800 $\pm$60MPa), given that the tensile strength of Jushi E-Glass is given as 2513 MPa [29]. The theoretical maximum tensile strength is 1630 MPa given a fibre fraction of 65 vol%. In comparison, the tensile strength of the rods filled with Omyacal 10 was 1085 $\pm$18MPa (Figure 6.3), which is closer to the expected theoretical value. The theoretical values of strength are not achieved due to the detrimental effects of the fillers (Chapter 5) and damage associated with clamping the specimen during testing.

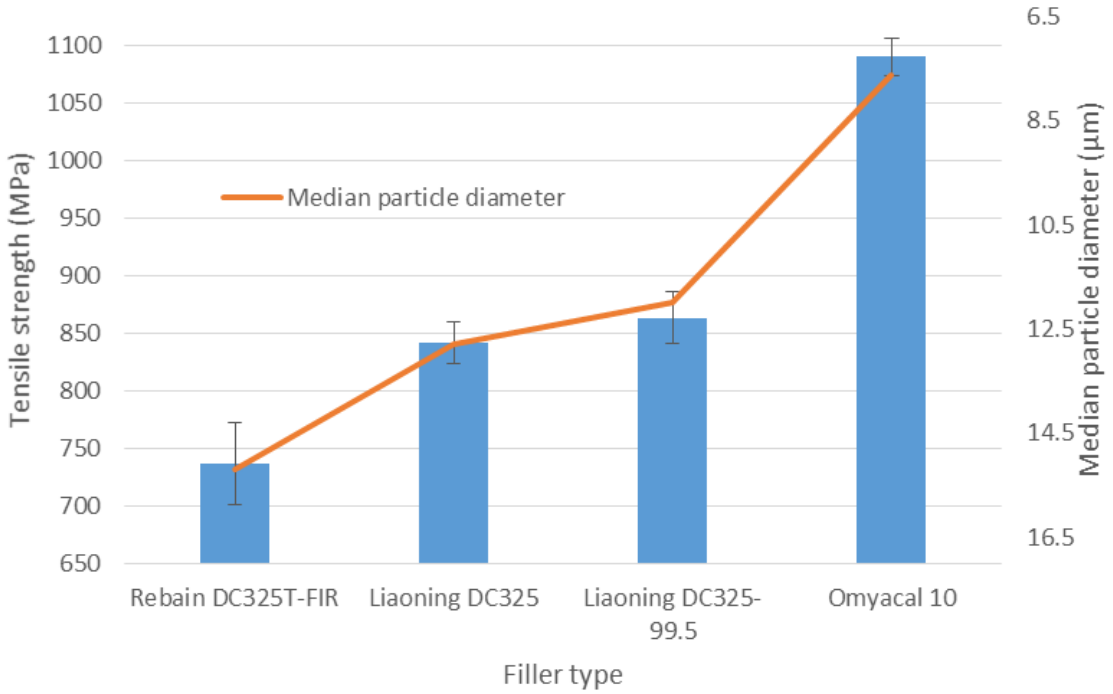

FIGURE 6.3: Tensile strength as a function of the filler type. Filler content is 25 phr. Error bars represent 95% confidence interval.

The tensile strength corresponded well with the median particle diameter for each filler. For example, Omyacal 10 has the smallest median particle diameter of the four fillers and exhibited the highest tensile strength, while Rebain DC325T-FIR with the largest median diameter, exhibited the lowest tensile strength. Both of the Liaoning fillers have similar a median diameter and tensile strength (842 ± 18MPa for Liaoning DC325 and 863 ± 23MPa for Liaoning DC325-99.5). An overlap of the 95% confidence intervals indicates that there is no significant difference in tensile strength between the materials. The higher grade product (Liaoning DC325-99.5) provides little benefit in terms of tensile strength.

Based on the above observations, it could be proposed that the tensile strength of a pultruded rod is inversely proportional to the median particle diameter of the filler for a given glass fibre fraction.

The level of contaminants and batch-to-batch variations may also contribute to variations in the tensile strength of composites containing Rebain DC325T-FIR. Rebain DC325T-FIR may be composed of up to 50% contaminants as the filler is mined from the edges of the mine site. Contaminants may include thermally unstable compounds, hygroscopic compounds and minerals that may damage the glass fibres under tensile loading conditions.

6.3.2 Effect of filler type on thermomechanical and curing behaviour

Dynamic mechanical analysis (DMA) provides an insight to differences in the thermal and curing behaviour of composites.

The extent of cross-linking in the resin may be studied by monitoring changes in the glass transition temperature (T_g). The DMA tests were initially run up to a temperature of 200 °C. The resin may undergo some post-curing during this initial run. The glass transition temperature of the thermoset matrix will increase with increasing degree of cure (Figure 6.4). The glass transition temperature is also affected by the presence of plasticisers or thermal decomposition of the resin matrix.

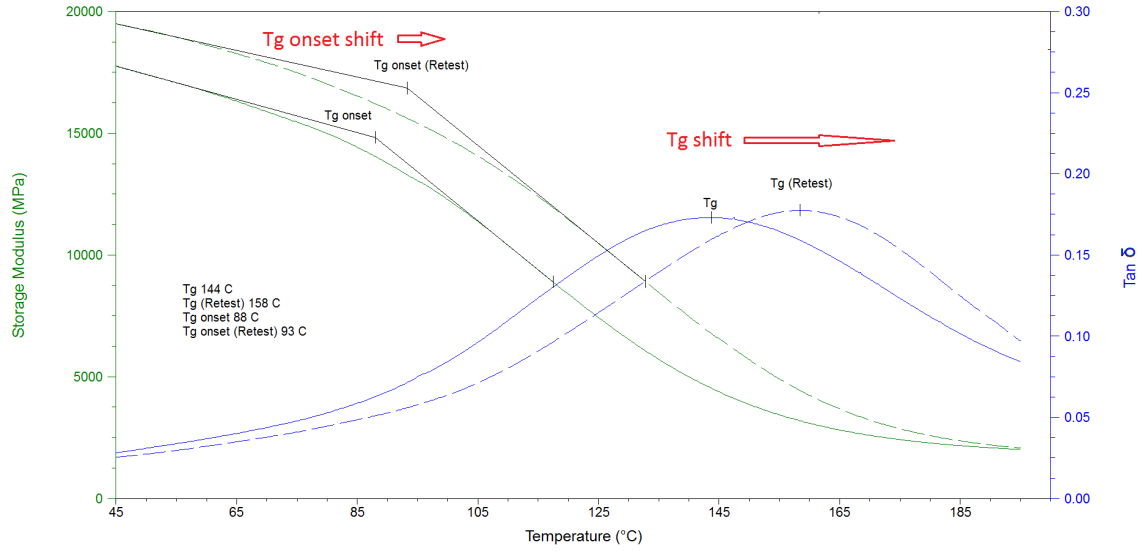

FIGURE 6.4: The storage modulus (E′) and tan(δ) of a 3.2 mm diameter rod as a function of temperature (Liaoning DC325 filler).

It was observed that for all composites tested the T_g increased when the specimen was retested in DMA, indicating an increase in the degree of cure between the initial run and the second run (Figure 6.5). The DMA results show that complete curing of the polyurethane did not occur during the pultrusion process. The pultruded composites filled with Rebain DC325T-FIR exhibited the smallest change in T_g ($\Delta T_g \approx 3\,°C$), indicating a high degree of cure during pultrusion.

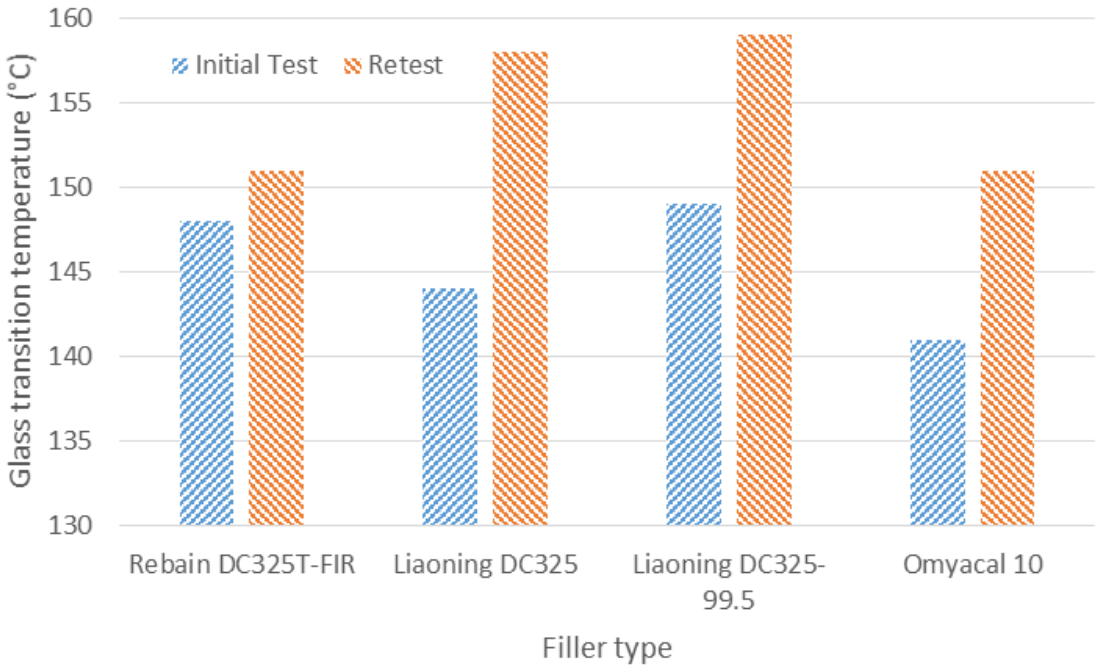

FIGURE 6.5: Changes in the glass transition temperature as a function of filler type.

The products manufactured with the Liaoning talc fillers exhibited different curing behaviour. The composites attained a similar final T_g upon retesting, with the composite filled with Liaoning DC325 having a glass transition temperature of 158 °C and the composite filled with Liaoning DC325-99.5 having a glass transition temperature of 159 °C. However, the initial test results indicated a difference in the degree of cure in the as-pultruded state. The Liaoning DC325 filled composite had an initial glass transition temperature of 144 °C, while that of the Liaoning DC325-99.5 filled composite was 149 °C. The above results indicate that the higher grade of filler results in a higher degree of cure during pultrusion. A higher T_g generally results in higher and more stable mechanical and thermal properties. Composites that are partially cured may be expected to change in properties due to curing post-manufacturing.

Composites filled with Omyacal 10 exhibited the lowest degree of cure based on an initial T_g of 141 °C. Retesting resulted in a T_g of 151 °C, which was comparable with the Rebain DC325T-FIR filled composite. A low initial T_g is indicative of a lower degree of curing during manufacturing. The Omyacal 10 filler is of high purity and thermal stability (up to 800 °C). Therefore, the effects of Omyacal 10 on the curing behaviour is likely to be dominated by the morphology of the filler.

All samples exhibited an increase in the onset of the T_g upon retesting in the DMA (Figure 6.6). The above results indicate that talc fillers generally provide enhanced curing during pultrusion, although the tensile properties are significantly impaired compared with $CaCO_3$ fillers. The calcium carbonate fillers appear to inhibit the degree of curing but result in an increase in tensile strength of $\approx$ 50% when compared to that of Rebain DC325T-FIR. Therefore, further experiments were carried out to compare the tensile and flexural properties of calcium carbonate filled composites as a function of filler content and particle size.

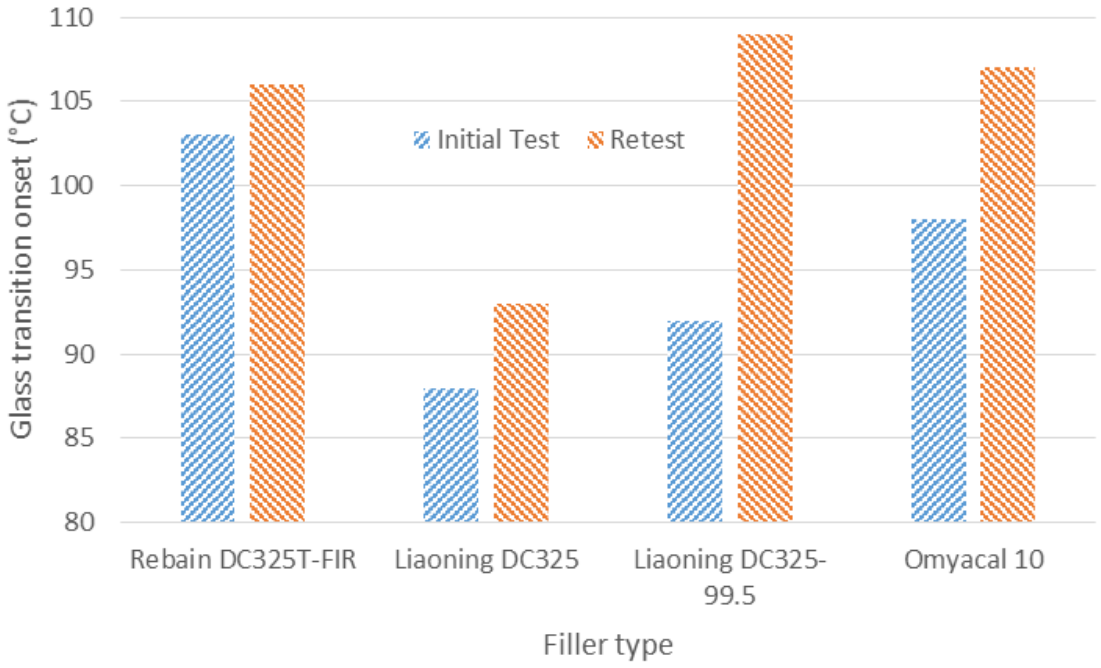

FIGURE 6.6: Glass transition onset temperature test results for products manufactured using competitive fillers

6.3.3 Effect of filler content and particle size on the tensile properties of $CaCO_3$ filled pultruded composites

A full factorial experiment was performed to determine the relationship between median filler particle size, filler content and tensile strength of pultruded composites containing calcium carbonate fillers. Batches of 3.2 mm diameter rods were manufactured using the GEC-EXP1 pultrusion machine. Three rovings of 4400 tex Jushi E-glass were used, giving a nominal glass content of 64.5 vol%.

Tensile failure was not localised within gauge length of the specimen (3.2 mm diameter

rod). The fracture behaviour suggests that the majority of the glass fibres failed simultaneously and that localised stress concentrations do not cause failure (Figure 6.7).

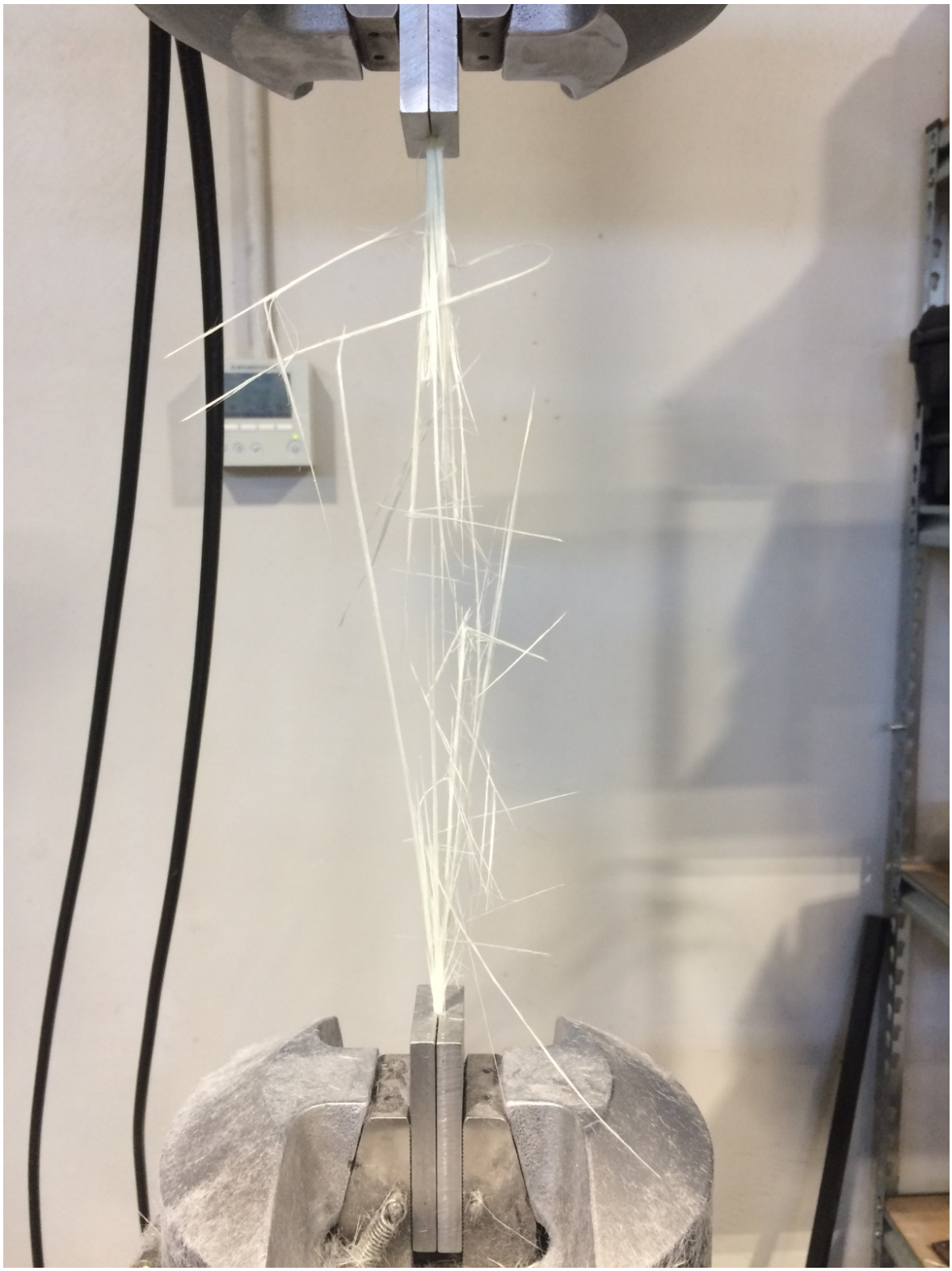

FIGURE 6.7: Photograph of tensile fracture of a 3.2 mm diameter rod (30 phr Omyacal 10).

The tensile strength of pultruded composites is not directly correlated to the type of filler per se, as hypothesised in Section 6.3.1. The tensile properties appear to be strongly influenced by the median particle diameter of the fillers, where an inverse linear relationship can be observed (Figure 6.8). A regression coefficient of $R^2 = 0.9873$, combined with non-biased scatter of data points indicates that a linear model provides a suitable fit to the data (Figure 6.8) in agreement with work on the effects of a spherical glass bead filler on the tensile strength of a cast thermosetting polyurethane resin (without fibre reinforcement) by Landon *et al.* [9].

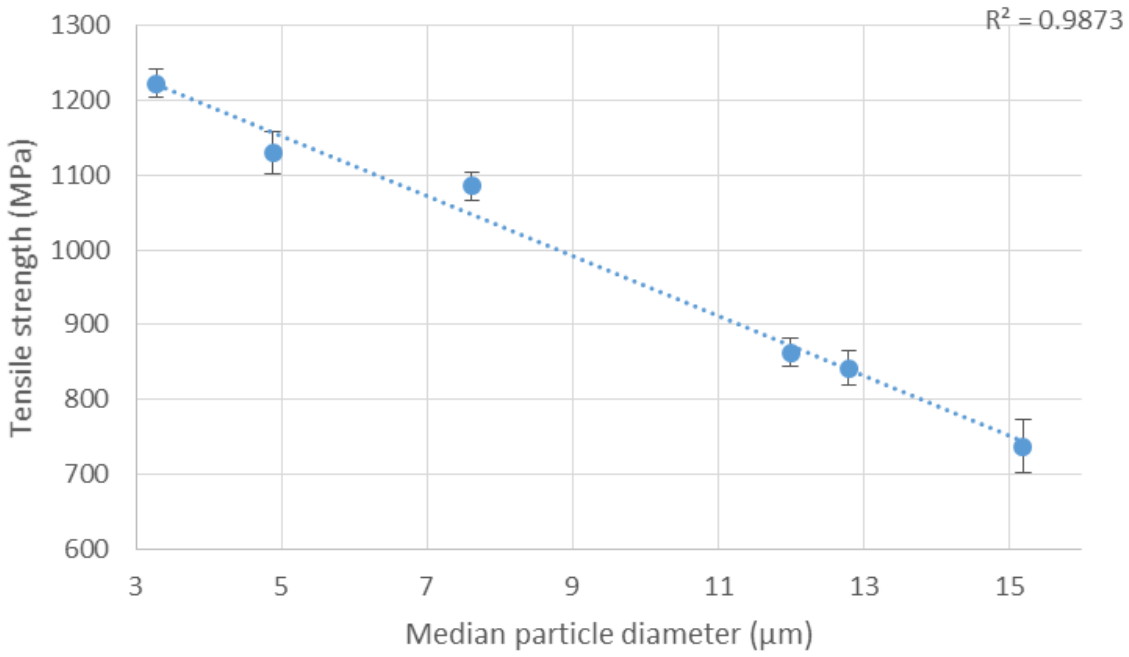

FIGURE 6.8: The tensile strength of 3.2 mm diameter rods as a function of the median particle diameter at a content of 25 phr, both talc and $CaCO_3$ fillers are represented. Error bars represent 95% confidence interval for strength.

The observed linear decrease in tensile strength as a function of median particle diameter is explained in terms of micro-crimping that occurs within the microstructure of the composite when the dimensions of the filler particles exceed the allowable spacing between the glass fibres (Figure 6.9). Equation 6.1 gives the shear stress within a glass fibre which is not oriented in a direction parallel to the loading of a composite,

$$\tau_{glass} = \sigma_x cos(\phi) sin(\phi) \tag{6.1}$$

where σ_x is the applied normal stress in the nominal axial direction of the part, and ϕ

is the angle of deviation for the fibre from the axial direction of the part. The angle ϕ is determined by the filler particle diameter and filler content. A larger filler particle will tend to increase the fibre spacing, while an increase in filler particles will tend to increase the number of micro-crimps throughout the composite.

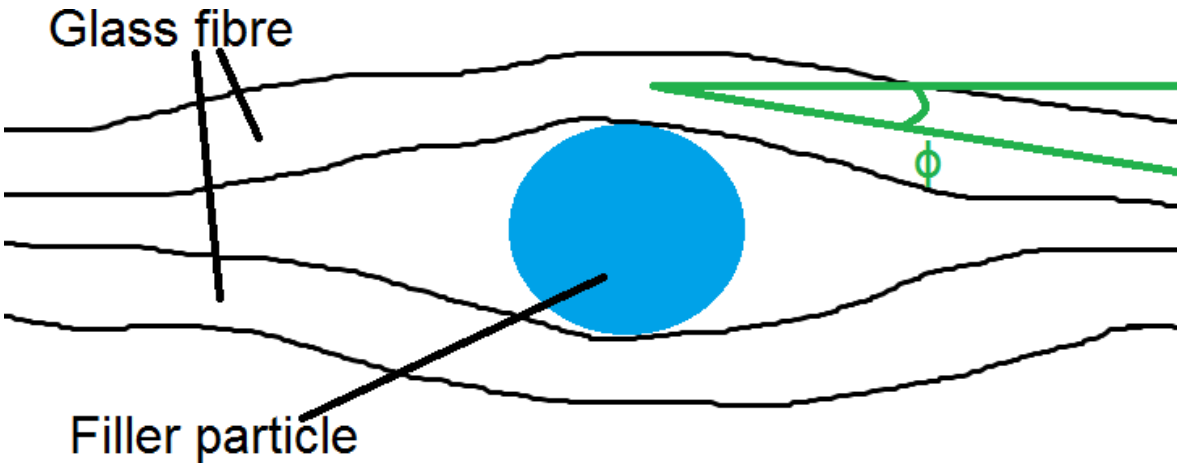

FIGURE 6.9: Schematic of micro-crimping behaviour in filled fibre reinforced composites.

Jushi gives the shear strength of individual glass fibres as 67 MPa which is approximately 3% of the tensile strength of the fibres. Therefore, it is expected that shear failure will occur for a fibre with a deviation of just four degrees from the nominal axial direction and a normal stress of 1000 MPa on the part. When fillers consisting of large particles are used, there is the potential for substantial micro-crimping throughout the part as the glass fibres must necessarily undergo localised displacement to accommodate the filler particles when the glass fraction is high.

A general downwards trend in tensile strength is observed for higher filler content across all filler types (Figure 6.10). However, the decrease in tensile strength is greatest with fillers having the largest median particle diameter. The samples produced with Omyacal 10, Omyacal 5 and Omyacal 2 experienced a reduction in tensile strength of approximately 190 MPa (15%), 170 MPa (12%) and 69 MPa (5.5%) respectively between a filler content of 5 and 30 phr. The samples produced with Omyacal 1T actually exhibited a net increase in tensile strength of 45 MPa between a filler content of 5 and 30 phr.

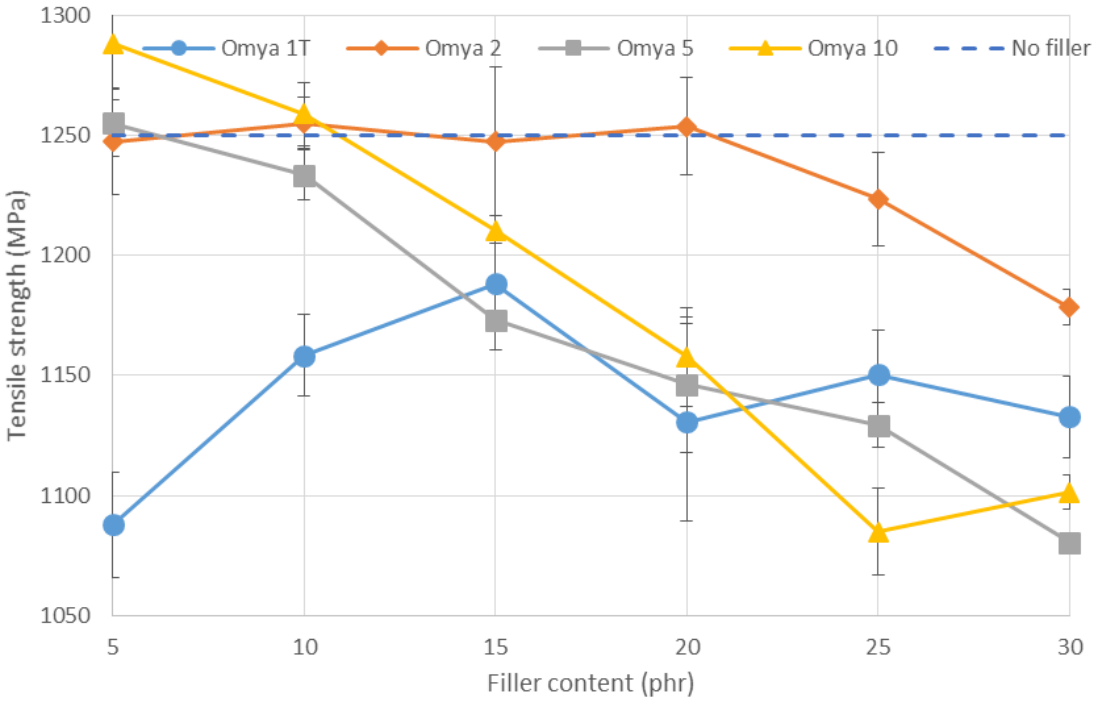

FIGURE 6.10: Tensile strength of 3.2 mm diameter rods using various Omyacal fillers between 5 phr and 30 phr content. Error bars represent 95% confidence interval for strength.

The tensile behaviour of Omyacal 1T filled composites is attributable to the filler particle size distribution and surface treatment of the particles. Omyacal 1T is difficult to mix into the Plexinate P100 resin due to the surface treatment of the particles, resulting in agglomeration of particles into relatively large but unstable clusters. As a result, the tensile data of the Omyacal 1T filled composites exhibits no distinct trend as a function of filler content.

At high filler content, the Omyacal 1T particles behave more like particles with a small median diameter (improved fibre packing is observed and strengths tend to be higher than with Omyacal 5 and Omyacal 10). The Omyacal 1T particles behave as large particles at low filler content, causing packing issues and reduced tensile strength.

The composites produced with Omyacal 2 generally provided the greatest tensile strength across the entire filler content range. As discussed in Section 5.2.2, the largest particle diameter that can be accommodated between the fibres for a hexagonal close packed glass structure with a fibre diameter of 23 µm is 3.6 µm. Although Omyacal 2 does contain particles with a larger diameter than this upper limit, the fibre fraction (65 vol%) of the composites results in only limited regions of hexagonal close packing. A fully hexagonal close packed microstructure requires a fibre fraction of approximately 90 vol%.

In reality, the microstructure is a mixture of hexagonal packing, square packing and random packing. The composite microstructure accommodates moderate quantities of large filler particles with a glass content of approximately 65 vol%. Hence, it is reasonable to expect the tensile strength is retained up to a filler content of 20 phr of Omyacal 2.

6.4 Summary

An inverse linear relationship was found between filler particle size and the tensile strength of pultruded composites, with the tensile strength decreasing from 1220 to 750 MPa between filler particle diameters of 3 and 15 µm at a content of 25 phr. Increased filler content results in a slight decrease in the strength of pultruded composites. The type of filler (talc or calcium carbonate) does not appear to affect the tensile strength of pultruded composites. It should be noted that small particle talc fillers were not studied in this research.

The tensile strength of a pultruded composite provides information regarding the interaction of particulate fillers and glass fibres but does not provide useful information regarding the performance of the matrix phase of the composite. Flexural tests may be used to characterise the effects of fillers on the matrix of a composite as flexural properties are more heavily influenced by the matrix properties.

Chapter 7

Effect of additives on the flexural properties of pultruded composites

7.1 Introduction

The design of structures using pultruded composites is often governed by service deflection limits that demand details of the flexural behaviour of the profiles. Flexural tests are faster and less complex to perform than tensile tests due to ease of alignment and specimen preparation, making them ideal for quality control purposes. Fillers have been shown to improve the flexural strength of pultruded composites when added at between 0 and 40 phr by Chen *et al.* [10]. However, Boukhili *et al.* found filler content had no effect on the flexural strength of pultruded composites [12] when added at between 0 and 40 phr.

7.2 Experimental methods

Flexural tests may be performed in either 3 point or 4 point loading, where 3 point loading consists of two supports and a single loading nose positioned midspan while four point loading consists of two supports and two loading noses positioned symmetrically about the midspan point. Thus, flexural testing imposes a combination of tensile, compressive and shear stresses on the specimen. For a unidirectional pultruded composite, properties can be assumed to be uniform throughout the thickness of the composite, resulting in a normal stress that varies linearly through the thickness. Maximum compressive stress occurs on the concave face at the loading nose while maximum tensile stress occurs on the convex face directly opposing the loading nose. With 3 point loading there are interlaminar shear

stresses throughout the entire span while with four point bending there are no interlaminar shear stresses present between the two loading noses such that only pure bending occurs in the central span. ASTM D790 provides standard test methods for determining the flexural properties of pultruded composites and specifies 3 point loading conditions. ASTM D790 is a commonly used standard in the pultrusion literature [30, 31, 32]

Energy dispersive X-ray spectroscopy (EDS) was used to detect zinc at the fracture surface of composites which exhibited unstable interlaminar shear failure during flexural tests. EDS is an analytical technique used for elemental analysis of a sample. The EDS technique detects X-rays emitted from the sample when it is bombarded by an electron beam. Each element produces a specific X-ray energy spectrum and thus elements may be differentiated through detection of characteristic energy peaks. Samples were prepared for EDS by coating the fracture surfaces with a thin layer carbon.

7.3 Results and discussion

The addition of fillers to pultruded composites influenced the flexural behaviour in a similar manner to the tensile properties. The flexural strength of filler-free composites was found to be 1320 ± 22MPa. All fillers have a similar effect on flexural strength of the pultruded composites. In general, the flexural strength was observed to decrease from approximately 1400 to 1275 MPa with filler contents of 5 and 30 phr, respectively (Figure 7.1). Similarly, the flexural strength is increased at low filler content, indicating that voids are reduced in the composites compared to that of unfilled composites. These results are in line with previous observations of polyester pultruded composites [12].

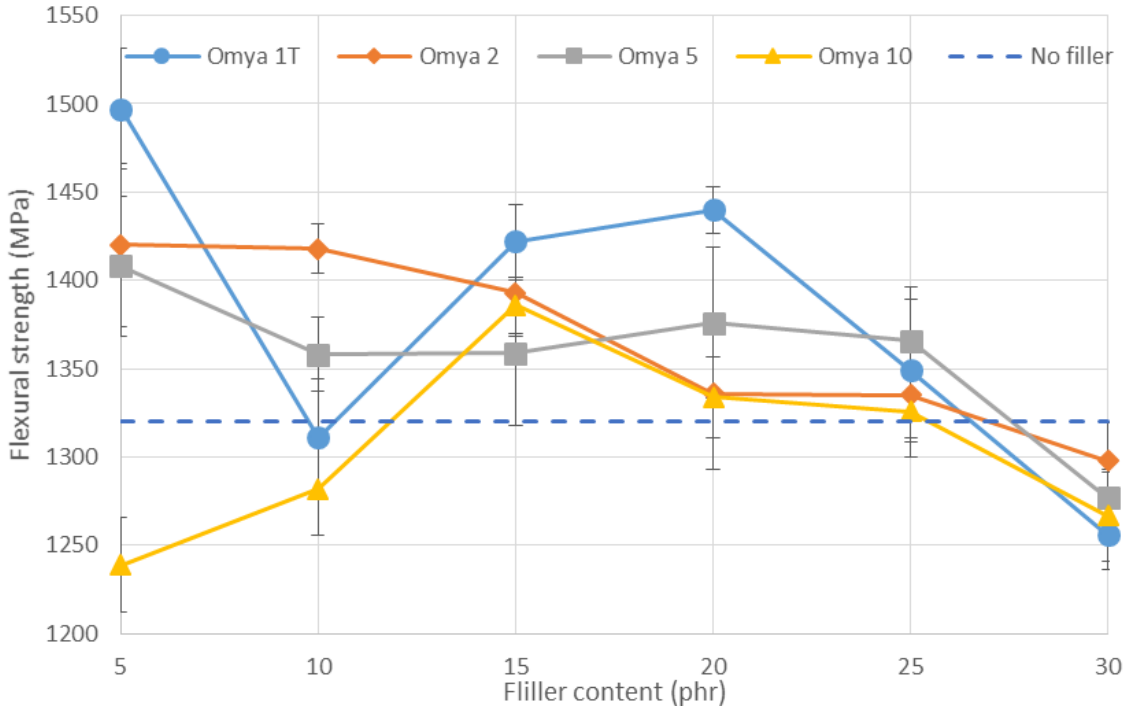

FIGURE 7.1: The flexural strength of 15 x 3.5 mm flat bars using various Omyacal fillers between 5 phr and 30 phr content. Error bars represent 95% confidence interval on mean strength.

The flexural modulus of the pultruded composites is largely unaffected by the addition of fillers (Figure 7.2). A slight decrease in flexural modulus was observed at a filler content of 30 phr, but these effects are probably due to the reduction in effective glass content in the profile as the cross-sectional areas increased slightly with added filler (Figure 7.3). The observed flexural moduli were within 1 to 5% of predicted values using the fibre and resin properties and a simple rule of mixtures. Previous research indicated a slight increase in flexural modulus with an increase in filler content [11], although this was not observed.

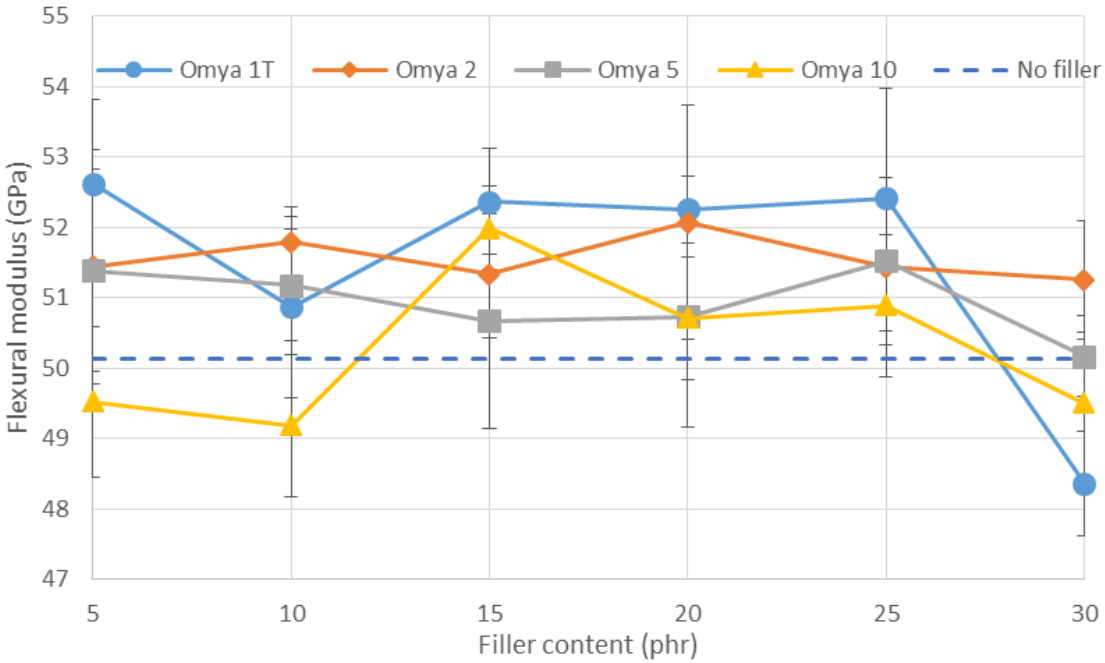

FIGURE 7.2: The flexural modulus of 15 x 3.5 mm flat bars using various Omyacal fillers between 5 phr and 30 phr content.

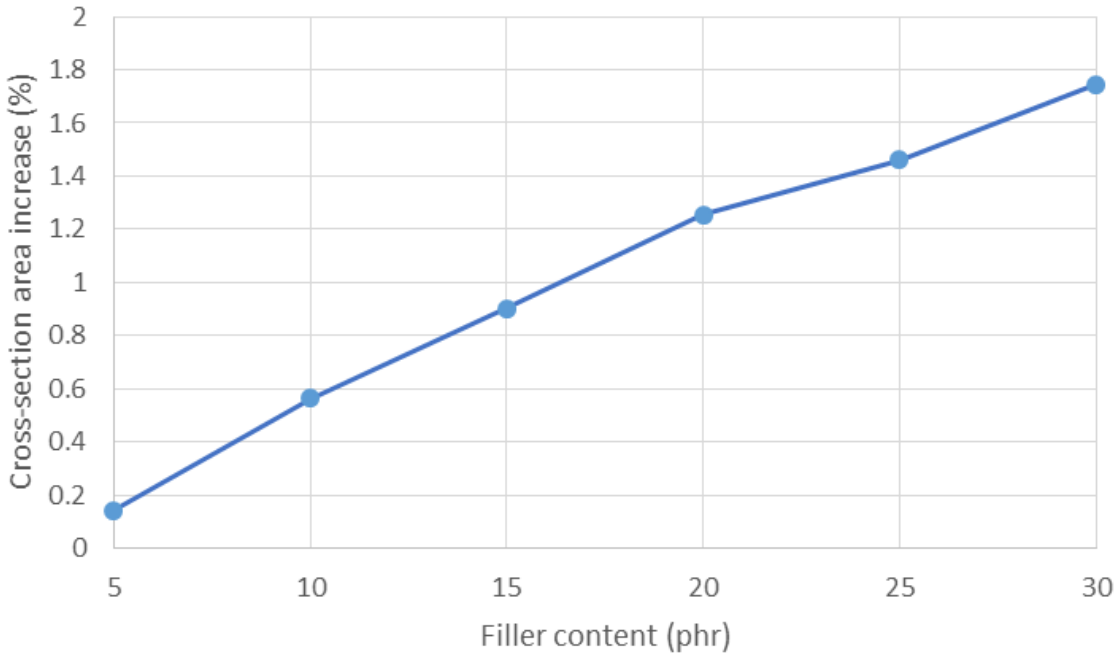

FIGURE 7.3: Cross-section area increase compared to an unfilled composite as a function of filler content (Omyacal 10).

Zinc stearate and P200 resin were both found to decrease the flexural strength of pultruded composites significantly. The addition of zinc stearate to the resin mixture decreased the flexural strength by 150 MPa. The addition of P200 to the resin mixture decreased the

flexural strength by 50 MPa. The addition of both zinc stearate and P200 to the resin mixture decreased the flexural strength by 200 MPa (Figure 7.4). The reason for the decrease in observed flexural strength due to the addition of zinc stearate appears to be due to zinc stearate not migrating to the outer surface of pultruded composites and instead residing at the interface between the matrix and fibres, resulting in decreased matrix-fibre adhesion. The reason that zinc stearate does not migrate to the surface of the composite is likely due to the fact that the melting temperature of zinc stearate (120 - 130 °C) is higher than the resin gelation temperature ($\approx$ 90 °C) within the die, leading to the retention of zinc stearate within the bulk material. The majority of the composites containing zinc stearate exhibited mixed mode failure, with a combination of compressive failure of fibres and matrix on the upper surface, interlaminar shear throughout the sample and tensile failure of the fibres on the lower surface. In contrast, tensile failure of the fibres was the main failure mode in composites free of zinc stearate. A reduction in composite cross-section area of 1.7% was observed on the removal of zinc stearate from the resin formulation as the zinc stearate acted as a filler with large particles. Composites containing Omyacal 2 at a content of 45 phr were produced in an attempt to compensate for a reduction in fibre packing associated with removal of the larger zinc stearate particles. An increased filler content of 45 phr of Omyacal 2 resulted in a decrease in flexural strength (30 MPa) when compared to a composite with a resin formulation containing only P100 resin and Omyacal 2 at a content of 30 phr while providing an increase in flexural strength (20 MPa) when compared to a composite with a P100 resin formulation containing zinc stearate and Omyacal 2 at a content of 5 and 30 phr, respectively. As a result the filler content of industrial pultrusion resin formulations may be increased from 30 to 45 phr with no negative effects on flexural properties when zinc stearate is removed.

Increasing the loading support span from the standard 16:1 to 20:1 may reduce the risk of interlaminar shear failure within the flexural specimens [12], but as the tests were intended to be comparative in nature the decision was made to retain the loading span at 16:1 for all tests. It was noted that only two out of 150 samples exhibited pure interlaminar shear failure. Slow motion video footage captured during testing showed that failure occurred rapidly in the majority of the samples that resulted in a mixed mode failure, although some samples initially exhibited tensile failure on the lower surface prior to the onset of other failure modes.

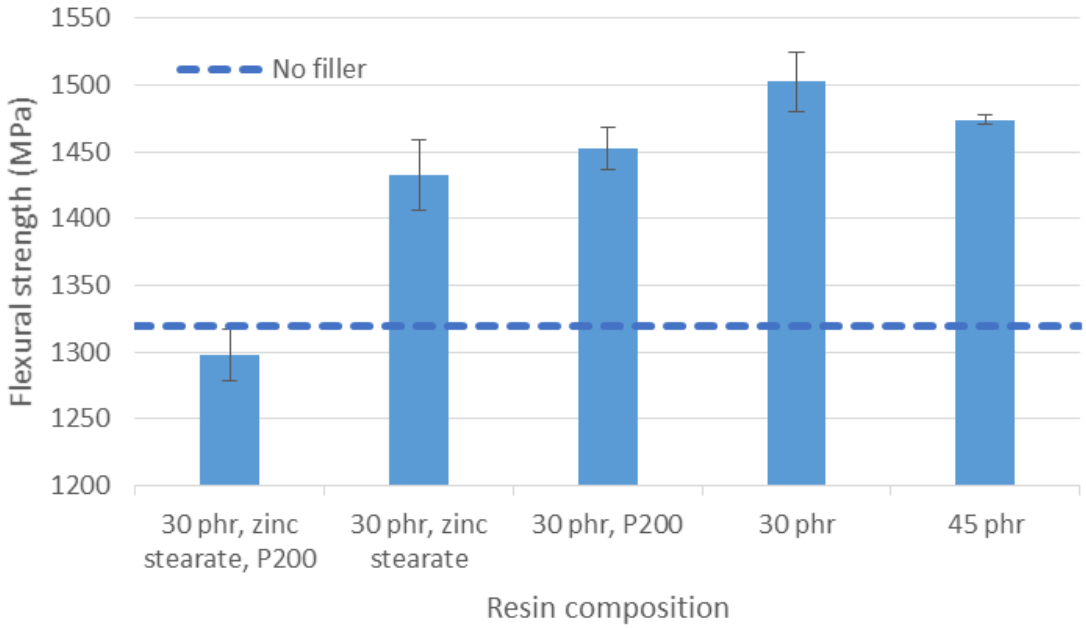

FIGURE 7.4: Mean flexural strength of 15 x 3.5 mm flat bars containing Omyacal 2 at 30 phr and 45 phr, characterising the effects of removing zinc stearate and P200 resin. Error bars represent 95% confidence interval on mean strength.

Some samples containing zinc stearate exhibited pure unstable interlaminar shear failure, with a crack propagating through the entire length of the sample. Interlaminar shear failure suggests poor interfacial bonding between the matrix and fibres, potentially due to the presence of zinc stearate rich regions at the interface between the matrix and fibres. The above failure has also been observed by Irfan *et al.* in trials regarding external application of mould release agents [3]. Zinc was shown to be concentrated at the surface of the glass fibres, rather than the matrix (Figure 7.5). Negligible quantities of zinc were detected in the bulk composite. Therefore, the presence of zinc at the fracture surface suggests that interlaminar failure is initiated as a result of the zinc stearate not migrating to the surface of the composite. It appears that zinc stearate migrates to the to the fibre and matrix interface, reducing the interfacial bonding.

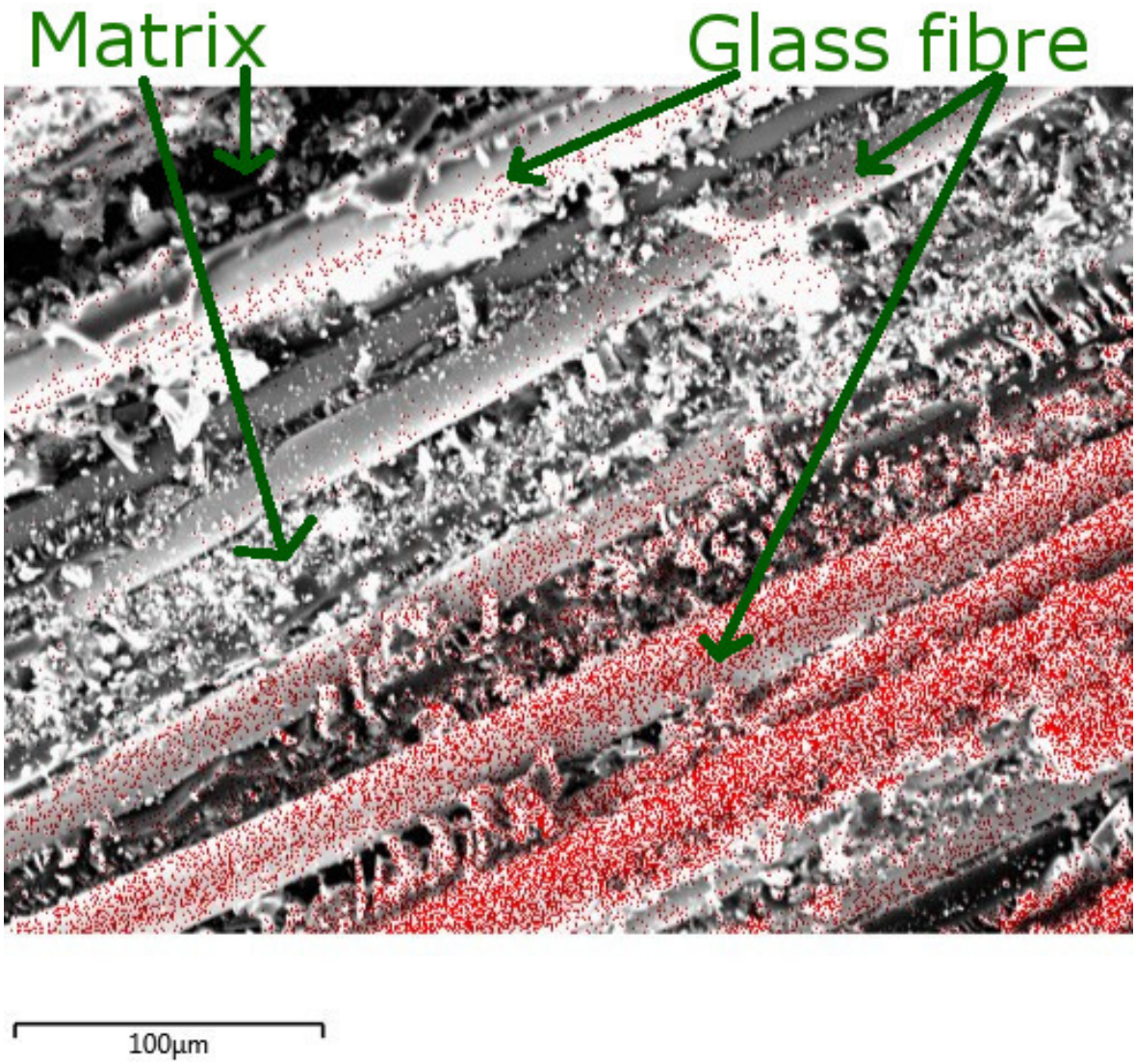

FIGURE 7.5: Scanning electron micrograph of a pultruded zinc-stearate containing composite that exhibited unstable interlaminar shear failure during a flexural test. Red dots indicate the presence of zinc as detected by EDS.

7.4 Summary

Particulate fillers were found to have a slight negative effect on the flexural strength of pultruded composites when added in high concentrations (> 25 phr), decreasing the flexural strength by 3.5% compared to unfilled composites. Flexural strength was found to increase by 7 - 14% at 5 phr compared to unfilled composites. A maximum flexural strength of 1500 MPa was observed upon the removal of zinc stearate and P200 from the resin formulation, while maintaining a filler content of Omyacal 2 at 30 phr. The size of the filler particles does not have a significant effect on the flexural strength as the failures appear to be initiated by matrix damage rather than fibre damage.

Zinc stearate was found to reduce the flexural strength of pultruded composites significantly by reducing the fibre-matrix bonding - resulting in interlaminar shear failure.

Interlaminar shear stresses were significant during the flexural tests, with interlaminar shear failure being observed in the majority of flexural tests. Therefore, a more detailed study of the interlaminar shear properties of pultruded composites was necessary.

Chapter 8

Effect of additives on the short beam properties of pultruded composites

8.1 Introduction

Interlaminar shear properties of pultruded composites is often a limiting design factor in structures, with shear strengths on the order of one tenth to one twentieth of flexural strengths in common pultruded composites (Table 8.1). Short beam shear testing takes advantage of the fact that shear stresses always occur in a flexural test. Shear stresses dominate in comparison to normal stresses when the span is small compared to the specimen thickness. The literature regarding the effects of additives on interlaminar shear strength and damage evolution mechanisms during short beam loading of pultruded composites is sparse.

TABLE 8.1: Comparison of properties of pultruded unidirectional epoxy/E-glass composites. Adapted from Irfan *et al.* [3].

Resin system	**Fibre fraction** (vol%)	**Flexural strength/ILSS**
EPON 9310	65.7	8.60[@]
EPON 9405	64.3	9.00[@]
EPON 9420	64.3	12.4[@]
EPON 9302	57.4	15.6[@]
Filled EPON 9500	68.0	26.7[@]
Araldite LY556	69.3	15.6[+]
Araldite LY556*	63.7	14.8[+]

[@]ASTM D790/D2344, [+]ASTM D6272/ISO 14130, *Externally applied mould release agent

8.2 Experimental methods

ASTM D2344 provides a standard test method for determining the short beam strength of pultruded composites. The test method is simple to employ, requiring only low cost fixtures, and is fast to perform. The above characteristics make the test ideal for use in quality control and comparison of resin formulations.

Specimens of rectangular sections manufactured with no filler, Omyacal 2 and Omyacal 10 at contents of 20 phr and 30 phr were subjected to short beam testing (ASTM D2344) with the aim of studying damage evolution. Damage evolution specimens contained P200 at 10 phr and zinc stearate powder at 5 phr.

Testing was also interrupted at pre-determined strain levels throughout the load-deflection curve to study the evolution of damage of the composites. Samples were analysed at deflections of 0.3, 0.6 and 1.0 mm. Samples were sectioned through the central loading point using a diamond saw blade. The samples were then mounted in acrylic and 1.5 mm was ground from each sample using a Buehler Powerhead grinder-polisher (Figure A.5) to remove surfaces damaged by the cutting procedure. Samples were then polished with progressively finer sand papers (Beuhler CarbiMet (P100, P240, P320, P600)) and polishing compounds (Buehler MataDi Supreme Polycrystalline Diamond Solution) down to a final polishing compound of 1 µm using a central load of 20 N spread between six samples. Each polishing stage was carried out for 6 minutes.

Polished samples were cleaned using an ultrasonic cleaning bath and coated in a thin carbon layer using a Quorum EMS150T ES Turbo-Pumped Sputter Coater. Samples were then imaged with secondary electrons using a JEOL JSM-IT300 scanning electron microscope (Figure A.6) using an accelerating voltage of 20 kV, probe current of 55 µA and 10 mm working distance.

8.3 Results and discussion

8.3.1 Short beam properties as a function of filler content and particle size

The interlaminar shear strength (ILSS) of composites containing no added filler (yet still retaining zinc stearate and P200 resin) was found to be 61.6 $\pm$0 8MPa. ILSS was not strongly affected by the presence of the fillers that were tested (Figure 8.1). An average net decrease in

ILSS of 10% was observed when filler content was varied between 5 and 30 phr, decreasing from 68 to 61 MPa (Figure 8.1). Interestingly, an increase in ILSS was observed with the addition of filler, indicating that the filler helped to reduce the presence of voids when added in small concentrations.

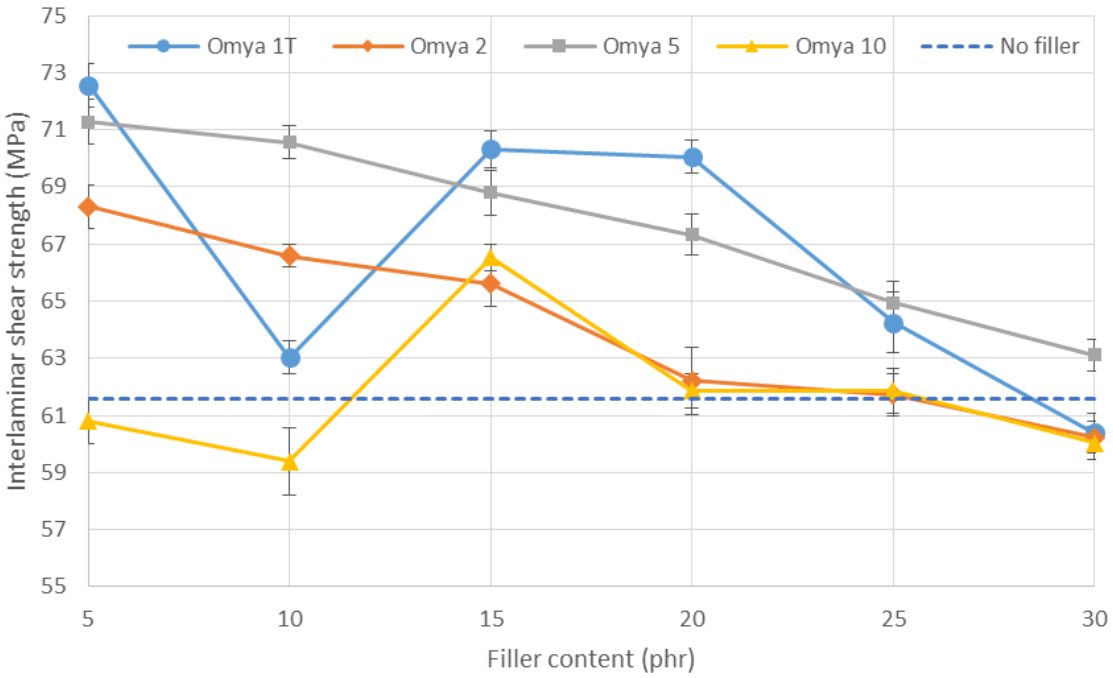

FIGURE 8.1: Short beam strength of 15(w) x 3.5 (t)mm flat bars using various Omyacal fillers between 5 phr and 30 phr content. Error bars represent 95% confidence interval on mean strength.

Zinc stearate and P200 resin were both found to decrease the ILSS of pultruded composites significantly (Figure 8.2). The addition of zinc stearate to the resin mixture decreased the ILSS by 18 MPa (21%). The addition of P200 to the resin mixture decreased the ILSS by 7 MPa (8%). The addition of both zinc stearate and P200 to the resin mixture decreased the ILSS by 28 MPa (33%). The reason for the decrease in observed ILSS is due to zinc stearate not migrating to the outer surface of pultruded composites as discussed in Section 7.3.

8.3.2 Damage evolution under short beam loading conditions

Figure 8.3 gives a representative stress-displacement curve for a pultruded glass reinforced composite under short beam loading configuration. Three distinct stages are observed throughout the loading response of these samples. The first stage is linear elastic response (I), where little to no damage occurs within the sample. The second stage is damage formation (II)

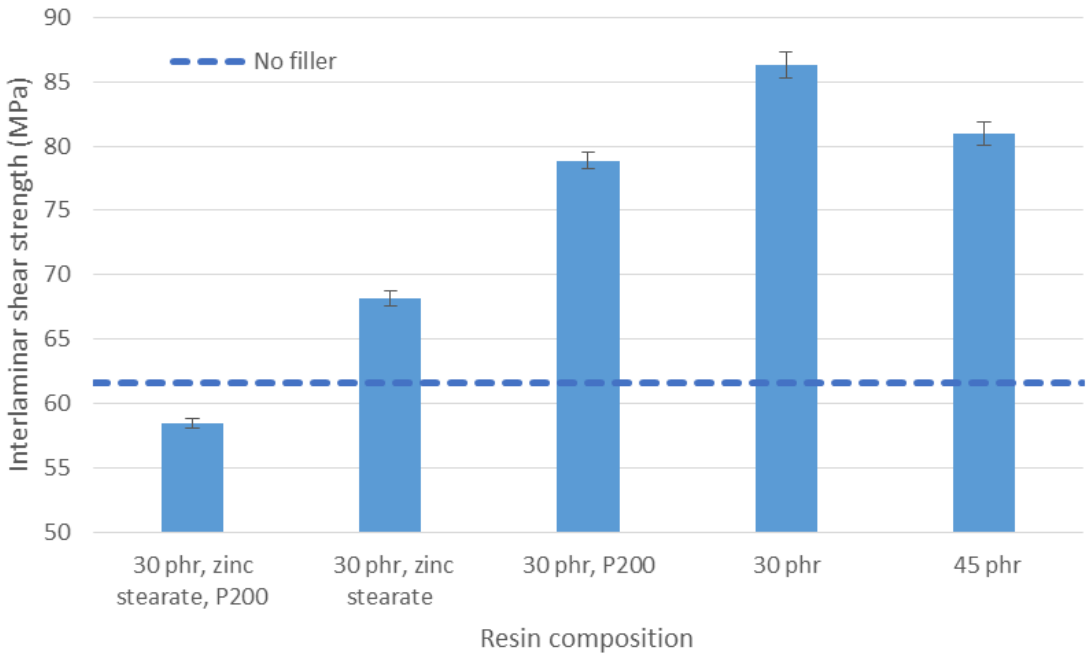

FIGURE 8.2: Interlaminar shear strength of 15(w) x 3.5 (t)mm flat bars as a function of Omyacal 2, zinc stearate and P200 resin content. Error bars represent 95% confidence interval on mean strength.

where cracks begin to form within the sample and the third stage is damage growth (III) where existing cracks grow substantially.

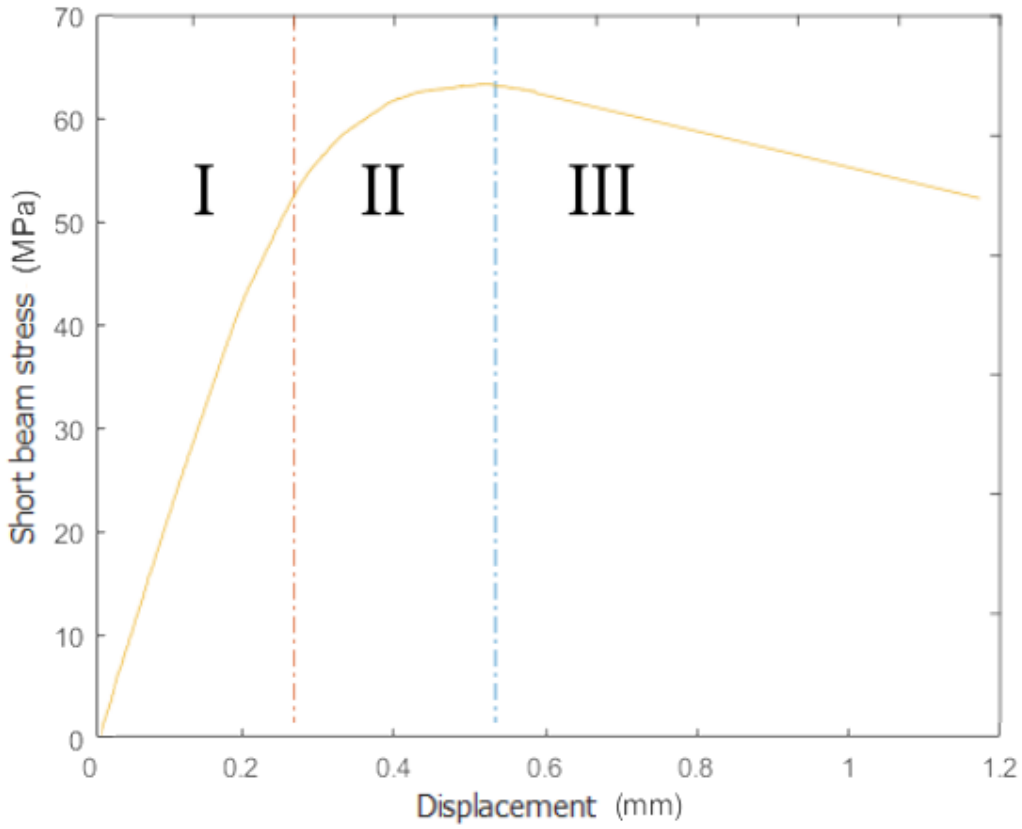

FIGURE 8.3: Representative stress-displacement curve for a pultruded glass reinforced polyurethane matrix composite under short beam loading configuration.

Sparse debonding is observed at the fibre-matrix interface surrounding a fibre-lean regions following Stage I loading (Figure 8.4). Cracks are not observed to propagate through the matrix phase, rather the cracks propagate along the fibre-matrix interface. Resin shrinkage may also partially cause initiation of damage at the fibre-matrix interface. Similar damage was observed with unfilled and Omyacal 2 and Omyacal 10 filled composites following Stage I loading.

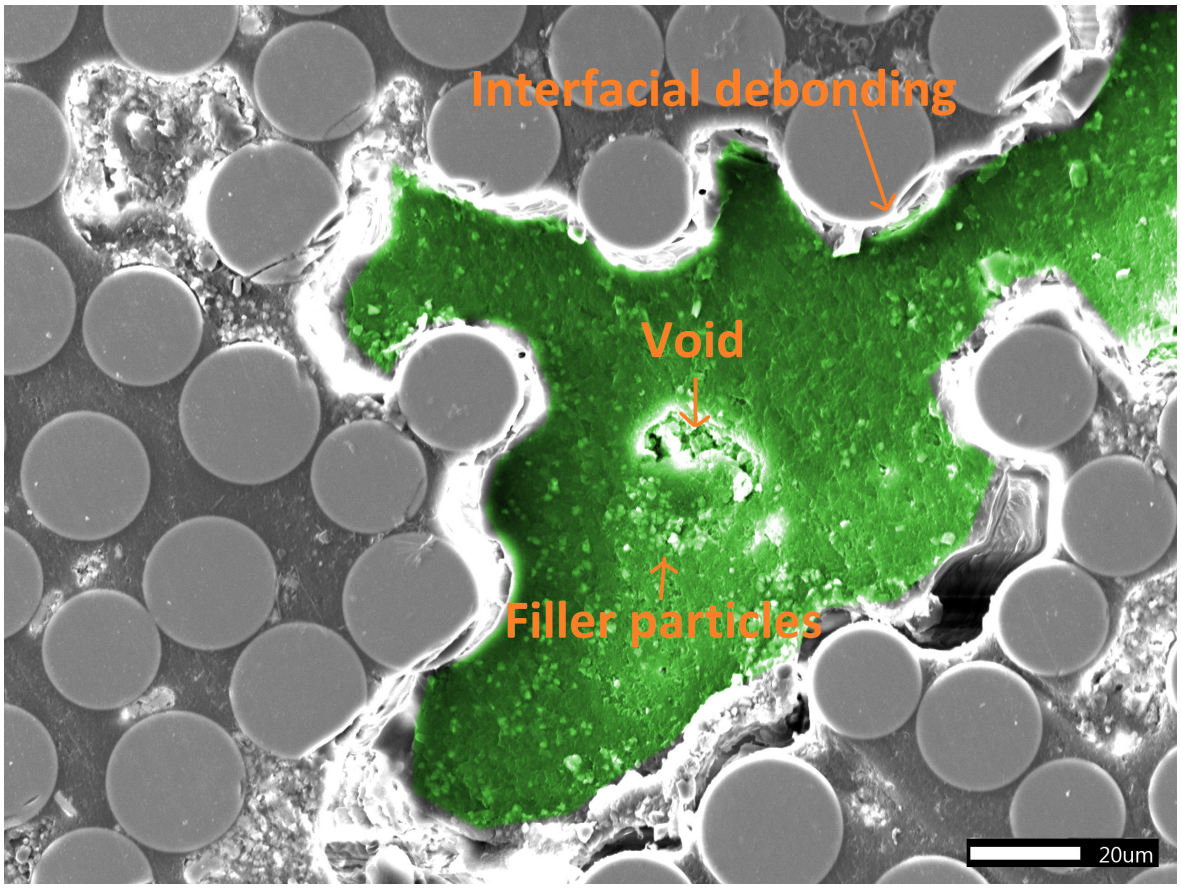

FIGURE 8.4: Scanning electron micrograph of a pultruded composite part after short beam testing through Stage I loading. Fibre lean region is green. Omyacal 2 at 20 phr.

A higher density of isolated regions of debonding at the fibre-matrix interface was observed at multiple sites throughout specimens by the end of Stage II loading (Figure 8.5). The damage mechanism is the same as observed after late Stage I loading (damage initiation), with more damage initiation sites present. Similar damage was observed for all samples that were loaded through to the end of Stage II.

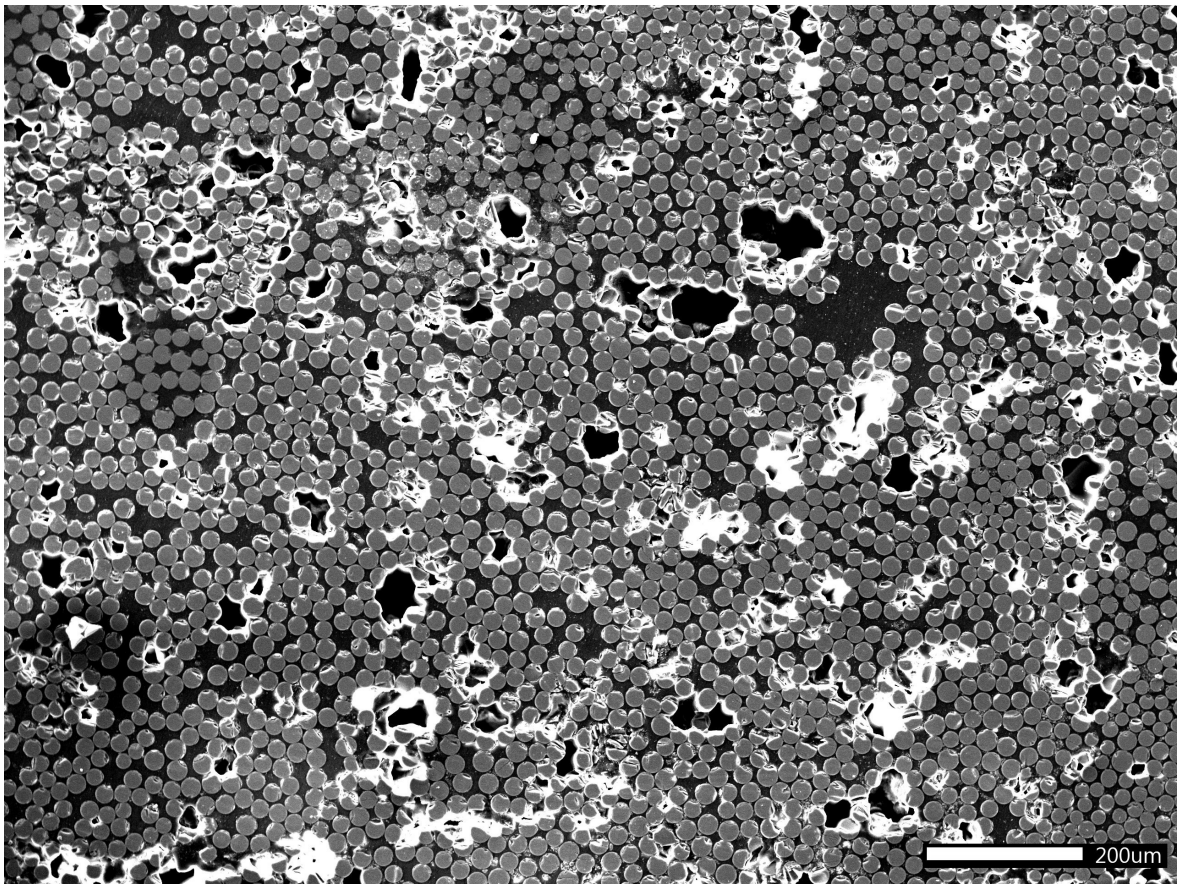

FIGURE 8.5: Scanning electron micrograph of a pultruded composite part after short beam testing through Stage II loading.

Microcracking developed into a network by the end of Stage III (Figure 8.6). The resin mixture of the part contained Omyacal 2 at 30 phr, P200 at 10 phr and zinc stearate powder at 5 phr. Similar levels of damage were observed for all samples following Stage III loading. The damage is widespread such that many isolated cracks link together to form larger macroscopic cracks..

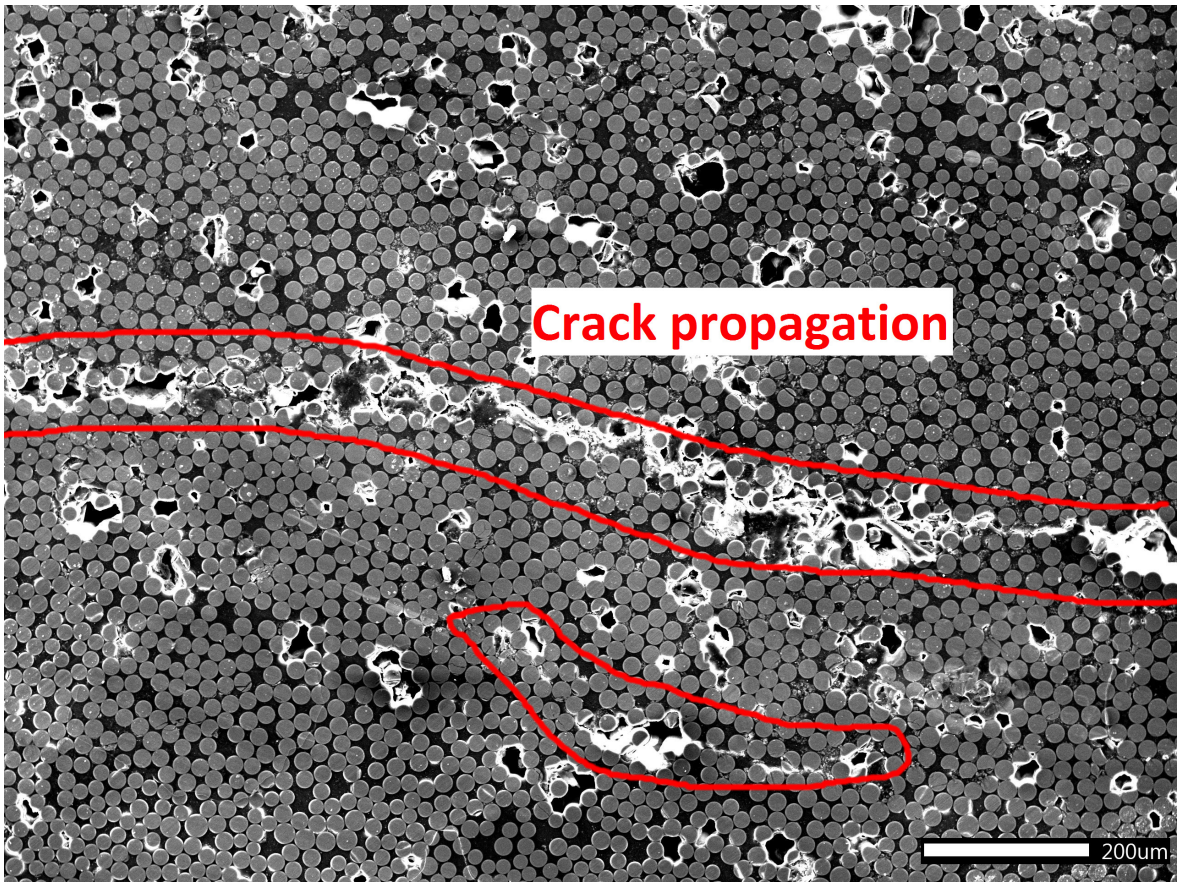

FIGURE 8.6: Scanning electron micrograph of a pultruded composite part after short beam testing through Stage III loading.

8.4 Summary

The short beam strength of pultruded composites was found to behave in a similar manner to the flexural strength. A slight decrease in interlaminar shear strength was observed with increased filler content. Filler particle size had a negligible effect on the interlaminar shear strength, indicating that filler particle size does not play a major role in interfacial bonding between the matrix and fibres. Zinc stearate (5 phr) and P200 (10 phr) were shown to dramatically decrease the interlaminar shear strength of pultruded composites by 33% from 86 to 58 MPa.

Short beam loading of composites results in a stress-strain response consisting of three distinct regions: (I) linear elastic, (II) damage formation and (III) damage growth. Damage was mainly observed as interfacial debonding around fibre-lean regions of the microstructure.

Chapter 9

Statistically representative microstructure generation

9.1 Introduction

The effects of fibre packing on the elastic properties of a transversely random distributed, longitudinally unidirectional glass-epoxy composite was described by Gusev *et al.* [15]. Random microstructure generation (RMG) was used as a method for predicting elastic properties of real and simulated fibre arrangements in unidirectional long fibre composites with high volume fractions by Melro *et al.* [16] and Romanov *et al.* [17]. A modified nearest neighbour algorithm method similar to the RMG method was developed for generating representative volume elements (RVEs) as reported by Wang et al. [18]. A reprentative volume element is a small volume element over which a measurement can be made that represents the whole composite, Gusev *et al.* found a square region with side lengths of 25x the average fibre diameter provide adequate RVEs [15].

None of the above models considered the presence of filler particles, only considering the fibres and matrix in composites. This work aims to fill the gap in literature regarding generation of statistically representative microstructures of composites containing fillers in addition to glass fibres.

9.2 Statistically representative microstructure generation

A model was created using MATLAB to generate random microstructure cross-sections in the form of representative volume elements (RVE). The model aims to predict shrinkage

and density of pultruded composites as a function of the filler content and type.

A RVE is generated containing fibres and fillers created from statistical distributions relating to the particular products (glass fibres, filler particles) being used. The micrograph is then analysed to determine the fibre volume fraction, filler volume fraction, product density and expected shrinkage of the part.

The first step in generating the RVE involves generating an allowable region in which the components of the composite may be placed. A maximum allowable region is generated using a matrix of pure zeros, with each element representing one square micron multiplied by a scaling factor (which is generally one). This region is then subdivided into multiple overlapping subregions which may then be filled with components (Figure 9.1).

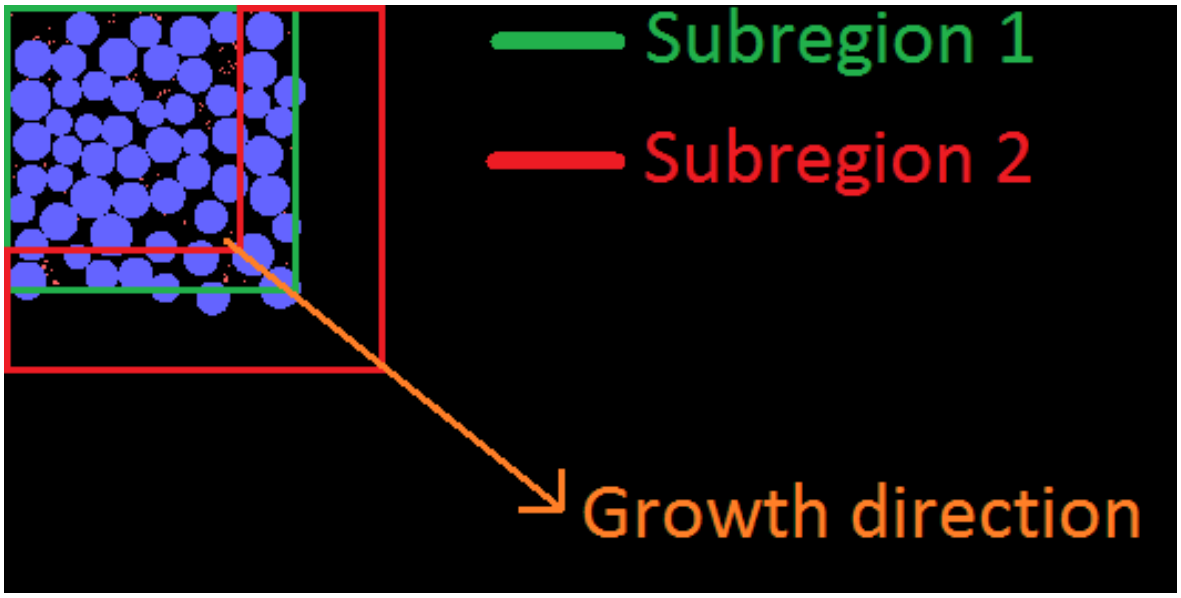

FIGURE 9.1: Overlapping subregion generation method, initial subregion populated.

Once a subregion has been defined, the algorithm begins to attempt placing fibre and filler particles within the region. A random point within the subregion is generated, this point represents the centre of the first object. In order to optimise the process of object placement, a sub matrix is generated for each object. This submatrix has dimensions corresponding to a square that contains a circular object located at the centre of the submatrix. The object is defined within this submatrix by replacing the corresponding elements with a 1. In order to determine whether the object overlaps any existing objects within the subregion, the submatrix is dot multiplied with the region of the same dimensions as the submatrix surrounding the attempted centre location of the object within the subregion. If there is

any overlap with an existing particle, the maximum value of this dot multiplication will be greater than zero.

If any overlap between objects is detected, the attempted centre location of the new object will be mutated by a small amount (mutation factor), corresponding to the number of attempts made at placing the particle. When a situation of non-overlapping is detected, the object is placed within the subregion matrix and given a value between 0 and 255, depending on whether it is a filler particle or glass fibre. Each particle is attempted to be placed 2000 times. If the object cannot be placed within 1000 attempts through mutation, a new random centre will be selected, this will continue until the object is placed, or a total of 2000 attempts have been made.

For filler particles, the entire particle must be placed within the subregion, but glass fibres are allowed to be placed with their centres on the boundary of the subregion, eliminating issues where lines are formed between subregions where all of the glass fibres are aligned with the edge of the subregions.

Once a subregion has reached a lower limit for glass volume fraction and filler volume fraction, the script moves on to the next subregion and repeats the process. This process continues until either the specified quantity of glass fibres have been placed or the script runs out of objects to place.

9.3 Deterministic density modelling

A simple model using the rule of mixtures to determine the density of composites was initially used. The predicted (ideal) density of a 15(w) x 3.5 (t)mm rectangular pultruded composite containing 20 rovings of 4400 tex E-glass (glass volume fraction calculated from measured dimensions of each specimen), with a matrix consisting of a P100/P200 blend increases approximately linearly from 2.066 to 2.103 $\mathrm{g\,cm^{-3}}$ with an increase in filler (Omyacal 2) content from 0 to 30 phr (Figure 9.2). The ideal prediction exceeds measured values when the composite is unfilled and when the filler content exceeds 20 phr. The reason for this is due to the increased presence of voids within the unfilled and highly filled composites. Raper *et al.* showed the formation of voids in unfilled composites is due to styrene gas bubble nucleation at the fibre-matrix interface as a result of lowered pressure resulting from excessive resin stripping at the die entrance with low viscosity resins [33]. The formation

of voids in highly filled composites is due to two possible mechanisms: (i) close-packing of filler particles that exclude resin penetrating the agglomerates and (ii) filler particles acting as gas bubble nucleation sites that cause evolution of styrene gas or CO_2 by racting with catalysts during the pultrusion process as described by Zhang *et al.* [13]. Data sheets for the Omyacal fillers indicate that the packed bulk density for Omyacal 1T and Omyacal 2 is $0.8\,\mathrm{g\,cm^{-3}}$ (ISO 787/11) and for Omyacal 5 and Omyacal 10 is $1.0\,\mathrm{g\,cm^{-3}}$ (ISO 787/11). The density for bulk calcium carbonate is $2.75\,\mathrm{g\,cm^{-3}}$. Therefore, the likelihood that agglomeration occurs (and resin is excluded from the agglomerate interstices) is increased with increasing concentration of filler particles. A reasonable fit to the measured data is obtained by modelling the effective density of the filler as constant at $2.7\,\mathrm{g\,cm^{-3}}$ up to a content of 20 phr and then decreasing the density to 1.8 and $1.6\,\mathrm{g\,cm^{-3}}$ at a content of 25 phr and 30 phr, respectively, (Figure 9.3).

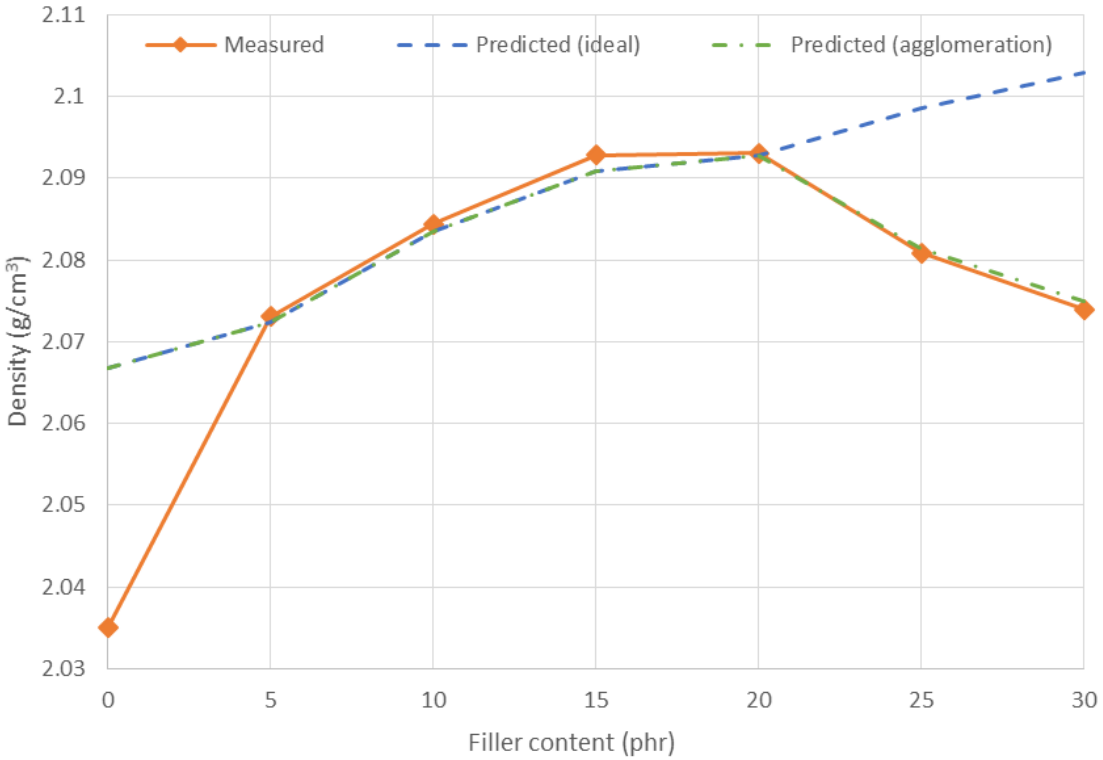

FIGURE 9.2: Predicted and measured density for a composite filled with Omyacal 2 between 0 phr and 30 phr.

Using the rule of mixtures for predicting density of pultruded profiles has several limitations. The rule of mixtures does not account for greater effects on packing of larger filler particles compared to smaller filler particles, nor does the model account for resin shrinkage

- this necessitates measuring the actual glass content of a composite before any modelling may commence. The rule of mixtures also assumes all particles and fibres are spread evenly throughout the composite with no clustering. In reality, the particles tend to cluster at interstices between the fibres and form agglomerates. Allowing a longer rest period between mixing resin and pultruding the profiles may decrease the effects of agglomeration by allowing the resin to permeate into the agglomerates.

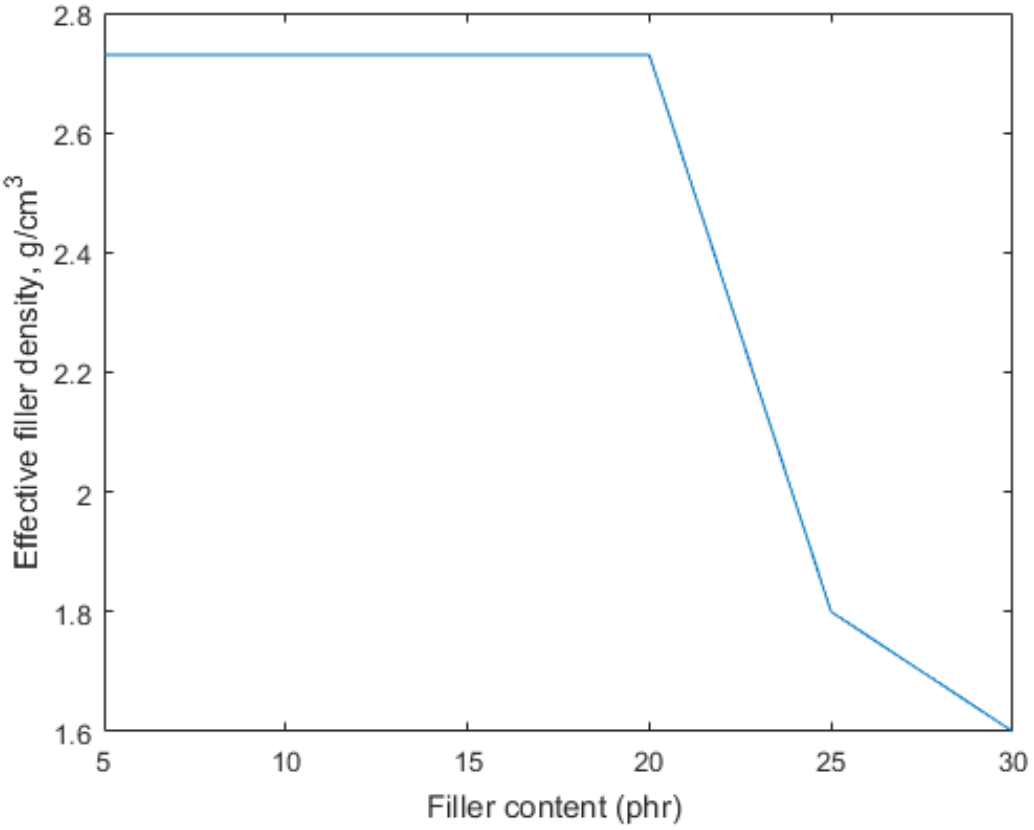

FIGURE 9.3: Effective density of a calcium carbonate filler between 5 phr and 30 phr.

9.4 Modelling the packing arrangement

The fibre packing arrangement varies chaotically throughout a pultruded composite, exhibiting a combination of random, hexagonal and square packing [11] (Figure 9.4).

Ideally, a model used to generate a representative microstructure of a pultruded composite must attempt to replicate the actual packing arrangement. This work involves a modified

nearest neighbour algorithm (NNA) to place particles within a representative volume element. The model initially attempts to place new particles near the most recently placed particle. If a certain number of attempts at placing the particle are unsuccessful, then the model attempts to place the particle at random throughout the allowable region. In order to tune the model to produce realistic results, mutation factors and attempt allowances are adjusted. Wang *et al.* used a similar modified NNA to model carbon fibre/epoxy composites and showed the method is capable of producing realistic clustering [18].

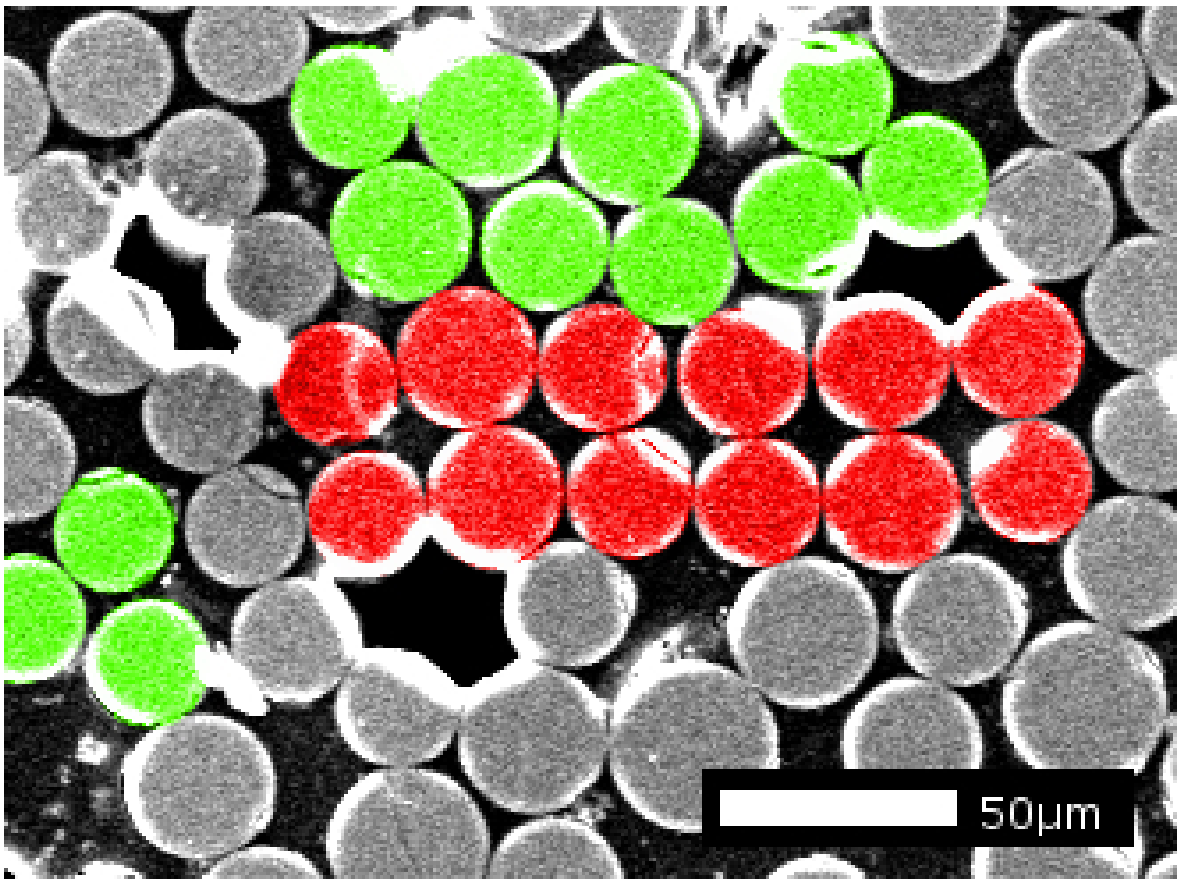

FIGURE 9.4: Micrograph showing various fibre configurations present in real composites. Red fibres exhibit square packing, green fibres exhibit hexagonal packing and grey fibres exhibit random packing.

9.5 Particle size determination

The diameter of particles (fibres and fillers) to be placed is determined using various methods, although the model is limited to objects with a circular cross-section.

For glass fibres, a random value is selected from an array of values corresponding to measured fibre radii from a micrograph of a pultruded composite manufactured with 4400

tex Jushi rovings (Figure 9.5).

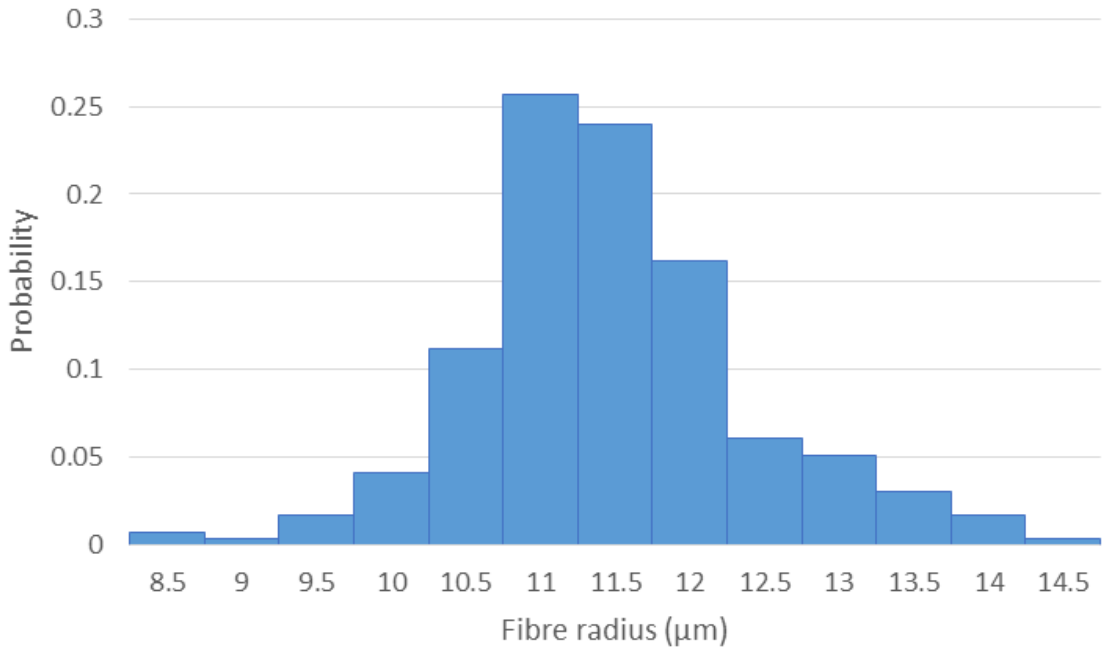

FIGURE 9.5: Probability distribution for measured fibre radii of 4400 tex Jushi rovings.

Two methods were developed for generating filler particle sizes. The first method involves using the particle size distributions obtained in Section 5.2.2 and selecting particle diameters based on the cumulative distribution function for each filler type. However, this method has a major limitation in that the particle distribution curves are not entirely representative of the true filler particle distributions due to issues with agglomeration. Hence, this method is not preferred. However, this method may be useful if a density correction factor is applied to larger particles in an effort to account for resin exclusion from agglomerates.

The second method for generating filler particle sizes involves generating a Weibull random number representing the particle radius. Two parameter Weibull distributions are applicable to describing particle distributions generated by milling and crushing operations [34]. Using a scale parameter of 1.0 and a shape parameter of 1.5 gives a Weibull distribution corresponding closely to particles of Omyacal 2.

9.6 Statistical characterisation

Nearest neighbour angle analysis and fibre radius distribution analysis was performed using MATLAB to analyse the generated RVEs.

Nearest neighbour angle analysis considers the angle between a reference fibre and its nearest neighbour with respect to the positive x-axis, to give a cumulative distribution function for the RVE. A straight diagonal line is produced for a completely spatial random (CSR) distribution of fibres, indicating an equal probability of a fibre being at each angle. A deviation from the straight diagonal line is observed if there is an element of regularity in the fibre distribution. Experimental measurements in the literature have found such deviations to occur [18, 16, 17], indicating clustering and a degree of regularity in real composites.

The fibre radius distribution was established by comparing histograms generated from the experimental and generated RVEs.

9.7 RVE analysis

RVEs are automatically analysed by MATLAB to determine key properties of the composite. The predicted density, glass content, filler content in phr and expected shrinkage of the composite were calculated. Density is calculated by summing the products of volume fractions and constituent density of each constituent. The glass content is calculated by summing the elements of glass fibres in the RVE and dividing the sum by the total number of elements in the RVE. Filler content in phr is calculated by determining the mass fraction(s) of the filler(s) within the matrix and converting the mass fraction to parts per hundred resin using Equation 9.1,

$$phr_n^f = \frac{m_n^f phr^r}{m^r} \tag{9.1}$$

where phr_n^f is the parts per hundred resin of filler n, m_n^f is the mass fraction in the matrix of filler n, phr^r is the parts per hundred resin of the resin - 100 - and m^r is the mass fraction of resin in the matrix.

Part shrinkage was modelled by applying a 2.2% linear shrinkage (determined by comparing the dimensions of cast neat P100 resin and the casting mould) to the resin component of the matrix in the RVE, keeping the volume of the glass fibres and fillers constant.

9.8 Results and discussion

Figure 9.6 gives a representative volume element for a pultruded composite containing unidirectional reinforcement in the form of 4400 tex Jushi 312 rovings and Omyacal 2 as a filler. This particular RVE gives a fibre content of 64.0 vol% and a filler content of 31.0 phr.

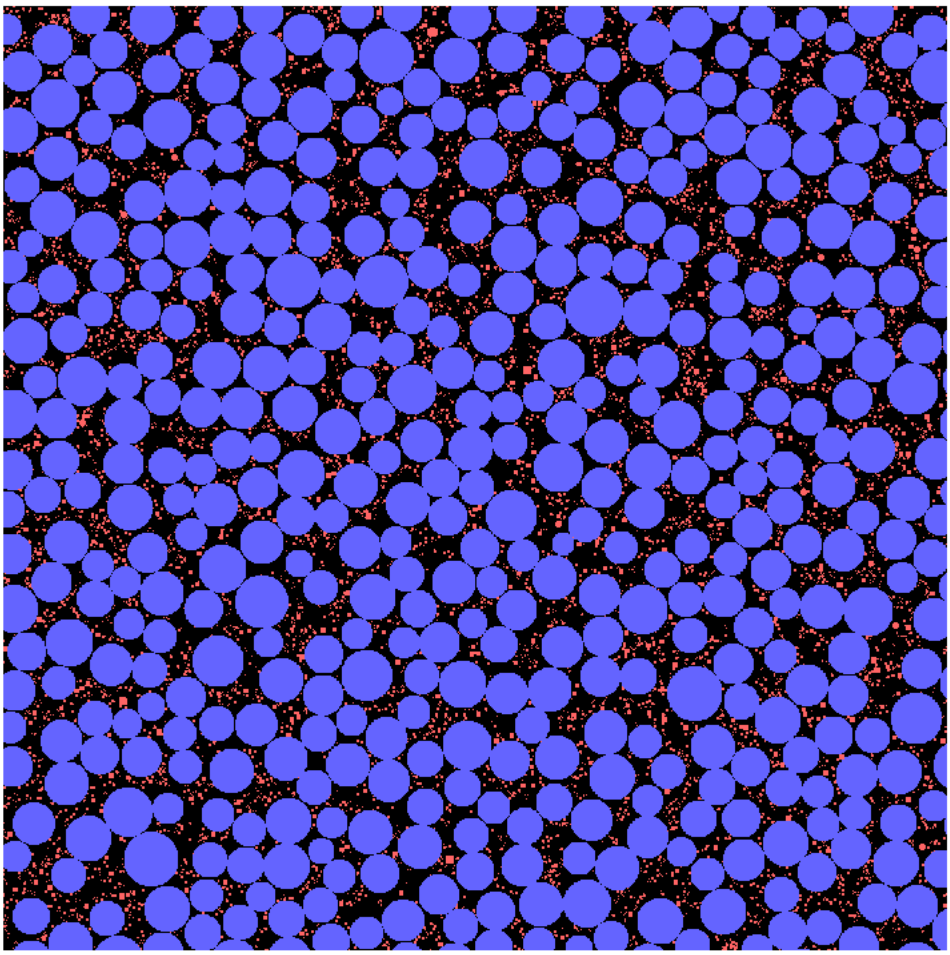

FIGURE 9.6: Representative volume element of a pultruded composite. Fibres are blue, filler particles are red and the matrix is black.

Nearest neighbour angle analysis for a generated RVE shows an essentially random packing of glass with little stepping as observed in square packed microstructures and hexagonally packed microstructures (Figure 9.7). These results are in agreement with nearest neighbour angle analysis given in by Wang *et al.*, indicating that the model provides an adequately representative microstructure [18].

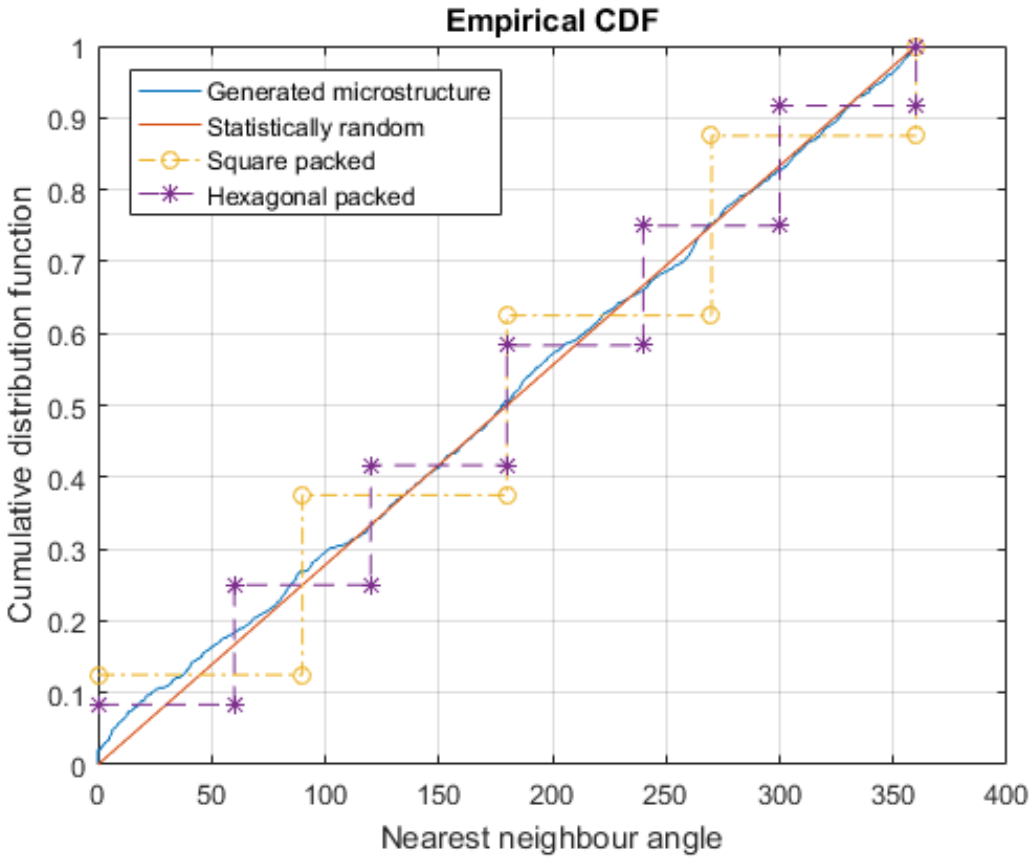

FIGURE 9.7: Nearest neighbour angle analysis for a generated RVE.

The microstructure generation algorithm produces accurate predictions of product density and glass packing (Figure 9.8, Figure 9.9), the modelled structure consists of unidirectional reinforcement in the form of 4400 tex Jushi 312 rovings and Omyacal 2 as a filler. The matrix resin does not include Plexinate P200 or zinc stearate powder. The samples which were used for the comparison were manufactured with resin which was mixed and left to sit for at least one hour after the filler particles had been added, reducing the effects of resin exclusion in close packed filler particle agglomerates. Some variation and oscillatory behaviour is evident in the prediction, but this is an expected result when using stochastic methods for determining properties, especially when a small RVE is used. The RVE used in this case had dimensions of 800 µm by 800 µm. Running the simulation for larger RVEs reduces the variation in results but increases computational time significantly.

The generated microstructures tend to be biased slightly towards fibres with a smaller radii (Figure 9.10). A bias toward smaller fibres is due to the fact that as the fibre content increases in the generated microstructure, larger fibres become more difficult to place than

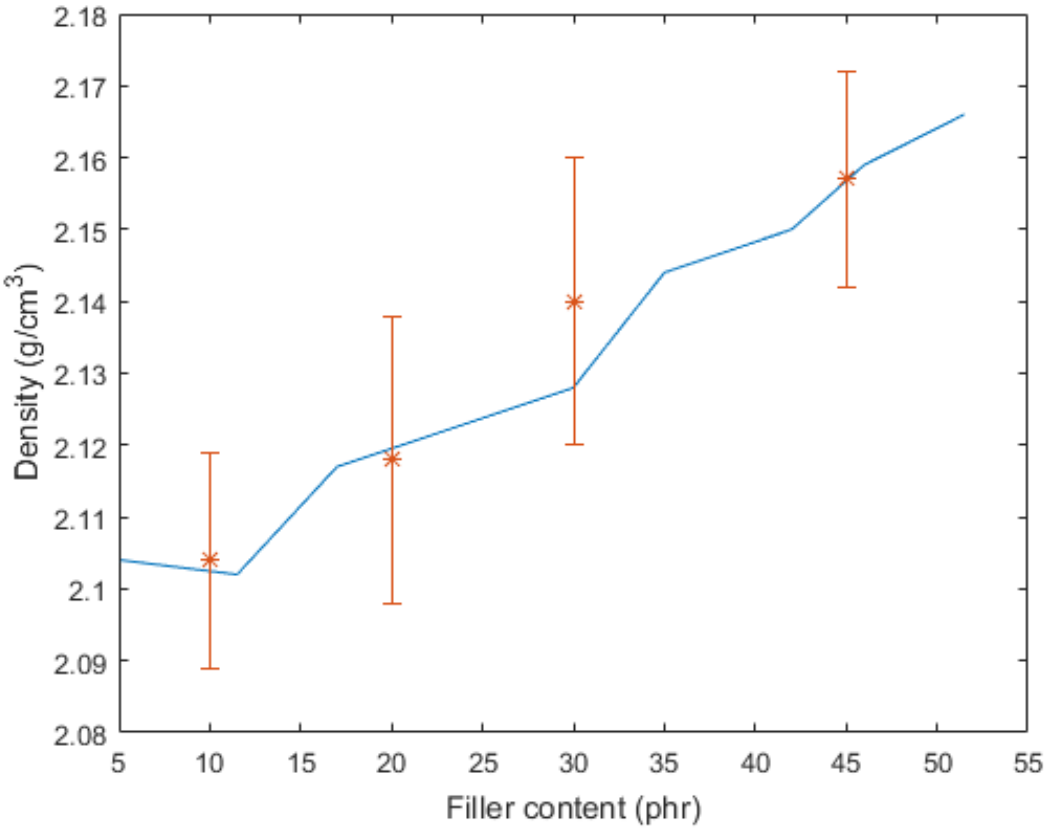

FIGURE 9.8: Predicted density of a pultruded composite using a generated RVE. The line represents the prediction, while the individual points represent measured data from manufactured composites.

smaller fibres. After a specified number of attempts the model eventually gives up on placing the larger fibres. This is partially accounted for by dynamically adjusting the number of attempts made at placing fibres depending on their radius, allowing greater numbers of attempts to place larger fibres than for smaller fibres. Future work should involve implementing a "stirring" algorithm to continually relocate fibres during the packing sequence in an effort to improve packing efficiency, similar to work by Chen *et al.* [8].

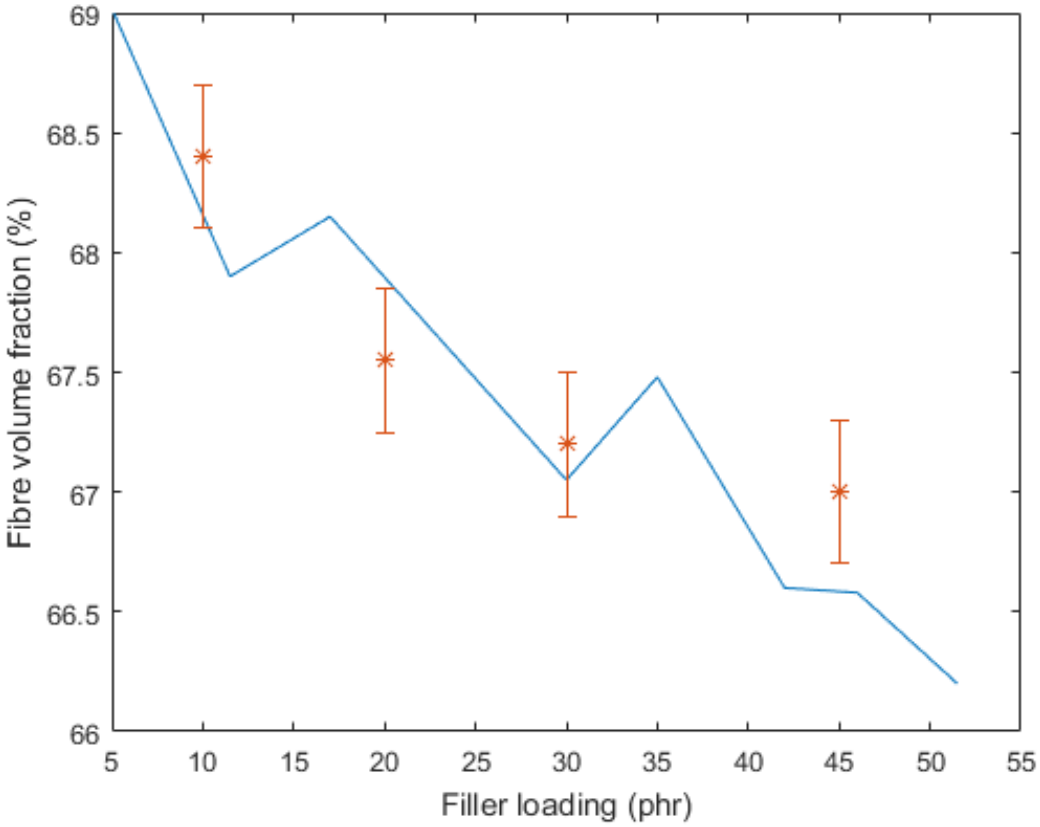

FIGURE 9.9: Predicted fibre content of a pultruded composite using a generated RVE. The line represents the prediction, while the individual points represent measured data from manufactured composites.

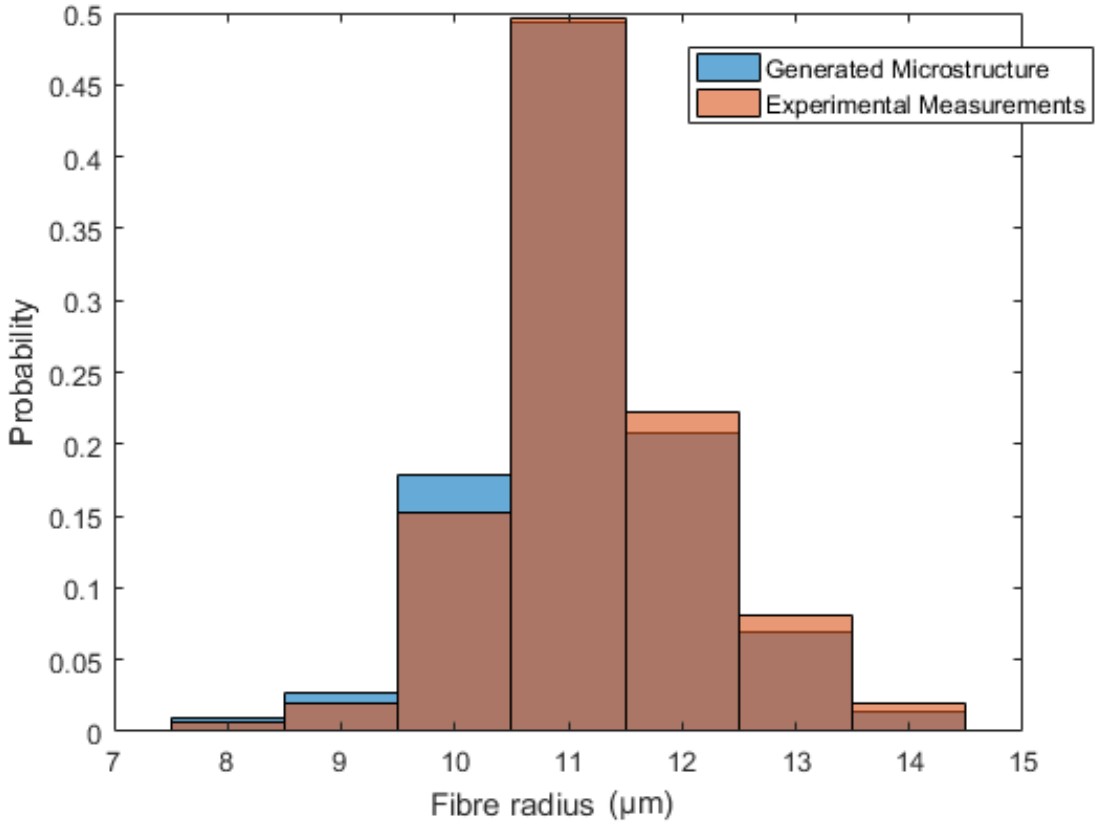

FIGURE 9.10: Distribution of fibre radii for a generated microstructure (blue) and for an experimentally measured microstructure (peach).

9.9 Summary

A stochastic model was developed to generate microstructures representative of pultruded composites containing fillers. Density and fibre volume fraction predictions were in agreement with measured values from real composites.

The model is currently limited as it does not incorporate a "stirring" algorithm which is used in other works, as a result the model produces microstructures that are biased towards smaller fibre diameters than true microstructures. A "stirring" algorithm repositions previously placed fibres to increase the fibre volume fraction when the model encounters difficulty in placing new fibres. The model does not consider void formation.

Microstructures generated using this model may be used for FEA to predict the tensile, flexural and interlaminar shear properties of pultruded composites in future work. The model is also useful for predicting the maximum allowable number of rovings that may be incorporated into pultruded profiles.

Chapter 10

Conclusions

10.1 Summary of the main findings

- Tensile strength of unidirectional pultruded composites is slightly sensitive to filler content and is affected significantly by the filler median particle diameter. Fibre crimping caused by large filler particles appears to be responsible for these effects.
- The type of filler used (talc or calcium carbonate) does not appear to directly affect the tensile strength. A linear decreasing relationship between median particle diameter and tensile strength is observed.
- Filler content and particle size have little effect on the flexural and short beam strengths of pultruded composites, a net negative effect is noticed but is only on the order of 3 to 10% at a filler content of 30 phr when compared to 5 phr and a positive effect when compared to products manufactured containing no filler.
- The addition of zinc stearate and P200 polyurethane resin appears to decrease the interlaminar shear strength of unidirectional pultruded composites by approximately 33%. The effects do not appear to interact, with the P200 being responsible for one third of the decrease and the zinc stearate being responsible for the remaining two thirds of the decrease. Zinc stearate was found to accumulate at the interface between the matrix and fibres in pultruded composites, resulting in reduced bonding.
- Similar effects on flexural strength are observed when zinc stearate and P200 polyurethane resin are added to the resin mixture, giving an decrease in flexural strength of approximately 15%. However, the effects of the P200 and zinc stearate appear to swap roles,

with the P200 being responsible for two thirds of the loss of strength while the zinc stearate is responsible for only one third of the loss of strength.

- Incorporation of filler particles into a random microstructure generation algorithm allows for the prediction of maximum density and fibre packing fraction in real pultruded composites.

It is recommended that the use of Rebain DC325T-FIR as a filler in pultruded composites be discontinued and a replacement filler with smaller particle sizes and better UV performance be specified. Omyacal 2 at 30 phr has been shown to perform well when used as a filler in pultruded composites.

Removal of Zinc stearate and P200 resin from the industrial resin formulation is recommended as there is no apparent benefit to the pultruded composites, with significant impairment of properties being observed when these components are present. If zinc stearate is to be removed from the resin formulation, the concentration of filler particles may be increased to 45 phr in order to account for increased product shrinkage without significant detriment to product properties.

When mixing filler into resin, a significant waiting period is required to allow for particle agglomeration to be overcome and thus reducing the void content of manufactured products. If the resin is used too soon after the filler powder is added there will tend to be large agglomerates of filler particles which have excluded resin from their body, these agglomerates act as hosts for voids. Table 10.1 gives the suggested resin formulation as a result of this research.

TABLE 10.1: Suggested resin formulation.

Material	**Weight (phr)**	**Weight (percent)**
Plexinate P100 polyurethane resin	100 (base reference)	67.6 %
Norox Pulcat AWM catalyst	1.5	1.0 %
Norox TBPB catalyst	1.0	0.68 %
Mold Wiz INT-PUL-24	0.5	0.34 %
Omyacal 2 Filler	45.0	30.4 %

10.2 Future work

Due to time limitations of this project, further study of the random microstructure generation algorithm was not able to be performed. Future study should involve determining the statistical validity of the algorithm. Wang et al. [18] give a good overview of methods which are suitable for determining statistical validity. These methods include nearest neighbour distance (completed as a part of nearest neighbour angle analysis), nearest neighbour angle (completed), Ripley's K function and the radial distribution function.

Representative volume elements from the random microstructure generation algorithm should be used to perform FEA and model the elastic properties of filled pultruded composites.

The three dimensional microstructure of pultruded composites has not been studied and as such no model has been produced to predict the degree of micro-crimping throughout the sample. MicroCT may provide a means for observing micro-crimping behaviour within a part.

Further research should be conducted into the effects of zinc stearate and P200 resin on the properties of the products and the processing robustness associated with the changes.

Appendices

Appendix A

Images of Equipment

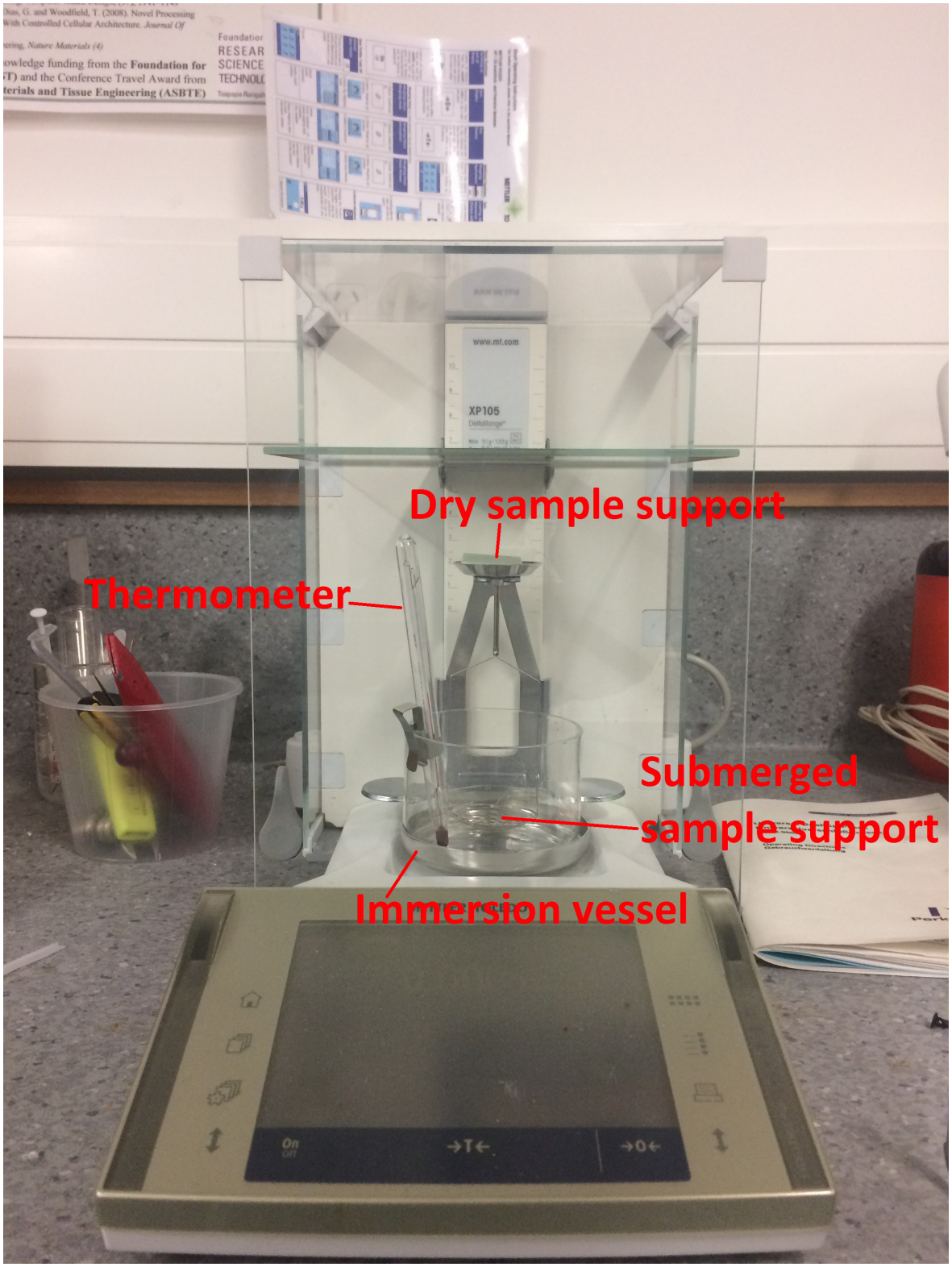

FIGURE A.1: Metler Toledo density testing apparatus.

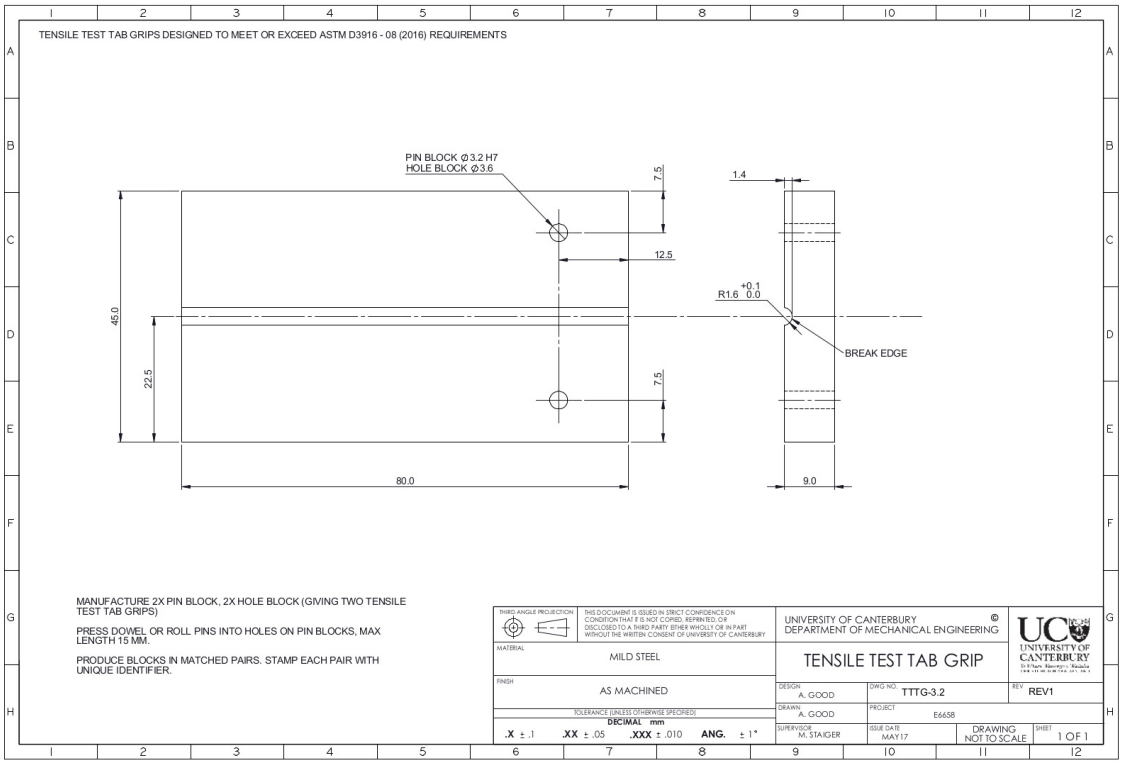

FIGURE A.2: CAD drawing of tensile testing clamp fixtures used in experiments, fixtures designed to meet and exceed ASTM D3916

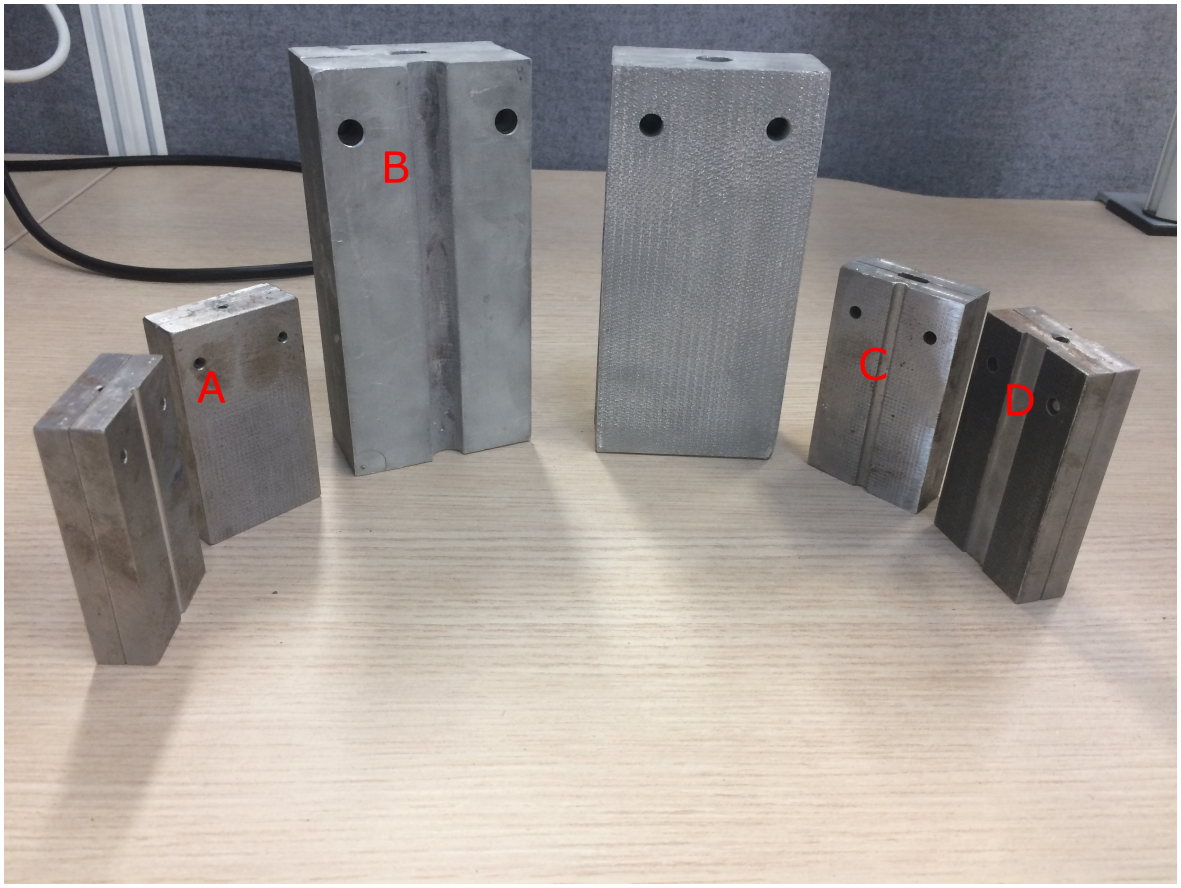

FIGURE A.3: Tensile testing clamp fixtures manufactured as a part of this project. A: 3.2 mm diameter rod, B: 12.7 mm diameter rod, C: 5.0 mm diameter rod, D: 11 mm by 4.0 mm rectangular bar.

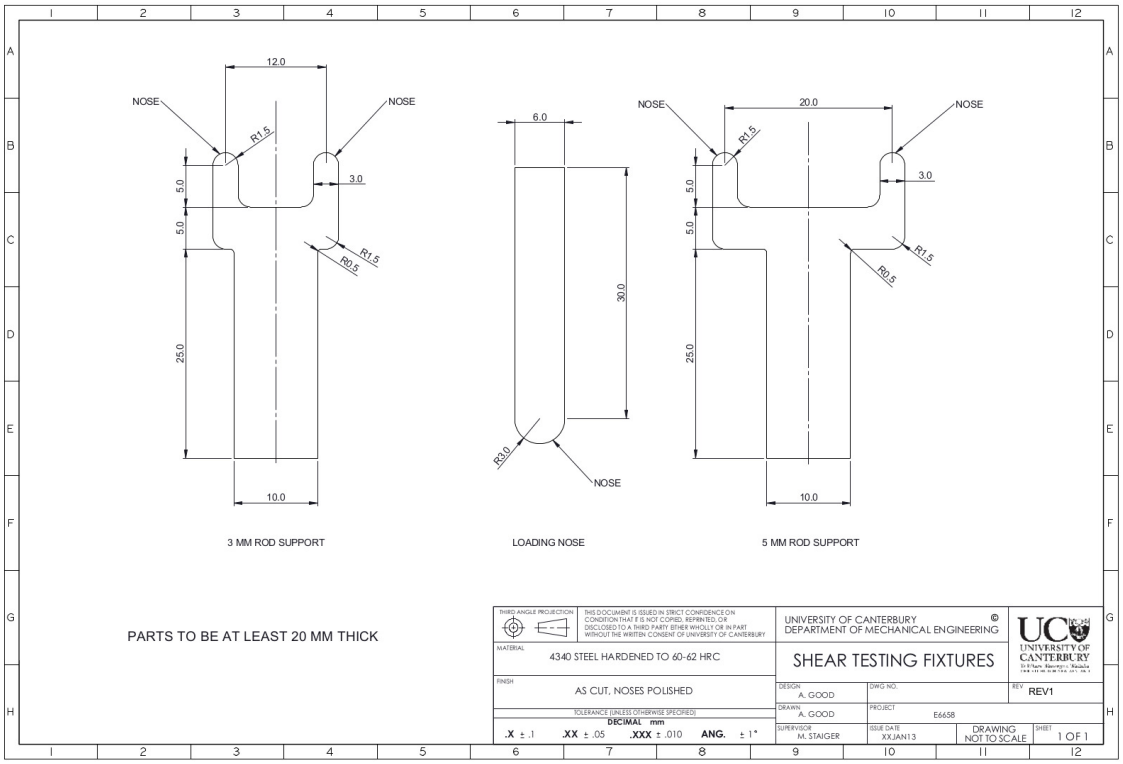

FIGURE A.4: CAD drawing of short beam loading fixtures used in experiments, fixtures designed to meet ASTM D2344

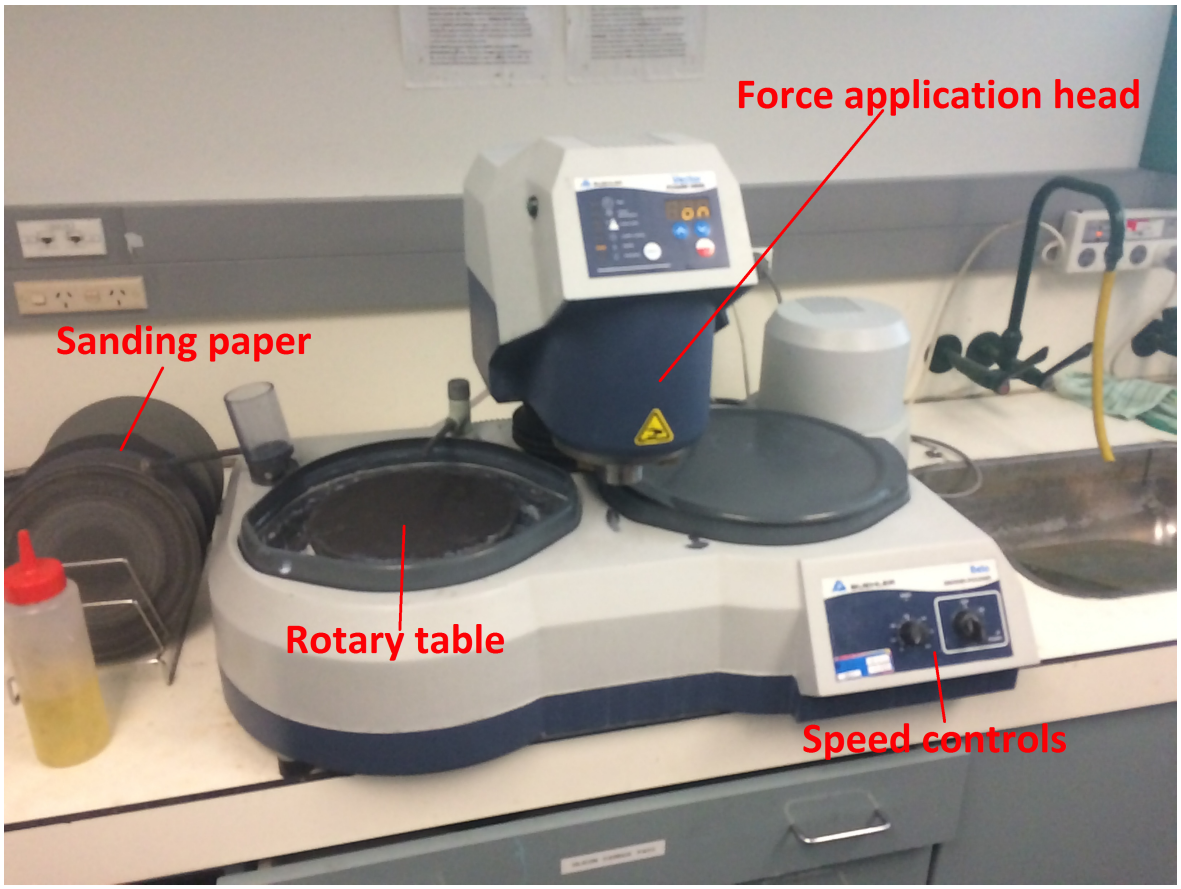

FIGURE A.5: Beuhler Powerhead grinder-polisher.

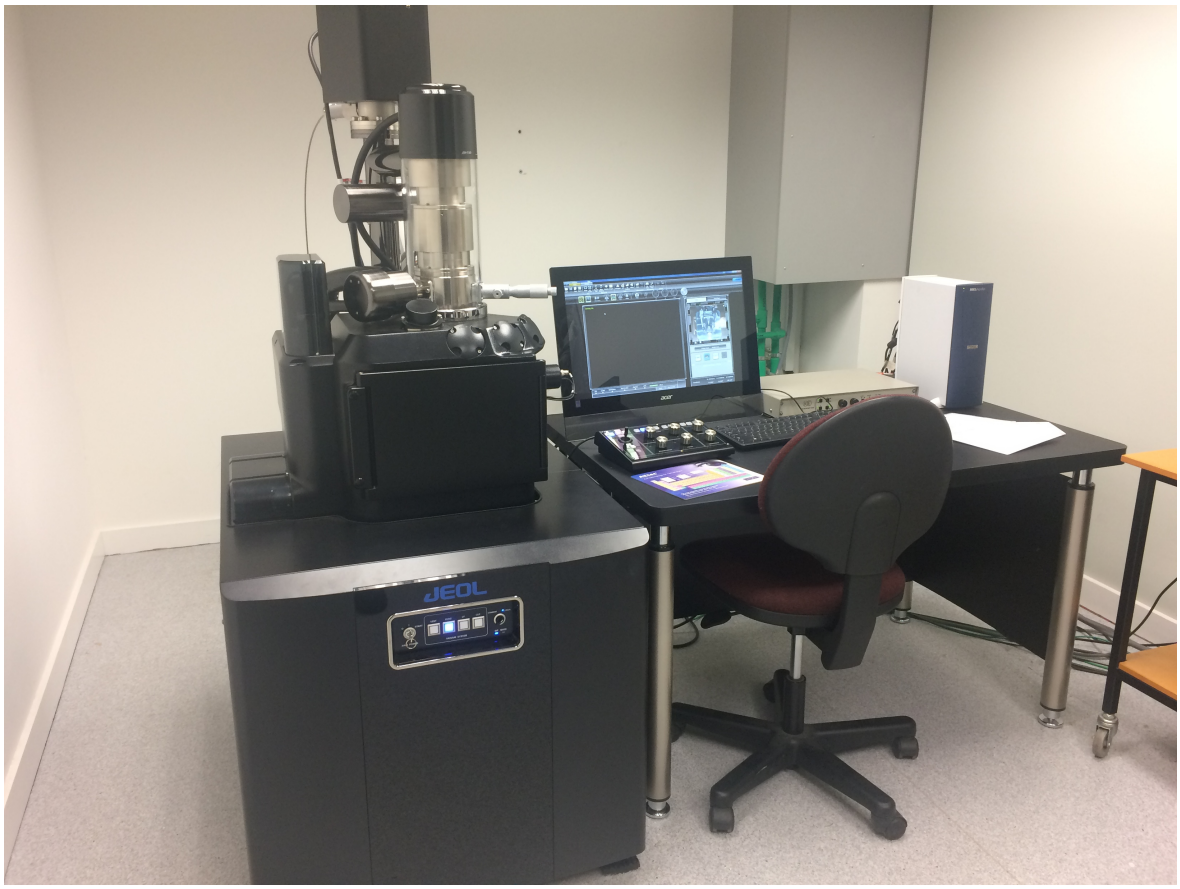

FIGURE A.6: JEOL JSM-IT300 scanning electron microscope

Appendix B

Matlab code

Microstructure generation script

```
clear all, close all, clc
load('expdiam.mat'); % Load experimental diameter data
fillercontent = [5:5:30]; % Attempted filler loadings in phr
results = zeros(length(fillercontent),4); % Initialise result
    matrix
subvolpercglass = 0; % initialize subregion volume percentage glass
submfiller1 = 0; % initialize subregion filler loading
for n = 1:length(fillercontent) % Loop through each filler content
    % product dimensions
    width = 1; % width in mm
    height = 1; % height in mm
    ID = 6; % internal diameter if used, mm
    nglass = 15000; % Number of fibers to try and place
    nf1 = 35000;%/n^0.4*fillercontent(n);%19000;%24000; % Number of
        filler1 to try and place
    nf2 = 0;%150; % Number of filler2 to try and place
    t = 1; % 1, rectangle; 2, round rod; 3, round tube
    f1type = 2; % Type of filler for filler 1, 1: given
        distribution, 2: poisson distribution
    initsubreglim = 60; % Lower limit on fibre content for initial
        subregion
    gensubreglim=63-fillercontent(n)/30; % Lower limit for glass
        percentage in subvolume
    subreglim = initsubreglim; % Set the sub region limit
    scalefactor = 2; % how much to scale the matrix and associated
        calculations by
    actnumrov = 0.1; % Actual number of rovings
    actglassarea= actnumrov*1.73; % Each 4400 roving is 1.73 mm^2
    dmid = 20; % delta growth for subregion mid sections
    dend = 20; % delta growth for subregion ends
    % Upper limits for fillers
    limf1 = fillercontent(n);%15; % limit in phr for the filler
    limf2 = 0; % limit in phr of filler 2
    warning ('off','all'); % Disable warnings
    global matcomposite smatxl smatyl smatxll smatyll smatx smaty
        fibrelist % Initialise global variables
```

```
30      fibrelist = zeros(nglass,3); % List of fibre diameters and x,y
            coordinates
31      smatx = 1e3*width*scalefactor; % width in micron
32      smaty = 1e3*height*scalefactor; % height in micron
33      initsmatxl = smatx/5;%/17;
34      initsmatyl = smaty/5;%/17;
35      smatxl = initsmatxl; % initial limit of guess region
36      smatyl = initsmatyl; % initial limit of guess region
37      smatxll = 1; % initial lower limit of guess region
38      smatyll = 1; % initial lower limit of guess region
39      matcomposite = zeros(smatx,smaty,3); % matrix for fiber/
            particle positions and size
40      %--- Define region which is composite and which is die
41      switch t
42          case 1 % Rectangle
43              cutoffperc = actnumrov*1.73/(width*height)*100; % Stop
                    adding glass when we get to this point
44          case 2 % Round rod
45
46              cutoffperc = actnumrov*1.73/(width^2/4*pi)*100; % Stop
                    adding glass when we get to this point
47              % Outside diameter
48              r = smatx/2*scalefactor; % radius of hole
49              [nc nr] = meshgrid(1:smatx,1:smaty);
50              xc = smatx/2; % centre x coord
51              yc = smaty/2; % centre y coord
52              submat = 150*((nr-yc).^2+(nc-xc).^2>=r.^2);
53              matcomposite = matcomposite+submat;
54              % Circular tube, 10 mm x 4 mm
55          case 3
56              % Centre hole
57              cutoffperc = actnumrov*1.73/(width^2/4*pi-ID^2/4*pi)
                    *100; % Stop adding glass when we get to this point
58              r = width*scalefactor; % radius of hole
59              [nc nr] = meshgrid(1:smatx,1:smaty);
60              xc = smatx/2;
61              yc = smaty/2;
62              submat = 150*((nr-yc).^2+(nc-xc).^2<=r.^2);
63              matcomposite = matcomposite+submat;
64              % Outside diameter
65              r = 5000*scalefactor; % radius of hole
66              [nc nr] = meshgrid(1:smatx,1:smaty);
67              xc = smatx/2;
68              yc = smaty/2;
69              submat = 150*((nr-yc).^2+(nc-xc).^2>=r.^2);
70              matcomposite = matcomposite+submat;
71      end
72      %--- Load in data for fillers
73      datf1 = importdata('omyacal10.csv'); % filler 1
74      radf1 = datf1.data(:,2)*scalefactor; % radius data
75      cumf1 = datf1.data(:,3); % cumulative quantity
```

```
76      rhof1 = datf1.data(1,5); % density of filler particles
77      % Just assume a particle size distribution
78      lambda = 1; % mean particle radius
79      wb1 = 1;%1; % weibull factor lambda
80      wb2 = 1.5; % weibull factor k
81      sf = 1.0; % scaling factor for weibull
82      datf2 = importdata('zincstearate.csv'); % filler 2
83      rhof2 = datf2.data(1,5); % density of filler particles
84      radf2 = datf2.data(:,2)*scalefactor; % radius data
85      cumf2 = datf2.data(:,3); % cumulative quantity
86      %--- Glass fiber size distribution
87      muglass = 11.24*scalefactor; % Mean radius of glass fibre
88      stdglass = 0.925*scalefactor; % Stdev of glass radius
89      rhoglass = 2.54;
90      %--- Particular properties
91      rhoresin = 1.05; % Density of resin
92      phrf1 = 30; % Parts per 100 resin of filler 1 by weight
93      phrf2 = 5; % Parts per 100 resin of filler 2 by weight
94      totweight = 100+phrf1+phrf2; % Total weight of mixture
95      wpercf1 = phrf1/(totweight); % Weight fraction of filler 1 in
            resin
96      wpercf2 = phrf2/(totweight); % Weight fraction of filler 2 in
            resin
97      wpercresin = 100/(totweight); % Weight fraction of resin in
            resin mixture
98      totvol = wpercresin*rhoresin+wpercf1*rhof1+wpercf2*rhof2; %
            Total volume of mixture
99      vpercf1 = wpercf1*rhof1/(totvol); % Volume fraction of filler 1
             in resin
100     vpercf2 = wpercf2*rhof2/(totvol); % Volume fraction of filler 2
             in resin
101     vpercresin = wpercresin*rhoresin/(totvol); % Volume fraction of
             resin in mixture
102     %--- Generate filler matrix
103     gx = 0;
104     gy = 0; % Initial guesses for locations
105     %Filler 1
106     f1 = f1type; % Preset the filler 1 type
107     numsteps = max([nf1,nf2,nglass]);
108     numexp = length(exp);
109     for i=1:numsteps
110         subproductarea = numel(matcomposite(max(5,smatxll):smatxl
                ,5:smatyll))+numel(matcomposite(5:smatxll,max(5,smatyll)
                :smatyl))+numel(matcomposite(max(5,smatxll)+1:smatxl,max
                (5,smatyll)+1:smatyl))-(sum(sum(matcomposite(max(smatxll
                ,5):smatxl,5:smatyll,1)==150))+sum(sum(matcomposite(5:
                smatxll,max(5,smatyll):smatyl,1)==150))+sum(sum(
                matcomposite(max(5,smatxll)+1:smatxl,max(5,smatyll)+1:
                smatyl,1)==150)));
```

```
111         subglassarea = sum(sum(matcomposite(max(5,smatxll):smatxl
                ,5:max(5,smatyll),3)==255))+sum(sum(matcomposite(5:max
                (5,smatxll),max(5,smatyll):smatyl,3)==255))+sum(sum(
                matcomposite(max(5,smatxll)+1:smatxl,max(5,smatyll)+1:
                smatyl,3)==255));
112         subvolpercglass = subglassarea/(subproductarea)*100;
113         if subvolpercglass < subreglim+round(0.7*rand)
114             rglass = scalefactor*round(exp(ceil(numexp*rand))/2)
                    *(0.8+0.4*rand);
115             [gx,gy]=  particleplot(rglass,gx,gy,3);
116         end
117         perc = (i/numsteps)*100;
118         if mod(perc,0.3) ==0
119             clc
120             display(['Progress: ' num2str(perc) '%']);
121             productarea = numel(matcomposite(:,:,1))-numel(find(
                    matcomposite(:,:,1)==150));
122             glassarea = sum(sum(matcomposite(:,:,3)==255));
123             volpercglass = glassarea/(productarea)*100;
124             display(['Fibre fraction: ' num2str(volpercglass) ' %'
                    ]);
125             imshow(matcomposite./255);
126             drawnow
127             if volpercglass >=cutoffperc
128                 while submfiller1<limf1
129                     rf1 = sf*wblrnd(wb1,wb2);
130                     [gx,gy] = particleplot(rf1,gx,gy,1);
131                     subvolfiller1 = (sum(sum(matcomposite(max(5,
                            smatxll):smatxl,5:max(5,smatyll),1)==255))+
                            sum(sum(matcomposite(5:max(smatxll,5),max(5,
                            smatyll):smatyl,1)==255))+sum(sum(
                            matcomposite(max(5,smatxll)+1:smatxl,max(5,
                            smatyll)+1:smatyl,1)==255)));%./(
                            subproductarea-subglassarea)*100;
132                     subvolmat = subproductarea-subglassarea;
133                     subvolres = subvolmat-subvolfiller1;
134                     svff1 =subvolfiller1/subvolmat; % volume
                            fraction filler 1 in matrix
135                     svfr =subvolres/subvolmat; % volume fraction
                            resin in matrix
136                     smm = subvolfiller1*rhof1+subvolres*rhoresin;
137                     smff1 = subvolfiller1*rhof1/smm; % mass
138                     smfr = subvolres*rhoresin/smm;
139                     phrr = 100;
140                     submfiller1 = smff1*phrr/smfr;
141                 end
142                 break
143             end
144         end
145         if mod(perc,0.02) == 0
146             glassarea = sum(sum(matcomposite(:,:,3)==255));
```

```
147         trueglassarea = glassarea/scalefactor/scalefactor/1e6;
                % How many square mm are glass?
148         subproductarea = numel(matcomposite(max(5,smatxll):
                smatxl,5:smatyll))+numel(matcomposite(5:smatxll,max
                (5,smatyll):smatyl))+numel(matcomposite(max(5,
                smatxll)+1:smatxl,max(5,smatyll)+1:smatyl))-(sum(sum
                (matcomposite(max(smatxll,5):smatxl,5:smatyll,1)
                ==150))+sum(sum(matcomposite(5:smatxll,max(5,smatyll
                ):smatyl,1)==150))+sum(sum(matcomposite(max(5,
                smatxll)+1:smatxl,max(5,smatyll)+1:smatyl,1)==150)))
                ;
149         subglassarea = sum(sum(matcomposite(max(5,smatxll):
                smatxl,5:max(5,smatyll),3)==255))+sum(sum(
                matcomposite(5:max(5,smatxll),max(5,smatyll):smatyl
                ,3)==255))+sum(sum(matcomposite(max(5,smatxll)+1:
                smatxl,max(5,smatyll)+1:smatyl,3)==255));
150         subvolpercglass = subglassarea/(subproductarea)*100;
151         subvolfiller1 = (sum(sum(matcomposite(max(5,smatxll):
                smatxl,5:max(5,smatyll),1)==255))+sum(sum(
                matcomposite(5:max(smatxll,5),max(5,smatyll):smatyl
                ,1)==255))+sum(sum(matcomposite(max(5,smatxll)+1:
                smatxl,max(5,smatyll)+1:smatyl,1)==255)));%./(
                subproductarea-subglassarea)*100;
152         subvolmat = subproductarea-subglassarea;
153         subvolres = subvolmat-subvolfiller1;
154         svff1 =subvolfiller1/subvolmat; % volume fraction
                filler 1 in matrix
155         svfr =subvolres/subvolmat; % volume fraction resin in
                matrix
156         smm = subvolfiller1*rhof1+subvolres*rhoresin;
157         smff1 = subvolfiller1*rhof1/smm; % mass
158         smfr = subvolres*rhoresin/smm;
159         phrr = 100;
160         submfiller1 = smff1*phrr/smfr;
161         if trueglassarea>=actglassarea && subvolpercglass>=
                gensubreglim && submfiller1>=limf1
162             break
163         end
164         if submfiller1>=limf1
165             f1 = 3; % Disable filler 1 if there is more than
                    the limit of it
166         else
167             f1 = f1type;
168         end
169         if smatyl == initsmatyl;
170             subreglim = initsubreglim; % Accounting for wall
                    effects, reduce limit for sub region
171         else
172             subreglim = gensubreglim;
173         end
```

```
174             if (subvolpercglass >=subreglim && submfiller1 >=(limf1
                    -1))
175                 smatxll = max([1,round(smatxl-0.2*smatx/dmid)]);
176                 smatyll = max([1,round(smatyl-0.2*smaty/dmid)]);
177                 if (smatyl > 0.9*smaty)
178
179                     smatyl = round(min(smatyl+smaty/dend,smaty));
180                     smatxl = round(min(smatxl+smatx/dend,smatx));
181                 else
182                     smatyl = round(min(smatyl+smaty/dmid,smaty));
183                     smatxl = round(min(smatxl+smatx/dmid,smatx));
184                 end
185                 if smatxl == smatx
186                     smatxll = 1;
187                 end
188                 if smatyll == smaty
189                     smatyll = 1;
190                 end
191             end
192         end
193         if subvolpercglass>initsubreglim && smatxl == initsmatxl ||
                subvolpercglass>=gensubreglim% mod(i,round(numsteps/nf1
                ))) ==0 &&
194             switch f1
195                 case 1
196                     rval = 100*rand;
197                     [m,n] = min(abs(cumf1-rval));
198                     rf1 = scalefactor*radf1(n);
199                     gx = round(smatx*rand);
200                     gy = round(smaty*rand);
201                     particleplot(rf1,gx,gy,1);
202                 case 2
203                     rhof1 = 2.7; % Define a filler density
204                     rf1 = sf*wblrnd(wb1,wb2);
205                     [gx,gy] = particleplot(rf1,gx,gy,1);
206             end
207         end
208         if mod(i,round(numsteps/nf2))==0
209             rval = 100*rand;
210             [m,n] = min(abs(cumf2-rval));
211             rf2 = radf2(n);
212             [gx,gy] = particleplot(rf2,gx,gy,2);
213         end
214     end
215     matcomposite = matcomposite(20:smatxl-20,20:smatyl-20,:);
216     smatyl = smatyl-40;
217     smatxl = smatxl-40;
218     imshow(matcomposite./255);
219     productarea = numel(matcomposite(1:smatxl,1:smatyl,1))-numel(
            find(matcomposite(1:smatxl,1:smatyl,1)==150));
220     glassarea = sum(sum(matcomposite(1:smatxl,1:smatyl,3)==255));
```

```
221     volpercglass = glassarea/(productarea)*100;
222     totalfillerarea = sum(sum(matcomposite(1:smatxl,1:smatyl,2)
            ==255))+sum(sum(matcomposite(1:smatxl,1:smatyl,1)==255));
223     totalvolpercfiller = totalfillerarea/productarea*100;
224     volpercmatrix = 100-volpercglass;
225     vf1 = sum(sum(matcomposite(1:smatxl,1:smatyl,1)==255)); %
            number of elements with f1
226     vf2 = sum(sum(matcomposite(1:smatxl,1:smatyl,2)==255)); %
            number of elements with f2
227     vr = numel(matcomposite(1:smatxl,1:smatyl,1))-numel(find(
            matcomposite(1:smatxl,1:smatyl,1)==150))-vf1-vf2-sum(sum(
            matcomposite(1:smatxl,1:smatyl,3)==255)); % number of
            elements with resin
228    vm = vf1+vf2+vr;
229     vff1 =vf1/vm; % volume fraction filler 1 in matrix
230     vff2 = vf2/vm; % volume fraction filler 2 in matrix
231     vfr =vr/vm; % volume fraction resin in matrix
232    mm = vf1*rhof1+vf2*rhof2+vr*rhoresin;
233     mff1 = vf1*rhof1/mm; % mass
234     mff2 = vf2*rhof2/mm;
235     mfr = vr*rhoresin/mm;
236     phrr = 100;
237     phrf1 = mff1*phrr/mfr;
238     phrf2 = mff2*phrr/mfr;
239     volpercfiller1 = 100*vff1;
240     volpercfiller2 = 100*vff2;
241     volpercresin = 100*vfr;
242     shrinkperc = 2.2; % how much the resin shrinks by on curing,
            percentage
243     trueglassarea = glassarea/scalefactor/scalefactor/1e6; % How
            many square mm are glass?
244     truefillerarea = totalfillerarea/scalefactor/scalefactor/1e6;
245     preshrinkresinarea = productarea*1e-6/scalefactor/scalefactor-
            trueglassarea-truefillerarea; % How much resin area is there
             before shrinkage?
246     postshrinkresinarea = preshrinkresinarea*(1-(shrinkperc)^2/100)
            ; % After shrinkage
247     trueproductarea = postshrinkresinarea+truefillerarea+
            trueglassarea; % What is the true area of the product after
            shrinkage?
248     shrinkfrac = (1-trueproductarea/(preshrinkresinarea+
            truefillerarea+trueglassarea))*100;
249     truevolpercfiller = (totalfillerarea/scalefactor/scalefactor/1
            e6)/trueproductarea*100;
250     numrovings4400 = trueglassarea/1.73; % Number of 4400 rovings
            capable
251     numrovings9600 = trueglassarea/3.77; % Number of 9600 rovings
            capable
252     display(['True Fibre fraction: ' num2str(trueglassarea/
            trueproductarea*100) ' %']);
253     display(['Filler 1 weight loading: ' num2str(phrf1) ' phr']);
```

```
254     display(['Filler 2 weight loading: ' num2str(phrf2) ' phr']);
255     %display(['Number of 9600 rovings: ' num2str(numrovings9600)]);
256     display(['Number of 4400 rovings: ' num2str(numrovings4400)]);
257     switch t
258         case 1
259             display(['Die area: ' num2str(width*height) ' mm^2,
                    Post shrinkage area: ' num2str(trueproductarea)]);
260             display(['Final width: ' num2str(smatyl/1000) ' mm,
                    Final height: ' num2str(smatxl/1000) 'mm. (Pre
                    shrinkage)']);
261         case 2
262             productdiam = sqrt(trueproductarea*4/pi);
263             display(['Die diameter: ' num2str(width) ' mm, Post
                    shrinkage diameter: ' num2str(productdiam)]);
264     end
265     results(n,1) = phrf1; % filler loading phr
266     results(n,2) = phrf2; % filler loading phr
267     results(n,3) = trueglassarea/trueproductarea*100;%volpercglass;
            % volume of glass
268     results(n,4) = results(n,3)*rhoglass/100+truevolpercfiller*
            rhof1/100+rhoresin*(1+shrinkperc^2/100)*(100-results(n,3)-
            truevolpercfiller)/100; % density
269     results(n,5) = shrinkfrac;
270 end
271 figure(2)
272 plot(results(:,1),results(:,3))
273 figure(3)
274 plot(results(:,1),results(:,4))
275 figure(4)
276 fibrelist(find(fibrelist(:,1)==0),:)=[];
277 h1 = histogram(round(fibrelist(:,1))/scalefactor);
278 hold on
279 h2 = histogram(round(exp/2));
280 h1.Normalization = 'probability';
281 h2.Normalization = 'probability';
282 xlabel('Fibre radius, micron');
283 ylabel('Probability');
284 legend('Generated Microstructure','Experimental Measurements');
```

Particle plotter function

```
1 function [xc,yc] = particleplot(r,gx,gy,type) % Type is whether
      glass or filler particle. 1 = filler1, 2 = filler2, 3 = glass
2 global matcomposite smatxl smatyl smatxll smatyll smatx smaty
      fibrelist
3 % Generate particle at origin
4 curfibrelist = fibrelist(find(fibrelist(:,1)>0),:); % will be used
      for checking for the nearest neighbour\
5 nnt = 2.5*r; % maximum distance allowed between fibres
6 r = round(r);
7 if type == 3
```

```
8
9       err=0.12*r^4; % attempts allowed to place a fiber
10  else
11      err = 1000;
12  end
13  [p,pp] = meshgrid(1:2*r+1,1:2*r+1);
14  c = r+1;
15  submat = (p-c).^2+(pp-c).^2  <=r.^2;
16  submat(1:end,1) = 0; % pull the particle away from the edge
17  submat(1:end,end) = 0;
18  submat(1,1:end) = 0;
19  submat(end,1:end) = 0;
20  % Pick a nominal position for the particle
21  xc = abs(gx +round(6*r*rand-3*r));%r+round((smatxl-2*r)*rand);
22  yc = abs(gy +round(6*r*rand-3*r));% r+round((smatyl-2*r)*rand);
23  dist = nnt+1;
24  while dist>nnt
25      if type == 1
26          dist = 0;
27      else
28          dists = (xc-curfibrelist(:,2)).^2+(yc-curfibrelist(:,3))
                .^2;
29          distmins = (min(dists(dists>0)));
30          mp = 0.6; % mutation parameer
31          shiftscale = (0.25)*mp*r;% how much to attempt to shift by
32          xc = round(xc+shiftscale*rand-0.5*shiftscale); % New x
                centre
33          yc = round(yc+shiftscale*rand-0.5*shiftscale); % New y
                centre
34          dist = sqrt(distmins);%/mean([r1,rs]);
35      end
36      check = ((xc>(smatxll+r)&&xc<(smatxl-r-1))&&(yc>(r)&&yc<(smatyl
            -r-1)))|((yc>(smatyll+r)&&yc<(smatyl-r-1))&&(xc>(r)&&xc<(
            smatxl-r-1)));
37      while (not(check)==1)
38          yc=round(smatyl*rand);
39          xc=round(smatxl*rand);
40          if (yc<(smatyll+r)&&xc<(smatxll+r))
41              dir = rand;
42              if dir >=(smatxl/smatyl)
43                  yc = round((smatyl-(smatyll+r))*rand+(smatyll+r));
44              else
45                  xc = round((smatxl-(smatxll+r))*rand+(smatxll+r));
46              end
47          end
48          if type == 3&&smatxl<smatx
49              check = ((xc>(smatxll+r)&&xc<(smatxl-1))&&(yc>(r)&&yc<(
                    smatyl-1)))|((yc>(smatyll+r)&&yc<(smatyl-1))&&(xc>(r
                    )&&xc<(smatxl-1)));
50          else
```

```
51              check = ((xc>(smatxll+r)&&xc<(smatxl-r-1))&&(yc>(r)&&yc
                    <(smatyl-r-1)))|((yc>(smatyll+r)&&yc<(smatyl-r-1))
                    &&(xc>(r)&&xc<(smatxl-r-1)));
52          end
53      end
54      rpart = max(max(matcomposite([xc-r:r+xc],[yc-r:r+yc],1).*submat
            )); % Radius of potential existing particle
55      nerr = 0;
56      while rpart > 0 % If we encountered an existing particle
57          if rpart == 150
58              xc = round((smatxl-smatxll)*rand+smatxll);
59              yc = round((smatyl-smatyll)*rand+smatyll);
60          end
61          nerr=nerr+1;
62          mp = 0.6; % mutation parameer
63          shiftscale = (0.25+nerr/err)*mp*r; % how much to attempt to
                shift by
64          xc = round(xc+shiftscale*rand-0.5*shiftscale); % New x
                centre
65          yc = round(yc+shiftscale*rand-0.5*shiftscale); % New y
                centre
66          if nerr > err/5 && type ==1
67              xc = r+round((smatxl-2*r)*rand);
68              yc = r+round((smatyl-2*r)*rand);
69          end
70          if nerr > err/1.05 && type ==3
71              xc = r+round((smatxl-2*r)*rand);
72              yc = r+round((smatyl-2*r)*rand);
73          end
74          if type == 3&&smatxl<smatx
75              check = ((xc>(smatxll+r)&&xc<(smatxl-1))&&(yc>(r)&&yc<(
                    smatyl-1)))|((yc>(smatyll+r)&&yc<(smatyl-1))&&(xc>(r
                    )&&xc<(smatxl-1)));
76          else
77              check = ((xc>(smatxll+r)&&xc<(smatxl-r-1))&&(yc>(r)&&yc
                    <(smatyl-r-1)))|((yc>(smatyll+r)&&yc<(smatyl-r-1))
                    &&(xc>(r)&&xc<(smatxl-r-1)));
78          end
79          while (not(check)==1)
80              yc=round(smatyl*rand);
81              xc=round(smatxl*rand);
82              if type == 3 && smatxl<smatx
83                  check = ((xc>(smatxll+r)&&xc<(smatxl-1))&&(yc>(r)&&
                        yc<(smatyl-1)))|((yc>(smatyll+r)&&yc<(smatyl-1))
                        &&(xc>(r)&&xc<(smatxl-1)));
84              else
85                  check = ((xc>(smatxll+r)&&xc<(smatxl-r-1))&&(yc>(r)
                        &&yc<(smatyl-r-1)))|((yc>(smatyll+r)&&yc<(smatyl
                        -r-1))&&(xc>(r)&&xc<(smatxl-r-1)));
86              end
87          end
```

```
88          rpart = max(max(matcomposite([xc-r:r+xc],[yc-r:r+yc],1).*
               submat)); % Radius of potential existing particle
89          if nerr>err
90              rpart=0;
91          end
92      end
93  end
94  if nerr<err
95      %generate a new guess for next particle
96      shiftscale = (0.25+nerr/1000)*1*r;
97      % Ensure particle does not go outside of allowable region
98      if type == 1; R = 255; G = 100; B = 100; end
99      if type == 2; R = 100; G = 255; B = 0; end
100     if type == 3; R = 100; G = 100; B = 255;  fibrelist(find(
           fibrelist(:,1)==0,1,'first'),:) = [r,xc,yc]; end
101     matcomposite([xc-r:r+xc],[yc-r:r+yc],[1]) = [R.*submat]+
           matcomposite([xc-r:r+xc],[yc-r:r+yc],[1]); % Drop the
           particle in
102     matcomposite([xc-r:r+xc],[yc-r:r+yc],[2]) = [G.*submat]+
           matcomposite([xc-r:r+xc],[yc-r:r+yc],[2]); % Drop the
           particle in
103     matcomposite([xc-r:r+xc],[yc-r:r+yc],[3]) = [B.*submat]+
           matcomposite([xc-r:r+xc],[yc-r:r+yc],[3]); % Drop the
           particle in
104 end
105 xc = round(xc+shiftscale*rand-0.5*(0.25+nerr/1000)*r); % New x
    centre
106 yc = round(yc+shiftscale*rand-0.5*(0.25+nerr/1000)*r); % New y
    centre
107 end
```

Nearest neighbour analysis script

```
1  rlist = fibrelist(:,1)-0.5;
2  for i = 1:length(fibrelist)
3      x1 = fibrelist(i,2);
4      y1 = fibrelist(i,3);
5      r1 = rlist(i);
6      dists = (x1-fibrelist(:,2)).^2+(y1-fibrelist(:,3)).^2;
7      distmins = (min(dists(dists>0)));
8      nns = find(dists==distmins);
9      nns = nns(1);
10     rs = rlist(nns);
11     rs = rs(1);
12     r1;
13     dist(i) = sqrt(distmins)/mean([r1,rs]);
14     nnd(i) = min(sqrt(distmins)-r1-rlist(nns));
15     x2 = fibrelist(nns,2);
16     y2 = fibrelist(nns,3);
17     if x2>x1 && y2>y1
18         nna(i) = atand((y2-y1)/(x2-x1));
```

```
19      elseif x2<x1 && y2> y1
20          nna(i) = 90+atand((x1-x2)/(y2-y1));
21      elseif x2<x1 && y2<y1
22          nna(i) =180+atand((y1-y2)/(x1-x2));
23      elseif x2>x1 && y2<y1
24          nna(i) = 270+atand((x2-x1)/(y1-y2));
25      end
26  end
27  figure(7)
28  %ksdensity(dist)
29  histogram(dist,100,'Normalization','probability')
30  figure(8)
31  cdfplot(nna)
32  hold on
33  plot([0,360],[0,1])
34  plot
        ([0,90,90,180,180,270,270,360,360],[0.125,0.125,0.375,0.375,0.625,0.625,0.875
        '-.o')
35  plot
        ([0,60,60,120,120,180,180,240,240,300,300,360,360],[0.0833,0.0833,0.0833+0.166
        '--*')
36  hold off
37  xlabel('Nearest neighbour angle')
38  legend('Generated microstructure','Statistically random','Square
        packed','Hexagonal packed')
39  ylabel('Cumulative distribution function')
```

Bibliography

[1] Liaoning Metals and Minerals Enterprise Co. Limited. *Talc Product Specification*, 2015.

[2] Omya New Zealand Limited. *Product Information Omyacal*, 2005.

[3] Muhammad Shafiq Irfan. *Environmentally friendly pultrusion*. PhD thesis, University of Birmingham, 2013.

[4] Young S Song, Jae R Youn, and Timothy G Gutowski. Life cycle energy analysis of fiber-reinforced composites. *Composites Part A: Applied Science and Manufacturing*, 40(8):1257–1265, 2009.

[5] Anurag Gupta, Hari Singh, and RS Walia. Effect of fillers on tensile strength of pultruded glass fiber reinforced polymer composite. 2015.

[6] Q Quan and RE Johnson. Resin flow through a porous fiber collection in pultrusion processing. Technical report, TAM Report, 1993.

[7] Sandro G Borges, Carlos A Ferreira, Juliana M Andrade, and André LA Prevedello. The influence of bath temperature on the properties of pultruded glass fiber reinforced rods. *Journal of Reinforced Plastics and Composites*, 34(15):1221–1230, 2015.

[8] Chin-Hsing Chen and I-Ken Chen. The unidirectional glass fiber reinforced furfuryl alcohol for pultrusion. i. process feasibility and kinetic analysis. *Polymer Composites*, 29(6):611–616, 2008.

[9] G Landon, G Lewis, and GF Boden. The influence of particle size on the tensile strength of particulate—filled polymers. *Journal of materials Science*, 12(8):1605–1613, 1977.

[10] Chin-Hsing Chen and Chen-Chi M Ma. Pultruded fibre reinforced polyurethane composites ii. effect of processing parameters on mechanical and thermal properties. *Composites science and technology*, 45(4):345–352, 1992.

[11] SFMM Paciornik, FM Martinho, MHP De Mauricio, and JRM d'Almeida. Analysis of the mechanical behavior and characterization of pultruded glass fiber–resin matrix composites. *Composites science and technology*, 63(2):295–304, 2003.

[12] R Boukhili, H Boukehili, H Ben Daly, and A Gasmi. Physical and mechanical properties of pultruded composites containing fillers and low profile additives. *Polymer composites*, 27(1):71–81, 2006.

[13] Z Zhang and S Zhu. Microvoids in unsaturated polyester resins containing poly (vinyl acetate) and composites with calcium carbonate and glass fibers. *Polymer*, 41(10):3861–3870, 2000.

[14] Jin Y Park and Abdul-Hamid Zureick. Effect of filler and void content on mechanical properties of pultruded composite materials under shear loading. *Polymer composites*, 26(2):181–192, 2005.

[15] Andrei A Gusev, Peter J Hine, and Ian M Ward. Fiber packing and elastic properties of a transversely random unidirectional glass/epoxy composite. *Composites Science and Technology*, 60(4):535–541, 2000.

[16] AR Melro, PP Camanho, and ST Pinho. Generation of random distribution of fibres in long-fibre reinforced composites. *Composites Science and Technology*, 68(9):2092–2102, 2008.

[17] Valentin Romanov, Stepan V Lomov, Yentl Swolfs, Svetlana Orlova, Larissa Gorbatikh, and Ignaas Verpoest. Statistical analysis of real and simulated fibre arrangements in unidirectional composites. *Composites Science and Technology*, 87:126–134, 2013.

[18] Wenzhi Wang, Yonghui Dai, Chao Zhang, Xiaosheng Gao, and Meiying Zhao. Micromechanical modeling of fiber-reinforced composites with statistically equivalent random fiber distribution. *Materials*, 9(8):624, 2016.

[19] ASTM International. *Standard Test Method for Glass Transition Temperature (DMA Tg) of Polymer Matrix Composites by Dynamic Mechanical Analysis*, 2015.

[20] ASTM International. *Standard Test Methods for Standard Density and Specific Gravity (Relative Density) of Plastics by Displacement*, 2013.

[21] ASTM International. *Standard Test Method for Short-Beam Strength of Polymer Matrix Composite Materials and Their Laminates*, 2016.

[22] NIWA. Cliflo - national climate database, 2015.

[23] Leif Jilkén, Göran Mälhammar, and Ragnar Seldén. The effect of mineral fillers on impact and tensile properties of polypropylene. *Polymer testing*, 10(5):329–344, 1991.

[24] MJ Zaini, MY Ahmad Fuad, Z Ismail, MS Mansor, and J Mustafah. The effect of filler content and size on the mechanical properties of polypropylene/oil palm wood flour composites. *Polymer International*, 40(1):51–55, 1996.

[25] Victoria Jane Worner. Use of glass fibre reinforced polymer (gfrp) reinforcing bars for concrete bridge decks. Master's thesis, University of Canterbury, 2015.

[26] ASTM International. *Standard Test Method for Tensile Properties of Pultruded Glass-Fiber-Reinforced Plastic Rod*, 2016.

[27] W Thomas. An investigation of the factors affecting the strength of glass fiber. *Glass and Ceramics*, 17(10):549–550, 1960.

[28] F Ramsteiner and R Theysohn. The influence of fibre diameter on the tensile behaviour of short-glass-fibre reinforced polymers. *Composites Science and Technology*, 24(3):231–240, 1985.

[29] Jushi USA. *Direct Roving 312 for Filament Winding, Weaving and Pultrusion*, 2014.

[30] Lawrence C Bank. Flexural and shear moduli of full-section fiber reinforced plastic (frp) pultruded beams. *Journal of Testing and Evaluation*, 17(1):40–45, 1989.

[31] Kate Liao, CR Schultheisz, and Donald L Hunston. Effects of environmental aging on the properties of pultruded gfrp. *Composites Part B: Engineering*, 30(5):485–493, 1999.

[32] Almir Barros da S Santos Neto and Henriette Lebre La Rovere. Flexural stiffness characterization of fiber reinforced plastic (frp) pultruded beams. *Composite structures*, 81(2):274–282, 2007.

[33] KS Raper, JA Roux, TA McCarty, and JG Vaughan. Investigation of the pressure behavior in a pultrusion die for graphite/epoxy composites. *Composites Part A: applied science and manufacturing*, 30(9):1123–1132, 1999.

[34] Zhigang Fang, Burton R Patterson, and Malcolm E Turner Jr. Modeling particle size distributions by the weibull distribution function. *Materials characterization*, 31(3):177–182, 1993.